

EXPERIMENTAL STUDY ON THE ELECTRON SUPERCONDUCTING LINAC AND ITS APPLICATION*

Kexin Liu[†], Shengwen Quan, Jiankui Hao, Senlin Huang, Lin Lin,
Liwen Feng, Fang Wang, Feng Zhu, Huamu Xie, Limin Yang, Jia-er Chen
Institute of Heavy Ion Physics & State Key Laboratory of Nuclear Physics and Technology
Physics and Technology, Peking University, Beijing, China

Abstract

Experimental study on superconducting electron linac has been developed at Peking University. Stable operation of a DC-SRF photoinjector and a 2×9-cell SRF linac has been realized with an average beam current of mA scale in macro pulses of several ms with a repetition rate of 10 Hz. A compact high repetition rate THz radiation source has been developed based on DC-SRF photo-injector through velocity bunching. Superradiant THz radiation with a repetition rate of 16.25 MHz and a frequency that can be tuned from 0.24 to 0.42 THz was generated by varying the electron beam energy from 2.4 to 3.1 MeV. MeV UED at MHz repetition rate has been demonstrated experimentally using electron pulses from the DC-SRF photoinjector. THz undulator radiation of ~1 THz central frequency with an average power of 1 W has been achieved with 13 MeV electron beam from SRF linac and applications are underway.

INTRODUCTION

To obtain electron beams with high average current and low emittance, superconducting radiofrequency (SRF) photocathode guns, which combine the high brightness of normal conducting RF photocathode guns with the advantage of CW operation of superconducting RF cavities, have been developed in many laboratories worldwide [1, 2].

DC-SRF photoinjector, which combines a DC Pierce gun and a superconducting cavity, was first proposed by Peking University in 2001 [3] and demonstrated with a 1.5-cell TESLA type superconducting cavity in 2004 [4]. An upgraded DC-SRF injector with a 3.5-cell large grain niobium cavity was then designed and constructed [5]. Electron beam with a current of mA level has been obtained at long-term stable operation. At the same time, a 1.3 GHz superconducting linac containing two 9-cell cavities was designed, setup and commissioned. Electron beam of 8-25 MeV was obtained by combination of the DC-SRF photoinjector and SRF linac.

Some applications with superconducting electron linac have been carried out at Peking University. Based on the DC-SRF photoinjector, a compact THz radiation source through velocity bunching was constructed to generate THz pulses with a high repetition rate. MeV ultrafast electron diffraction (UED) at MHz repetition rate has been demonstrated experimentally using electron pulses

from the DC-SRF photoinjector. With 13 MeV electron beam from SRF linac, THz undulator radiation are generated and an average power of 1 W in macro pulse has been achieved.

In this paper, the experimental studies on DC-SRF photoinjector and superconducting linac, the applications with electron beam from superconducting injector and linac are reported.

STUDY ON DC-SRF PHOTOINJECTOR

DC-SRF Photoinjector

Figure 1 shows the schematic view of the upgraded DC-SRF photoinjector, which consists of the DC pierce gun, 3.5-cell SRF cavity, helium vessel, liquid nitrogen shield, input power coupler, tuner and auxiliary systems.

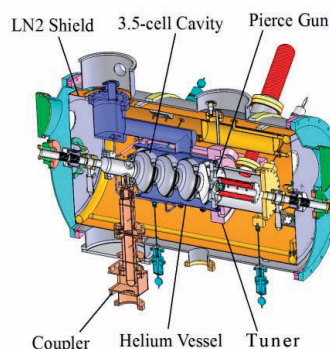


Figure 1: Schematic view of the DC-SRF photoinjector.

The designed DC voltage of Pierce gun is 90 kV. The surface electric field on the cathode is almost 5 MV/m and the peak electric field is lower than 13 MV/m. The 3.5-cell large grain niobium superconducting cavity comprises three TESLA type cells and a special designed half-cell. The accelerating gradient of the cavity reaches 23.5 MV/m and the intrinsic quality factor Q_0 is higher than 1.2×10^{10} in vertical test [5]. The input power coupler adopts compact capacitive coupling structure [6].

Cs_2Te photocathode is used for DC-SRF injector. The upgraded drive laser system composes of a Time-Bandwidth GE-100 XHP seed laser, amplifier, second harmonic generator, fourth harmonic generator and optical beam line to transport the UV pulses to the photocathode. The repetition rate of laser pulses is 81.25 MHz. The drive laser system can provide 1 W power in a train of 6 ps UV (266 nm) pulses with 5% power instability. The deposition of photocathode is accomplished in the vacuum of about 1.2×10^{-8} mbar. The Cs_2Te cathode is activated again with cesium just before

*Work supported by National Key Programme for S&T Research and Development (Grant NO.:2016YFA0401904)

[†] kxliu@pku.edu.cn

STATUS OF HEPS LATTICE DESIGN AND PHYSICS STUDIES*

Y. Jiao[†], X.H. Cui, Z. Duan, Y.Y. Guo, D.H. Ji, J.Y. Li, X.Y. Li, Y.M. Peng, Q. Qin, S.K. Tian, J.Q. Wang, N. Wang, Y.Y. Wei, G. Xu, H.S. Xu, F. Yan, C.H. Yu, Y.L. Zhao
Key Laboratory of Particle Acceleration Physics and Technology, IHEP, CAS, Beijing, China

Abstract

The High Energy Photon Source (HEPS) is a 6-GeV, kilometer-scale, ultralow-emittance storage ring light source to be built in Beijing, China. The HEPS is now under extensive design and study. In this report we will introduce the status of the HEPS lattice design and physics studies, including storage ring design, booster design, injection design, collective effects, error study, insertion device effects, longitudinal dynamics, etc.

INTRODUCTION

The High Energy Photon Source (HEPS) is a 6-GeV, kilometer-scale, ultralow-emittance storage ring light source to be built in the Huairou District, northeast suburb of Beijing, and now is under extensive design.

As the R&D project for HEPS, the HEPS test facility (HEPS-TF) has started in 2016, and is to be completed by the end of Oct., 2018. The goal of the HEPS-TF project is to develop key hardware techniques that are essentially required for constructing a diffraction-limited storage ring light source, meanwhile, to complete the design for HEPS. One of the goals of the HEPS-TF project is to obtain an ‘optimal’ lattice design for the HEPS, study the related accelerator physics issues and ensure there is no show-stopper from beam dynamics point of view, and give as detailed parameter list and tolerance budget table as possible for various hardware systems.

This year, we start to prepare the conceptual design report and the feasibility study report of the HEPS project. After iterative discussions, the goal emittance of the HEPS storage ring lattice design is to obtain a natural emittance of below 100 pm.rad, and the ring circumference is fixed to 1360.4 m.

For the sake of the R&D of key hardware techniques and related physics issues, a hybrid-7BA lattice with a natural emittance of ~ 60 pm.rad and large ring acceptance that promises different candidate injection schemes was proposed (see below for details).

Based on this lattice, we carry out related physics studies for the HEPS, including collective effect study, error effect and lattice calibration simulation, injection system design, injector design, etc. In addition, we also continuously do optimizations to look for lattice with even better performance.

In the following we will briefly introduce the status of the lattice design, and recent progress of studies on the related physics issues.

LATTICE DESIGN & PHYSICS STUDIES

Storage Ring Lattice Design

After various attempts of ultralow-emittance lattice designs and nonlinear optimizations [1-8], now the hybrid-7BA is chosen to be the basic layout of the HEPS storage ring. The optical function of one 7BA of the present lattice is shown in Fig. 1, and the main parameters of the ring are listed in Table 1.

After systematic optimization of both linear and nonlinear dynamics, as shown in Figs. 2 and 3, the ‘effective’ on-momentum dynamic aperture (DA) and momentum acceptance (MA) are 8 mm and 3.3 mm in x and y planes, and $\sim 3.5\%$, respectively (see [9] for definition and discussion of the ‘effective’ DA and MA). The large ring acceptance makes it feasible to use on-axis swap-out, on-axis longitudinal accumulation, or even off-axis multipole injection method in the HEPS storage ring.

It is worth mentioning that there is a trade-off between the emittance (which is positively correlated to the available maximum brightness) and the ring acceptance. On the other hand, the choice of injection method is related to the available of the ring acceptance. Generally speaking, conventional local-bump injection method requires a DA of larger than 10 mm, off-axis injection with multipole requires a DA of at least 5 mm, on-axis longitudinal injection requires that both on-momentum and off-momentum DAs are 1 to 2 mm, on-axis swap injection only requires an on-momentum DA of 1 to 2 mm.

Actually, this lattice is selected among those obtained from the global optimization of the hybrid-7BA lattice, where the linear and nonlinear dynamics are simultaneously optimized and all the available tenable element parameters are scanned. The results are presented in Fig. 4. It shows that with the hybrid-7BA lattice, if satisfying only the DA requirement of on-axis swap-out injection, the HEPS ring emittance can be down to ~ 45 pm.rad; if pursuing large ring acceptance that allows for accumulation injections, the DA can be optimized to be close to (if not larger than) 10 mm in the injection plane, while keeping the emittance to be around 60 pm.rad.

Except the layout presented in Fig. 1, we are exploring and comparing different types of lattice structures and globally scanning all tuneable parameters of the ring with stochastic optimization methods, with the aim to achieve lattice with even better performance. This will be reported in a forthcoming paper.

* Work supported by by NSFC (11475202, 11405187, 11205171)

[†] email address: jiaoyi@ihep.ac.cn

CEPC PARAMETER CHOICE*

D. Wang†, C. Yu, Y. Zhang, Y. Wang, J. Zhai, B. Sha, H. Geng, N. Wang, X. Cui, T. Bian, J. Gao, IHEP, Beijing, China

Abstract

The 100km Double Ring configuration with shared super conducting RF systems has been defined as baseline by CEPC steering committee. CEPC is compatible with W and Z experiment. Requirement for energy acceptance of Higgs has been reduced from 2% to 1.1% by enlarging the ring to 100 km. For CDR, W and Z will use the same lattice as Higgs, and the luminosity for Z is at the level of $10^{34}\text{cm}^{-2}\text{s}^{-1}$.

INTRODUCTION

According to the physics goal of CEPC at Higgs and Z-pole energy, it is required that the CEPC provides e+e-collisions at the center-of-mass energy of 240 GeV and delivers a peak luminosity of $2 \times 10^{34}\text{cm}^{-2}\text{s}^{-1}$ at each interaction point. At Z-pole the luminosity is required to be at least larger than $1 \times 10^{34}\text{cm}^{-2}\text{s}^{-1}$ per IP.

In the beginning of 2015, Pre-CDR of CEPC-SppC [1] has been completed with 54km circumference and single ring scheme. After that the size and the collision scheme of CEPC-SPPC was reconsidered. The 100km Double Ring configuration with shared SCRF has been defined as baseline by CEPC steering committee on Jan. 14th of 2016. The CDR report with 2mm β_y^* and 31 MW beam power will be finished by the end of 2017.

CEPC was proposed as a compatible machine which will allow stringent tests of the Standard Model (SM) with precision measurements at the Z pole and WW thresholds. At Higgs energy, all bunches distribute in the half ring due to the shared RF system. While for W and Z, bunches can distribute in the whole ring thanks to the independent RF system so that more bunches are possible. The scheme of CEPC bunch distribution is shown in Fig. 1.

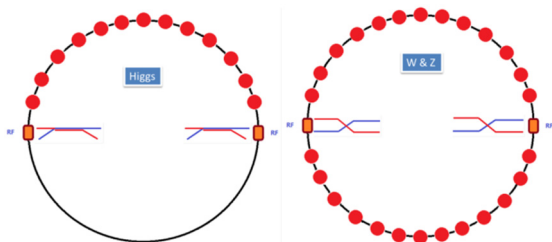


Figure 1: CEPC bunch distribution scheme (left: Higgs, right: W&Z).

BEAM LIFETIME LIMIT AND ENERGY SPREAD LIMIT DUE TO BEAMSTRAH-

LUNG

When two head-on colliding electron and positron beams penetrate each other, every particle in each beam will feel the electromagnetic field of the other beam and will be deflected. This deflection process has some undesirable effects. Firstly, the deflected particle will lose part of its energy due to the synchrotron radiation, called as beamstrahlung, which will increase the energy spread of the colliding beams, and hence increase the uncertainty of the physical experiments. If the beamstrahlung is so strong that particles' energy after collision is beyond the ring's energy acceptance, they may leave the beam and strike the vacuum chamber's walls, and hence beam lifetime is decreased. Secondly, the deflected particles will emit photons, hadrons, etc., which will increase the noise background level in the detector. Additionally, after the collision particles will change their flying direction with respect to the axis by a certain angle. If this angle is large enough the particles after the collision will interfere with the detection of small-angle events.

In order to control the extra energy spread by beamstrahlung to a certain degree, we introduce a constraint in this paper as

$$\delta_{BS} \leq \frac{1}{5} \delta_0 \quad (1)$$

where δ_0 is the nature energy spread and δ_{BS} is the extra energy spread due to beamstrahlung.

V. I. Telnov [2] pointed out that at energy-frontier e+e-storage ring colliders, beamstrahlung determines the beam lifetime through the emission of single photons in the tail of the beamstrahlung spectra. Unlike the linear collider case, the long tails of the beamstrahlung energy loss spectrum are not a problem because beams are used only once. If we want to achieve a reasonable beamstrahlung-driven beam lifetime of at least 30 minutes, we need to confine the relation of the bunch population and the beam size as follows [3]

$$\frac{N_e}{\sigma_x \sigma_z} \leq 0.1 \eta \frac{\alpha}{3 \gamma_e^2} \quad (2)$$

where η is the energy acceptance of the ring and α is the fine structure constant (1/137).

COLLISION SCHEME WITH LARGE PIWINSKI ANGLE AND CRAB WAIST

The crab waist scheme of beam-beam collisions can substantially increase the luminosity of a collider since it combines several potentially advantageous ideas. The first one is the large Piwinski's angle.

It is well known that decreasing β_y at the IP is very profitable for the luminosity, but the main limitation is set by the lower limit on the achievable bunch length. With

* Work supported by the National Key Programme for S&T Research and Development (Grant NO. 2016YFA0400400) and the National Natural Science Foundation of China (11505198, 11575218, 11605210 and 11605211).

† wangd93@ihep.ac.cn

PHASE SPACE GYMNASTICS

Alexander Chao, SLAC National Accelerator Laboratory

Abstract

Phase space gymnastics is a highly evolved accelerator physics technique based on the finest properties of the phase space. As modern accelerators become increasingly demanding, these techniques are finding a sharp increase in their applications. Here we intend only to introduce this topic to bring attention to the direction it points to.

INTRODUCTION

As accelerator technology advances, the requirements on accelerator beam quality become increasingly demanding. Facing these new demands, the topic of phase space gymnastics is becoming a new focus of accelerator physics research. In a phase space gymnastics, the beam's phase space distribution is manipulated and precision-tailored to meet the required beam qualities. On the other hand, all realization of such gymnastics will have to obey accelerator physics principles as well as technological limitations. Recent examples of phase space gymnastics include

1. Adapters
2. Emittance exchanges
3. Phase space exchanges
4. Emittance partitioning
5. Seeded free electron lasers
6. Steady-state microbunched storage rings

Each one of these applications involves half a dozen to a dozen inventions to special cases. It can only be expected that many more applications are yet to be found. This research field is very rich and active. In this report, however, we aim only to illustrate the subject and we will only briefly address the case of adapters (item 1 above) and give some of their example applications.

Just like the physical gymnastics, e.g. in the Olympic games, the skills needed in phase space gymnastics are highly technical and precise, while the resulting performance exquisite and beautiful. A comparison of these two gymnastics skills is shown in Fig. 1. Earlier phase space gymnastics have been mostly applied to the 2D longitudinal phase space, and took the form of RF manipulations in beam injection, extraction, and phase space displacement acceleration [1]. The recent advances, led by the seminal papers by Derbenev [2], begin to incorporate the transverse dimensions and become much more sophisticated, yielding a new wealth of additional applications mentioned above.

It should be mentioned here that phase space gymnastics permit precision manipulations because phase space is conserved to its finest details. Liouville theorem (more

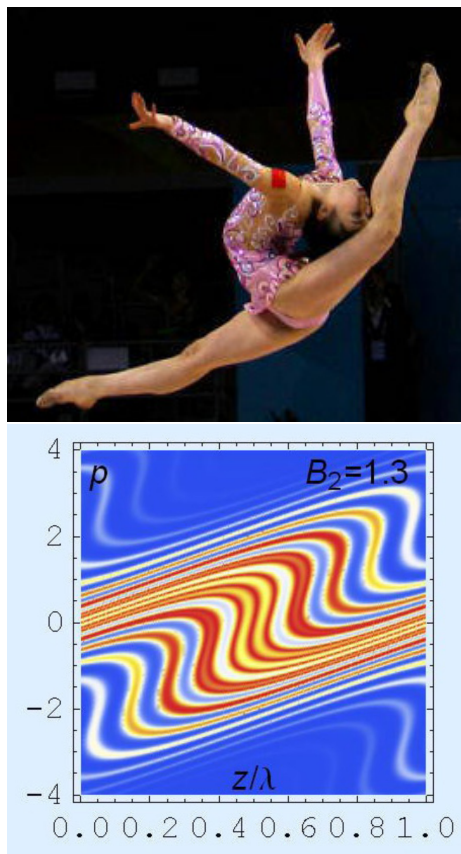


Figure 1: A comparison of phase space gymnastics and physical gymnastics.

accurately, the condition of symplecticity) is the root cause of this possibility of phase space technology. The very concept of phase space (a bold extension and abstraction of the 3D real space), and its intricate physical and mathematical properties (that pave the foundation of these phase space techniques), however, are not the subject of this report.

ADAPTERS

The idea of adapters was first introduced by Derbenev [2] and later rapidly extended by him and many others [3]–[14]. A few adapters of a different variety are shown in Fig. 2. Derbenev first envisioned applying it to a storage ring collider to form round beams at the collision point to mitigate the effect of the encountered beam-beam nonlinear resonances. This adapter idea has also been adapted for electron cooling [3, 7]. Furthermore, the production of a very flat beam from a round photocathode immersed in a solenoid followed by a round-to-flat adapter has been experimentally demonstrated [10–12].

Content from this work may be used under the terms of the CC BY 3.0 licence (© 2017). Any distribution of this work must maintain attribution to the author(s), title of the work, publisher, and DOI.

FABRICATION, ASSEMBLY AND TEST OF THE 2×4-CELL SUPERCONDUCTING LINAC MODULE FOR THE CAEP FEL-THz FACILITY *

X. Luo, C. L. Lao, L. J. Shan, K. Zhou[†], T. H. He, X. M. Shen, L. D. Yang,
 H. B. Wang, D. Wu, D. X. Xiao, J. X. Wang, S. F. Lin, X. F. Yang, M. Li
 Institution of Applied Electronics, CAEP, Mianyang, China
 X. Y. Lu, S. W. Quan, F. Wang, Peking University, Beijing, China

Abstract

A 2×4-cell superconducting linac module for the THz-FEL facility has been developed at the China Academy of Engineering Physics, which is expected to provide 6~8 MeV quasi-CW electron beams with an average current of 1~5 mA. The module consists of two 4-cell cavities, two power couplers, two tuners and the cryomodule. The main components are tested before the module assembly. The cavity test includes microwave measurement at room temperature and vertical test at 2 K. The conditioning and test of the couplers are also finished. The performances of the main components and the whole module are presented in this paper. The horizontal test indicated that the effective field gradients of both cavities have reached 10 MV/m, which have satisfied our designed goal.

INTRODUCTION

The FEL-THz facility in the China Academy of Engineering Physics (CAEP) is under construction at Chengdu, China. It is expected to provide 1 ~ 3 THz FEL with average power greater than 10 W [1]. Because of the advantages on working at CW mode or long pulse mode with high accelerating gradient, RF superconducting technology is employed in this project. As shown in Fig. 1, the superconducting module is used to accelerate the CW 1~5 mA beam from 320 keV to 6~8 MeV. The design of the module is based on the requirement of CW mode operation, such as beam loading and HOMs issues [2]. Two 4-cell TESLA-type cavities are adopted instead of one original 9-cell cavity, because of the limit of coupler power tolerance.

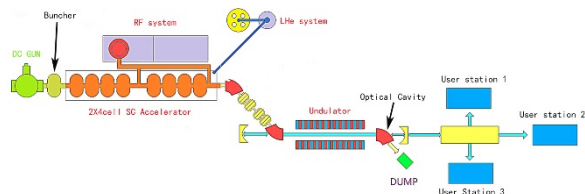


Figure 1: Layout of the CAEP THz-FEL facility.

Fig.2 shows the sectional view of the module. It consists of two 4-cell cavities, two power couplers, two tuners [3] and the cryomodule [4]. After the components are tested alone, the module are assembled and tested in Chengdu, China. The test technology and results are pre-

sented in this paper, as well as the components test.

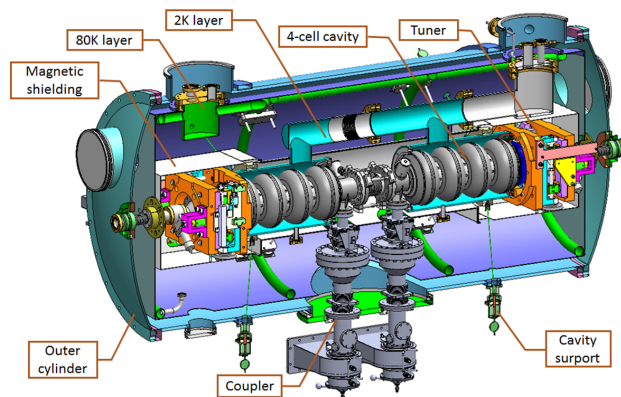


Figure 2: Schematic of the 2×4-cell module.

CAVITY PERFORMANCE

The 4-cell cavities are fabricated by Peking University. The RF character are measured by low power microwave test at room temperature. The frequency and electric field distribution of the fundamental mode and higher order modes are measured. After carefully adjust every cell length, the field flatness of each cavity reaches 95% (see Fig.3), and the fundamental mode frequency is adjusted to 1297.3 MHz, in order to make the frequency 1300 MHz after cooling down.

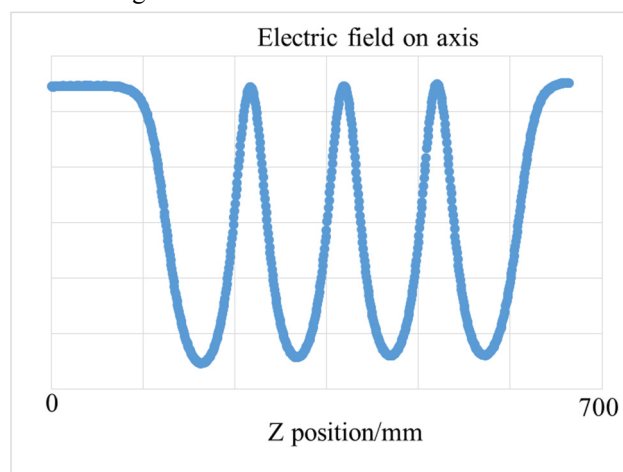


Figure 3: The electric field distribution of the fundamental mode in the 4-cell cavity.

The frequency and the field distribution of the HOMs are also measured. The modes type are identified by comparing with the simulation results before. The perfor-

* Work supported by China National Key Scientific Instrument and Equipment Development Project (2011YQ130018), National Natural Science Foundation of China with grant (11605190,11475159, 11505173 and 11576254).

[†] Email address: zhoudukui@163.com

ANALYSIS OF BEAM OPTICS FOR A HIGH POWER ION SOURCE*

Y. H. Xie, C. D. Hu[#], NBI Team, ASIPP, Hefei, China

Abstract

The high power ion source is the key parts of neutral beam injector. Generally speaking, the beam power should matching the extraction voltage for a given accelerator. In order to get higher beam power with lower beam extraction voltage, the beam optics of accelerator was analyzed based on the structure of EAST-NBI tetrode accelerator. The beam optics of a tetrode accelerator and a new designed three-electrode accelerator was analyzed with beam energy of 50 keV. The results shown that, the two types of accelerator can get high beam perveance (4.6 μp) with lower beam divergence angle compare to the EAST-NBI accelerator (2.8 μp). And the tetrode accelerator can gets lower beam divergence angle compare to the three-electrode accelerator, but the electric field between two electrode is much higher than three-electrode accelerator. The results can help for the ion source design of high power ion source.

INTRODUCTION

The Experimental Advanced Superconducting Tokamak (EAST) is the first fully superconducting tokamak in the world. It aims at the long-pulse operation (1000s) to study the physics and engineering questions of steady-state operation for controlled nuclear fusion sciences[1]. High auxiliary heating power was needed to support the physical research of EAST. So, a Neutral Beam Injection (NBI) system was designed and developed in the Institute of Plasma Physics, Chinese Academy of Sciences (ASIPP) for the EAST plasma heating and current driving[2-5].

The EAST-NBI system consist two ion sources, which has the same structure and designed parameters. According to the physical requirements of the EAST, a hot cathode multi-cusp ion source with four stage accelerator grids was employed for the EAST-NBI since the year of 2010. In September of 2013, one beam line with two ion sources are installed on the EAST and high power neutral beam of 2MW were injected into EAST in July of 2014. In the same year, other beam line with two modified accelerator with diamond plasma grids were installed on the EAST and it was contributed in the next campaign experiment of the EAST in 2015. The parameters of NBI can be achieved was mainly decided by the performance of ion source. In order to achieve high beam power with lower beam energy, the beam optics of a new designed accelerator based on the EAST-NBI accelerator was analyzed.

THE HIGH POWER ION SOURCE OF EAST-NBI

The hot cathode bucket ion source with tetrode accelerator was employed on the EAST-NBI system[6-7]. The ion source contains a plasma generator and a tetrode accelerator. The plasma generator has a rectangle cross section arc chamber with the dimension of 650 mm \times 260 mm \times 300 mm (W \times L \times H). In the top side, 32 pure tungsten filaments with diameter of 1.6 mm are installed near the back electron plate, which was used to provide sufficient primary electrons. The accelerator is a multiple slit type. It has a high transparence of 60%. Each layer of accelerator grid has 64 rails, which made of molybdenum and has cavity structure. The cooling water runs through the inner of rails, so, it has good performance of heating remove. The schematic map of ion source is shown in Figure 1. The cross-sectional picture of accelerator is shown in Figure 2. The designed beam energy of ion source is 50-80 keV, beam power is 2-4 MW. The beam cross section is 120mm \times 480mm and can be changed. The designed divergence angle in X direction is 0.6 degree and Y direction is 1.2 degree.

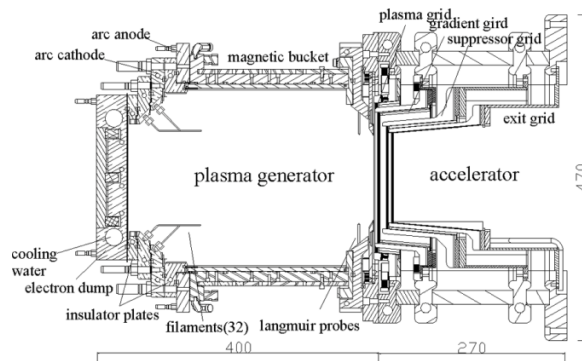


Figure 1: Schematic of high current ion source.

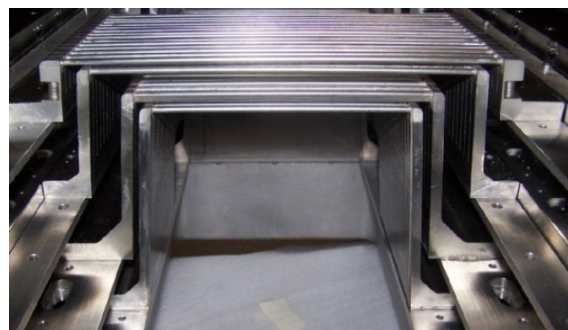


Figure 2: Cross sectional picture of accelerator with four stages of grids.

*Work supported by the National Natural Science Foundation of China (NNSFC) (Contract No. 11405207, 11507215 & 11675215)
[#]cdhu@ipp.ac.cn

THE ACCELERATION AND EXTRACTION SIMULATION FOR PULSED BEAM WITH DIFFERENT PHASE WIDTH FOR CYCIAE-100

Shizhong An[†], Luyu Ji, Sumin Wei, Ming Li, Fengping Guan, Tianjue Zhang, Chuan Wang, Dongsheng Zhang, LiPeng Wen, Yang Wang, Xiaotong Lu, Lei Cao
China Institute of Atomic Energy, Beijing, P.R. China

Abstract

A 100 MeV H- compact cyclotron (CYCIAE-100) has started operation from 2016 at China Institute of Atomic Energy (CIAE). The continuous proton beams of 75 MeV - 100 MeV has been extracted in dual opposite directions by charge exchange stripping devices. In order to analyze the extracted proton beam characteristics and control the beam loss for extracting 200 μ A proton beam, the acceleration and stripping extraction process for the pulsed beam for CYCIAE-100 are simulated with the code of COMA in detail in this paper. The simulations are mainly done for the different RF acceptance or acceleration phase width. Due to the simulation results, the extraction turns are more for the large phase width and it will be reduced effectively with small phase width. The transverse beam distribution and the extracted beam profile are not affected by the initial phase width due to the simulation, that's the characters of the cyclotron with the stripping extraction mode.

INTRODUCTION

The project of Beijing Radioactivity Ion-beam Facility (BRIF) has been constructed at China Institute of Atomic Energy (CIAE) for fundamental and applied research [1] [2]. As a major part of the BRIF project, the 100MeV compact cyclotron (CYCIAE-100) will provide proton beam with an intensity of 200 μ A ~ 500 μ A [3]. The extracted proton energy range is 75MeV~100MeV with dual direction foil stripping system [4]. The first beam of CYCIAE-100 was extracted on July 4, 2014 [5], the operation stability have been improved and beam current have been increased gradually. The main parameters for CYCIAE-100 are presented in Ref. [2]. For CYCIAE-100, the diameter of main magnet is 6160mm, corresponding to 4000mm for the magnet pole with the sector angle of 47 $^{\circ}$. The magnet is 2820mm high with a total weight of 435 tons. Two identical 100 kW RF amplifiers have been adopted to drive two cavities with the Dee angle of 38 $^{\circ}$ independently.

The CYCIAE-100 extraction system use two sets of stripping probes, can extract the beam from the symmetry direction to the various terminals. Two stripping probes with carbon foil are inserted radially in the opposite directions from the hill gap region and the two proton beams after stripping are transported into the crossing point in a combination magnet center separately under the

fixed main magnetic field. The combination magnet is fixed between the adjacent yokes of main magnet in the direction of valley region at ($R=2.75$ m, $\theta=100^{\circ}$).

The basic optic trajectories of extracted proton beams with various energies have been studied with the code CYCTR [6] and the transport matrix from the stripping foil to the crossing point is got from the code GOBLIN [7] including the dispersion effects. With the multi particle tracking code COMA [8], the beam dynamics are studied and the acceleration and stripping extraction process for the pulsed beam are simulated. The accelerate phase for the pulsed beam are selected after the simulation and the extracted proton beam turns are studied in detail for the pulsed beam with different initial phase width. The simulation results will give the references for the designing the beam pulsing system for CYCIAE-100. In order to analyze the extracted proton beam parameters for the pulsed beam, the simulation is mainly done for the different RF acceptance or acceleration phase width with the fixed initial transverse emittances.

THE BASIC CONSIDERATION FOR THE SIMULATION

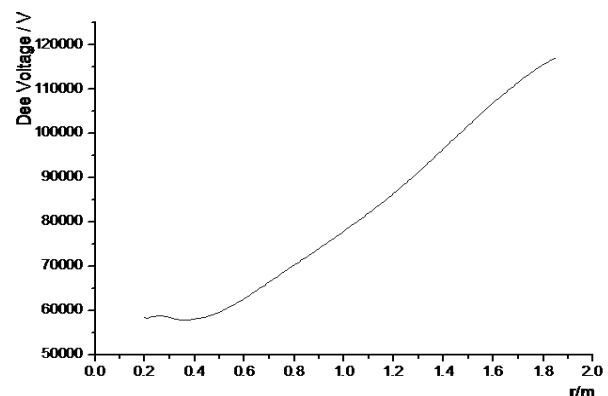


Figure 1: The voltage distribution versus along the radius of accelerating gap.

For CYCIAE-100, the outer radius of magnet yoke is 3.08 m and the combination magnet is located inside the yoke ($R=2.75$ m, $\theta=100^{\circ}$). The stripping foil is at the radial position of (1.609 m, 57.8 $^{\circ}$) for extraction energy of 70MeV and (1.875m, 59.6 $^{\circ}$) for extraction energy of 100MeV. The Dee Voltage is changed continuously from 60kV to 120kV along the radius of accelerating gap. Figure 1 shows the voltage distribution versus along the radius of accelerating gap.

[†] email address Szan@ciae.ac.cn

BEAM EXTRACTION SIMULATION FOR A 230 MeV SUPERCONDUCTING CYCLOTRON

Ming Li[†], Tianjue Zhang, Tao Cui, Tao Ge, Chuan Wang, Dongsheng Zhang, Jiuchang Qin, Sumin Wei, Shizhong An
China Institute of Atomic Energy, Beijing

Abstract

Introducing superconducting technologies, China Institute of Atomic Energy has designed a cyclotron to extract 230 MeV proton beam for cancer therapy. Extracted beam loss is one of the very crucial parameter in this machine. A low beam loss has benefit in reducing the dose level inside the cyclotron and preventing device damage, and consequently keeps the machine operate stable in long time. Two electrostatic deflectors are installed in the adjacent magnet hills to deflect the beam for extraction. The $v_r=1$ resonance and precession motion are introduced in extraction region to enlarge the turn separation. After the deflectors, passive magnetic channels provide radial focusing force to restrain the beam dispersion in the edge field. In this paper, the design process and simulation results will be presented in detail.

INTRODUCTION

Proton therapy is an effective way for cancer treatment with minimal side effect and widely investigated recent years. Due to the progress of superconducting techniques, very compact cyclotron can be manufactured with lower cost and less power consumption, which could be very suitable to be installed in hospital. In order to promote the development of proton therapy in china, CIAE (China Institute of Atomic Energy) has designed a superconducting cyclotron to extract 230 MeV, 300 nA proton beam [1]. The overall structure of the cyclotron is listed in Fig.1. The diameter and height of the magnet is 320 cm and 140 cm respectively, and the weight of the magnet is about 70 ton. The main parameters of the cyclotron are listed in Table 1 in detail. The excitation and field mapping of the coil has completed, the results of which shows the system operates stable and could generate the desired field. Meanwhile, the rough machining of the magnet is finished and the precision machining is ongoing.

As a proton therapy machine installed in hospital, beam extraction efficiency is very critical to reduce the dose level, which could prevent the devices from damage and hence increase the reliability of the machine in long time operation. There are four sectors in this machine. Spiral structure of the pole is adopted to increase the vertical focusing. Unlike the normal temperature magnet, the edge field of pole is very soft, i.e. the field drops slowly at the edge, leading to a long drift before extracted to the outside of the cyclotron. In order to drag the beam from acceleration, two deflectors placed at the adjacent hills are adopted to accel-

erate the beam deflection. Moreover, many magnetic channels are used to prevent the beam from blowing up resulted from the long drift in edge field.

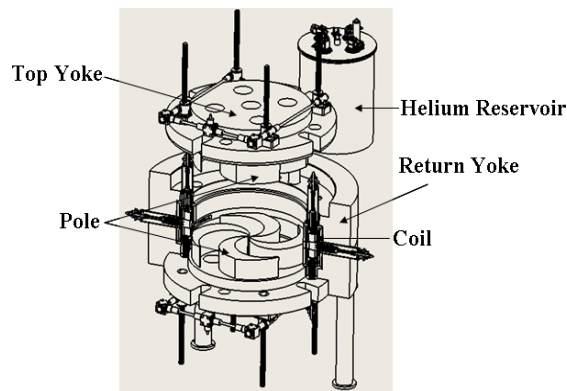


Figure 1: The overall structure of the cyclotron.

Table 1: The Main Parameters of the Cyclotron CYCIAE-230

Beam	
Extracted beam energy	240 MeV
Extracted beam current	300 nA
Magnet	
Pole structure	Spiral
Pole radius	85.0 cm
Outer radius of yoke	160.0 cm
Hill gap	5.0 cm
Central field	2.3 T
Coils	
Coil type	NbTi low temperature superconducting
Ampere-Turn Number	~600000 A.T×2
RF Cavity	
Number of cavity	4
RF frequency	72.0 MHz
Harmonic Mode	2
Cavity Voltage	80~110kV

BEAM PRECESSION

Beam precession with off center injection is always used to enlarge the turn separation in separated sector cyclotrons. A particle travel in the cyclotron with radial oscillation, the position of which at nth turn can be expressed as:

$$r = r_{seo} + x \sin(n(v_r-1)\theta + \phi) \quad (1)$$

Where r_{seo} is the according position of the static equilibrium, x and ϕ is the oscillation amplitude and phase, v_r is the tune value in radial direction and θ is the azimuth of the particle. Then the turn separation can be deduced,

[†]email address 393054642@qq.com

ENVELOPE CONTROL OF THE EXTRACTED BEAM FROM COMPACT CYCLOTRON

Sumin Wei[†], Ming Li, Tianjue Zhang, Shizhong An, Guofang Song, Pengzhan Li
 China Institute of Atomic Energy, Beijing, China

Abstract

Along with the fast development of cyclotrons, more and more compact cyclotrons are used in the medical treatment and the scientific research. Because of the compact structure, the magnetic field in the extraction area is complex and there is no room for the focusing elements, the new methods to control beam envelope in extraction area are needed. In this paper, the influence of envelope caused by the angle between the foil and the beam has been studied, the experiment on a 10 MeV compact cyclotron that construct in CIAE (China Institute of Atomic Energy) has been done, the result is well agrees with the theoretic design. For the small medical cyclotrons, this method can be used to adjust the beam spot on the liquid target which installs just on the exit of the cyclotron.

INTRODUCTION

A majority of the medical cyclotrons for the radio-pharmaceuticals production are compact cyclotrons, 10 MeV-30 MeV proton beams are extracted to produce radioactive nuclide for diagnosis such as F-18[1]. Usually, these kinds of cyclotron accelerate H- and extract proton beam by stripping foil because of the compact structure. Stripping is one of the most important methods in beam extraction of compact cyclotron because of the simple mechanical structure, the high extraction efficiency, the low cost, and the adjustable extraction energy.

For compact cyclotron, the dispersion caused by fringe field on the extract region will be obviously because of the small gap of the magnet, on the other hand, the energy dispersion of beams extracted by stripping foils usually large, which caused large increase in beam envelope and emittance, beam loss will be increased too. The extracted beam from these compact medical cyclotrons usually hit liquid target directly without long beam transfer line to produce short lifetime radioactive nuclide, there is no room for the focusing elements such as quadrupole, so we can't control beam envelope at this area and beam spot on target by focusing elements. The influence of envelope caused by the angle between the foil and the beam has been studied to control beam characteristic, both theoretical study and experiment study have been done. The results shows that one can control beam envelope effectively at extraction area only by adjusting the foil angle, it is of great significance for beam spot control on target, increasing the yield of radioactive nuclide and increasing of target lifetime.

For other cyclotrons with small extraction region that hard to install focusing elements, this method can be used

to control the extracted beam envelope, which is very important for the later beam transport, especially for high current cyclotron.

ANGLE EFFECT OF THE FOIL

Normally, the foil is perpendicular to beam direction and bring no influence for beam envelope. When there is an angle α between foil and the normal direction of beam, as shown in Fig. 1, it will bring a increment on x' after foil, could be expressed as formula 1.

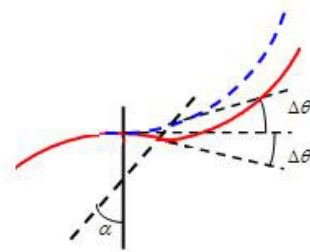


Figure 1: The angle between the foil and the beam.

$$\begin{aligned}
 \Delta x' &= 2 \int \frac{B_z}{B\rho} ds \\
 &= \frac{2}{(1+\delta)} \int \frac{B_0 + \frac{\partial B}{\partial x} x}{(B\rho)_0} ds \\
 &= \frac{2}{(1+\delta)} \frac{1 + \frac{\partial B}{\partial x} \frac{x}{B}}{\rho} x \tan \alpha \\
 &= \frac{2}{\rho} \left(1 - \frac{n}{\rho} x\right) (1 - \delta) x \tan \alpha \\
 &= \frac{2 \tan \alpha}{\rho} x - \frac{2n \tan \alpha}{\rho^2} x^2 - \frac{2 \tan \alpha}{\rho} x \delta
 \end{aligned} \tag{1}$$

In which α is the angle between foil and the normal direction of beam, ρ is the bending radius of the particles, δ is the momentum dispersion, n is the field-gradient index. Ignore higher order terms, the formula 1 can be wrote as:

$$\Delta x' = \frac{2 \tan \alpha}{\rho} x \tag{2}$$

Which means when there is an angle between foil and the normal direction of beam, it is a focusing effect in x direction, such as the pole-face rotation angle of the bending magnet.

Similarly, for z direction, the increment on z' after foil can be shown in formula 3.

[†] weisumin@tsinghua.org.cn

SOME INITIAL RESULTS OF CENTRAL REGION ORBIT TRACKING FOR SUPERCONDUCTING CYCLOTRON CYCIAE-230*

Dongsheng Zhang[†], Xianlu Jia, Ming Li, Fengping Guan,
Shizhong An, Tianjue Zhang, Chuan Wang, Sumin Wei,
China Institute of Atomic Energy, Beijing

Abstract

CYCIAE-230 superconducting cyclotron, a medical accelerator for proton therapy, is designing and constructing at CIAE now [1]. An internal PIG source was adopted to attain a compact and simple design. Central region electric and magnetic field design will directly affect the beam quality and reliability of the cyclotron in terms of phase selection, beam loss and beam stability. Moreover, a favourable central region will ensure single-turn extraction efficiency. The central region study was based on detailed orbit tracking results, including the beam behaviour in the push-pull RF mode and phase selection and axial focusing in the latest magnetic field and electrical field distribution from calculation. The physical design results of central region beam dynamics are presented here.

INTRODUCTION

CYCIAE-230 is a compact isochronous cyclotron with four spiral pole sectors and four spiral Dees in the valleys given the central field of 2.33 T and Dee voltage of 72 kV. This machine is designed to accelerate proton beam from the ion source to extraction energy of 230 MeV. Aims for clear single-turn extraction by electrostatic deflectors, second harmonic acceleration as well as push-pull RF mode was employed to get enough turn separation, which also benefits the central region design for larger energy-gain in the first turns. Internal ion source was adopted to simplify the machine, lead to a compact central region. Protons at the opening slit of the ion source was considered nearly zero energy, extracted by the puller at proper RF phase and accelerated in the first gap subsequently. Under the circumstances of internal ion source, the beam behaviour is strongly sensitive to the initial parameters of particles and the electric field distribution at the first gap. Meanwhile, without the injection beam line it is hard to satisfy all the demands of beam input properties (including energy, RF phase, radial phase space matching and vertical focusing) only by adjusting the position and opening direction of ion source. The general solution is to abandon the radial phase space matching in central region and rectify the radial oscillation by trim-rods or trim-coils located in the accelerator region. In our machine, four sets of trim-rods will be installed to provide radial beam alignment, but difficulties still remain in the ion source and central region design.

ORBIT CALCULATION

The calculation was conducted by single-particle tracking code CYCLONE [2] with the magnetic field in the symmetric plane and 3-dimensional electrical potential map in central region. The magnetic field calculations were carried out by 3-dimension finite element method code and the electric field was calculated by 2- or 3-dimension Laplace and Poisson equations solver RELAX3D [3]. The shape of central region electrodes was drawn in AutoCAD and imported to RELAX3D as boundary condition of electric potential.

Two electric field maps were used in CYCLONE. The small field, only covered the first gap, was fine meshed to make a more accurate orbit-tracking result, the field area is 1.6×1.6 cm and the grid size is $0.01 \times 0.01 \times 0.01$ cm, The large field in CYCLONE has an area of 20×20 cm and grid size of $0.05 \times 0.05 \times 0.05$ cm, contains about first 5 orbit turns. Simulation results implied such small grid in the small field region is necessary and the number of nodes in the large field is suitable for rapid iteration.

The initial coordinates of reference particle was chosen at the zero-potential surface in the opening of ion source, as recommended by Forringer's thesis [4] to provide accurate radial phase-space prediction. And the initial energy and RF phase of reference particle were scanned and determined in orbit-tracking.

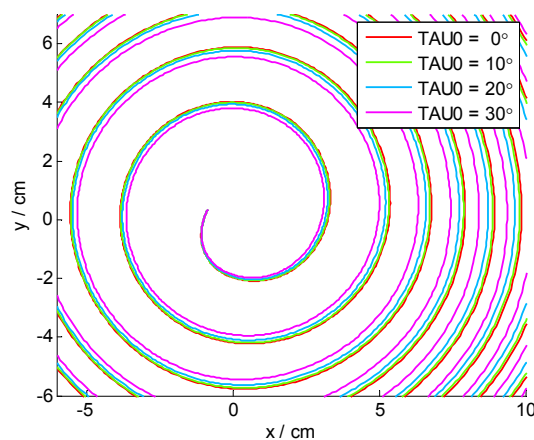


Figure 1: Orbits of particles with different initial RF phase.

The orbit tracking result shown in Fig. 1 contains the acceleration orbit of several particles within 30° phase width. In the current single-particle simulation period, the results shown that the phase acceptance of more than 30° is approachable, however a fixed phase slit will be

* This work was supported by the National Natural Science Foundation of China under Grand Nos.11375273 and 1146114103

[†] 18810681102@163.com

Content from this work may be used under the terms of the CC BY 3.0 licence (© 2017). Any distribution of this work must maintain attribution to the author(s), title of the work, publisher, and DOI.

DESIGN STUDY OF HEPS BOOSTER DESIGN*

Yuemei Peng[†], Zhe Duan, YuanYuan Guo, Daheng Ji, Yi Jiao, Cai Meng, Jingyi Li, Saike Tian, Haisheng Xu, Gang Xu, Key Laboratory of Particle Acceleration Physics and Technology, Institute of High Energy Physics, CAS, China

Abstract

The High Energy Photon Source (HEPS) is a 6GeV ultra-low emittance light source proposed to be built in Beijing. It will utilise a full energy booster synchrotron operating at a frequency of 1Hz as its injector. For meeting the requirement of high charge when using swap-out mode, the booster need to have the ability of beam accumulation. In this paper, a FODO lattice with 4 dispersion-free straight sections is presented.

INTRODUCTION

The light source HEPS with emittance less than 0.1nm.rad is proposed to be built in the suburb of Beijing. It will be composed of four main parts, a 0.3 GeV linac as the pre-injector, a full energy booster to accelerate the electrons from 300 MeV to 6 GeV, a storage ring at 6 GeV and the radiation synchrotron experimental hall.

The booster is located in a separate tunnel with a circumference about 453.5 m, 1/3 of that of the storage ring. It raises the energy of a 300 MeV electron beam up to 6 GeV in approximately 400 ms and operates at repetition rate of 1Hz.

Two filling patterns are mainly considered in HEPS storage ring, high-brightness mode (or low-bunch-charge mode, 90% buckets uniformly filled by about 680 bunches with beam current of 200 mA) and timing mode (or high-bunch-charge mode, 63 bunches uniformly filled in the ring). For the latter filling pattern, we need inject about 14nC charge to each bucket, this is a big challenge for injector, and so, the booster also used for beam accumulation is proposed.

For meet the storage ring operation requirements, the booster need support the beam with 2nC single bunch charge. The high bunch charge is a big challenge when beam energy is 300MeV.Under the detailed instability analysis, we change the booster lattice from TME cell with combined dipole [1] to FODO cell with separated dipole for larger momentum compact factor.

This paper is entirely about the lattice design and beam dynamics of the booster.

LATTICE DESIGN

The booster employs a classical FODO lattice structure as standard cell. It is a four-fold symmetry lattice with 14 identical cells together with two modified cells containing dispersion suppressors. The booster lattice is presented in Figure 1.The circumference is about 453.5 m, 1/3 of that of the storage ring.

There are four 8-m long straight sections with disper-

sion-free suitable for the installation of RF cavity, injection, and extraction systems. The main parameters are listed in Table 1.

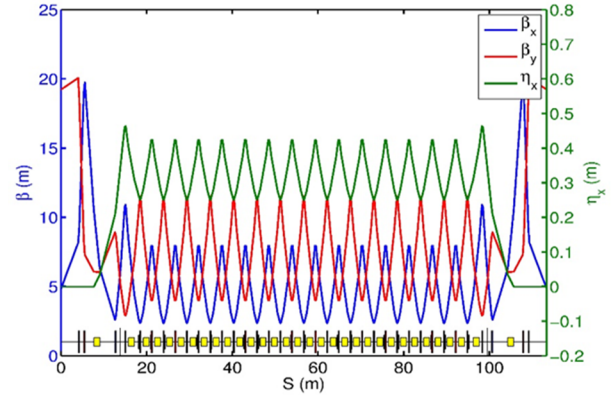


Figure 1: Optical functions and lattice structure of quarter.

Table 1: Main Parameters of HEPS Booster Lattice

Parameter	Unit	Value
Injection energy	GeV	0.3
Extraction energy	GeV	6
Number of super-periods		4
Length of the straight sections	m	8
Circumference	m	453.5
Repetition rate	Hz	1
Emittance @ 6 GeV	nm.rad	43
Emittance @ 0.3 GeV	nm.rad	70
Tune(H/V)		16.30/10.73
Energy spread @ 6 GeV		9.6×10^{-4}
Energy spread @ 0.3 GeV		0.5%
Natural chromaticity(H)		-17.70
Natural chromaticity(V)		-14.70
Momentum compaction factor		4.2×10^{-3}
Energy loss per turn @ 6 GeV	MeV	4
Long. damping time @ 6 GeV	ms	4.56
Hor. damping time @ 6 GeV	ms	4.51
Ver. damping time @ 6 GeV	ms	2.24
Maximum β_x	m	19.8
Maximum β_y	m	20.1
Maximum dispersion	m	0.5

We use six families of chromatic sextupoles to correct the chromaticity and nonlinear optimization. The nonlinear dynamics is simulated with AT program. The dynamic aperture of bare lattice and physical aperture in the middle of long straight is presented in Figure 2. The horizontal and vertical aperture can meet the requirements of beam

* Work supported by NSFC (11475202, 11405187, 11205171)

[†] pengym@ihep.ac.cn

Content from this work may be used under the terms of the CC BY 3.0 licence (© 2017). Any distribution of this work must maintain attribution to the author(s), title of the work, publisher, and DOI.

STUDY OF THE STABILITY OF LONGITUDINAL BEAM DYNAMIC OF CEPC FOR UNEVEN FILLING

Yuansheng SUN[†], Yuan Zhang, Na Wang, Jiyuan Zhai, Dianjun Gong
 Institute of High Energy Physics, CAS, Beijing, China

Abstract

PDR is a choice of CEPC design scheme, at any given time will contain a train of 50-70 bunches populate adjacent buckets and the remaining buckets unfilled. A consequence of an uneven filling scheme in the storage ring is that within train the synchronous phase will vary from bunch to bunch. This paper is to describe the tracking of the stability of longitudinal beam dynamic for CEPC, with the aim of including the main effects affecting the beam dynamics (i.e. the bunch-by-bunch feedback, the effect of the HOMs, the synchrotron radiation)..

INTRODUCTION

Table 1: The Machine Parameters of CEPC Partial Double Ring Scheme

Parameters	
Beam energy[GeV]	120
Beam revolution frequency [MHz]	5475.46
Energy spread total[%]	0.16
Number of IP	2
Circumference[km]	54
SR loss/turn[GeV]	3.1
Bunch number	50
Bunch current[mA]	16.67
Bunch length[mm]	6
Momentum compaction[10^{-5}]	3.4
RF Voltage[GV]	6.87
RF frequency[MHz]	650
Harmonic number	117081
Quality factor	4E10
Coupling factor	1.82E4
RF frequency[MHz]	650
Harmonic number	117081
Shunt impedance[MΩ]	5.72E2

CEPC is a circular electron-positron collider operate at 240GeV center-of-mass energy with a circumference of 54 km, serve as a Higgs factory. The parameters of CEPC is

[†] sunys@ihep.ac.cn

shown in Table 1. The main constraint in the design is the beam lifetime due to beamstrahlung(a process of energy loss by the incoming electron due to its interaction with the electron (positron) bunch moving in the opposite direction) and the synchrotron radiation power, which should be limited to 50MW per beam, in order to control the AC power of the whole machine. A new scheme called partial double ring was development recently and crab waist was adopted on CEPC. The layout of the CEPC partial double ring scheme is shown in Figure 1. The main advantage of crab waist is that the beam-beam limit can be significantly increased. At any given time, the ring contains a train of 50-70 bunches. Within the train bunches populate adjacent buckets and there is an extreme long gap that extends over 11731-11001 buckets. The time structure of bunch train is shown in Figure 2. A consequence of such uneven filling scheme is that within train the synchronous phase will vary significantly from bunch to bunch. For superconducting cavities with heavy beam loading, the transient effects result from fierce beam-cavity interaction should be carefully explored to provide information to the low level feedback system to ensure the accelerator can operate stabilized. In this paper we will study the beam loading of fundamental mode ignore the effect of other high order modes.

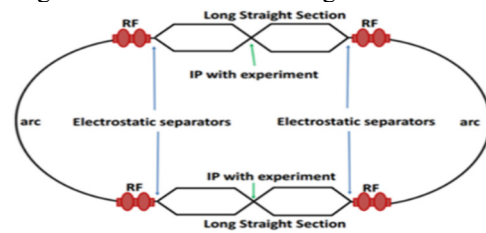


Figure 1: The layout of CEPC partial double ring.

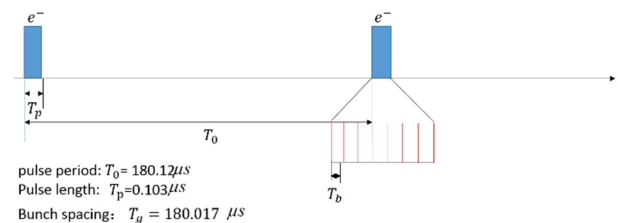


Figure 2: Time structure of bunch train.

COMPUTER SIMULATION OF THE BEAM LOADING

Tracking Model

MULTI-OBJECTIVE OPTIMIZATION OF DYNAMIC APERTURE AT OFF-AXIS INJECTION LATTICE OF HEPS

J. Wu[†], Y. Zhang, Y. M. Peng, IHEP, Beijing, China

Abstract

The off-axis injection scheme is also considered at HEPS. A large beta insertion section is need in the case, which breaks the symmetry of the machine. We introduce two designs of the injection section. There exist clear difference for the dynamic aperture between the two designs. The low-order nonlinear resonance driving terms is calculated and compared. The results show a correlation between momentum acceptance and the off-momentum driving terms. We enlarge the dynamic aperture by tuning the on-momentum and off-momentum non-linear driving terms with a multi-objective optimization code.

INTRODUCTION

Both on-axis injection scheme and off-axis injection scheme are considered in High Energy Photon Source (HEPS). Technology of off-axis injection is matured and it is well demonstrated in existing light sources. For ultra-low emittance storage ring, dedicated effort is required to reach the required dynamic aperture, but maybe at the expense of larger emittance.

Different lattices are adopted in different injection schemes. Compared with the standard 48-cell lattice, which is used for on-axis injection scheme, large-beta section is inserted in off-axis injection scheme that breaks the symmetry. As a result, dynamic aperture (DA) and momentum acceptance (MA) decrease a lot, especially MA, which falls from 3% to 2%. This result will be mentioned later.

Minimizing of the resonance driving terms (RDTs) is widely used for optimizing the dynamic aperture. This correction method is described in [1]. In consideration of the large reduction in momentum acceptance, we adopt both on-momentum and off-momentum resonance driving terms to carry out the optimization.

In this paper, we first introduce the lattice that includes the large-beta section and compare the DA and MA of two schemes. Then we give a short description for the resonance driving terms theory and analysis the 3rd and 4th order (Hamiltonian) terms with this method. According to the analytical results, we try to choose the objection functions to do the optimization.

LATTICE

To meet the demands of off-axis injection, standard 48-cell structure should be inserted large-beta ($\beta_x=90.86\text{m}$) linear section. As a result, the lattice includes: standard cell with 44 H7BA structure, injection cells with a high-beta section for injection, and the opposite two cells. See Figure 1 and Table 1.

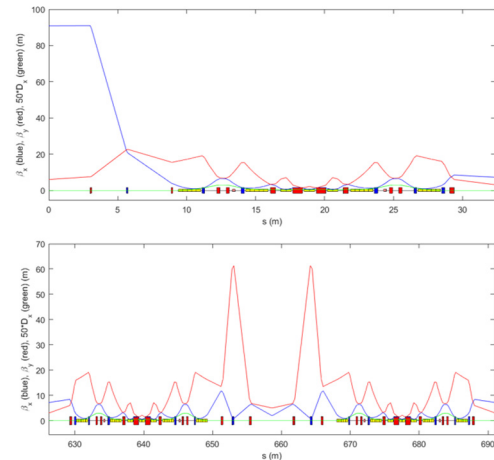


Figure 1: Half injection cell (above) and opposite cell for RF (below) [2].

Table 1: Main Parameters of the Lattice

Parameter	Value
Circumference(m)	1317.2783
Emittance(pm·rad)	60.2248
Q_x, Q_y	111.2839/41.1428
ξ_x, ξ_y	-2.4469/-2.3962
β_x, β_y (m)	90.8581/5.9937
Damping time(ms)	16.68/24.97/16.61
U_0 (Mev)	2.11

After inserting the high-beta section, we used this design lattice to do the particle tracking (1000 turns) and compared the DA result with the same work in the standard 48-cell lattice. Results are given below (See Figure 2).

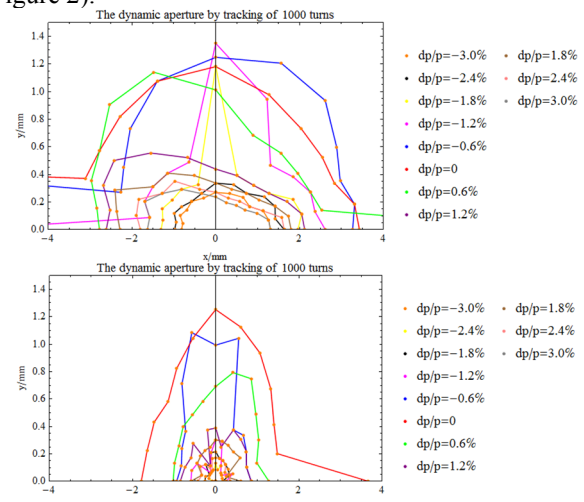


Figure 2: Dynamic aperture for HEPS on the x-y plane at the injection point for different off-energy values.

[†] wujin@ihep.ac.cn

THE BEAM DYNAMICS SIMULATION OF AN L-BAND ELECTRON GUN USING GENETIC ALGORITHM

Peiliang Fan[†], Xiaozhong He, Jian Pang, Liu Yang

Institute of Fluid Physics, China Academy of Engineering Physics, Mianyang, China

Abstract

The China Academy of Engineering Physics (CAEP) plans to build XFEL light source. In the beam dynamics simulation there are many parameters to be considered, so we need a high efficient method to find the optimal parameters. Genetic algorithm (GA) [1] is widely used as one kind of evolutionary algorithm and it can help us to find the optimal parameters in a shorter time. In this paper, we will use genetic algorithm to do the beam dynamics simulation of an L-band electron gun used for the XFEL. We put emphasis on the optimization of the transverse normalized projected emittance and the relevant result will be given and discussed.

INTRODUCTION

The China Academy of Engineering Physics (CAEP) plans to build XFEL light source. A normal conducting L-band photocathode electron gun will be used to produce high quality electron beam and its working frequency is 1.3 GHz. One of the most important parameters that influence the FEL process is the normalized transverse projected emittance, hereafter called emittance. There are many parameters to be considered in the beam dynamics simulation of the electron gun in order to get an optimized result. We need one efficient way to find these optimal parameters. Genetic algorithm is widely used as one kind of evolutionary algorithm and it can help us to find the optimal parameters in a shorter time. In this paper, we will use genetic algorithm to do the beam dynamics simulation.

THE BEAM LINE AND GA

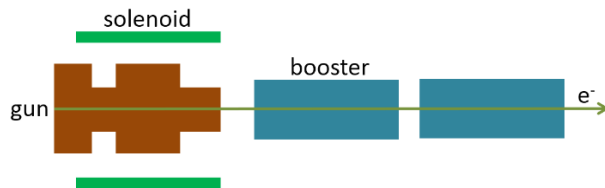


Figure 1: The simplified schematic of the beam line.

The electron source used for the XFEL is one normal conducting 1.6-cell L-band RF gun and its working frequency is 1.3 GHz (the field is shown in Fig. 2). The photocathode will use Cs₂Te or Cu, and they will be illuminated by UV laser pulses to produce high quality electron beams. The produced beams will be focused with solenoid installed around the gun. The beam will be further accelerated by the superconducting TESLA booster (9-cell). The simplified schematic of the beam line is shown in Fig. 1.

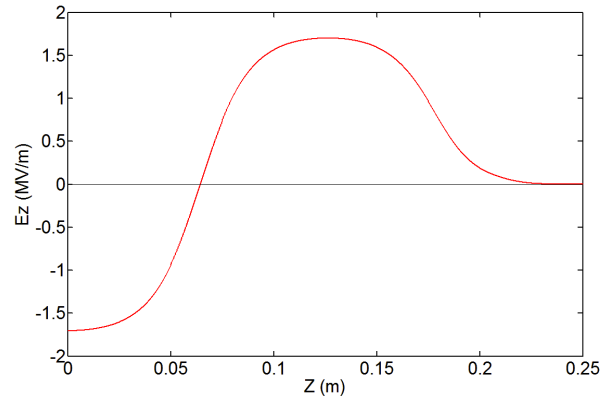


Figure 2: The electric field of the L-band gun.

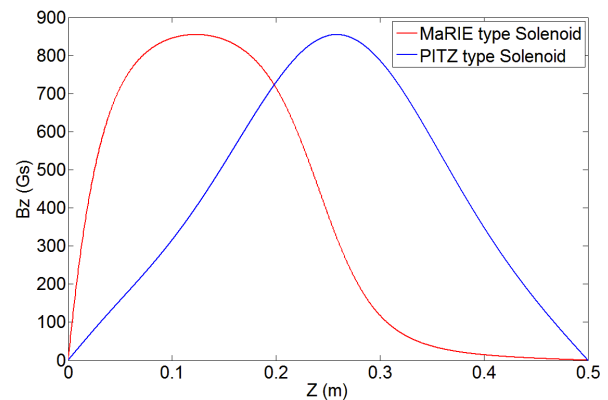


Figure 3: The magnetic field of solenoids.

In the simulation we compared the MaRIE [2] type solenoid, hereafter called M type, and the PITZ [3] type solenoid (P type). The magnetic field of the solenoids is shown in Fig. 3. We use ASTRA code [4] to do the beam dynamics simulation.

The initial condition is FWHM pulse length $Lt = 20\text{ps}$ and the rise time $rt = 2\text{ps}$. The laser pulse longitudinal shape is plateau distribution, and the transverse distribution is 2D uniform distribution. The E_{acc} of the booster is 20 MV/m and the gain energy is about 20 MeV for each 9-cell superconducting cavity.

Genetic algorithm solver is in the optimization tool of MATLAB. The GUI interface of the GA solver in MATLAB is shown in Fig. 4. We need to write the fitness function and set constrains. The population type is double vector and the population size is 50 ~ 100 for 4 variables. In the stop criteria option, *Generations* specifies the maximum number of iterations the genetic algorithm performs. In the plot function option, *Best fitness* plots the best function value in each generation versus iteration number.

[†] fanpeiliang@163.com

BEAM DYNAMICS OF A 325 MHz IH-DTL WITH KONUS

R.Tang, S. X. Zheng, Q. Z. Xing, X. L. Guan, X. W. Wang, C.X. Tang[†], Key Laboratory of Particle & Radiation Imaging (Tsinghua University), Ministry of Education, Beijing, China
 also at Laboratory for Advanced Radiation Sources and Application, Tsinghua University, Beijing,
 also at Department of Engineering Physics, Tsinghua University, Beijing, China

Abstract

A 325 MHz interdigital H-mode drift tube linac (IH-DTL), which is aimed at proton medical facilities, has been proposed and developing at Tsinghua University. The proton beam can be accelerated from 3 MeV to 7 MeV and the peak current of the beam at the exit of the cavity is about 15 mA. A KONUS dynamics without focusing element is applied in this cavity. The co-iteration of dynamics simulation and RF simulation is done. The process and result of the design is presented in this paper.

iteration of beam dynamics and RF field simulation [4]. The design process and results is presented in this paper.

Table 1: Parameters of 325 MHz IH-DTL

Parameters	
Particle species	proton
Frequency	325 MHz
Particle input energy	3 MeV
Particle output energy	7 MeV
Peak current	15 mA
Pulse width	40 μ s
Energy spread	$< \pm 0.3\%$ (> 8 mA)

INTRODUCTION

Since Munich University built the first IH-DTL accelerator at 1977, IH-DTL is widely used for heavy ion accelerators because of its high shunt impedance at low β range ($\beta < 0.1$) [1, 2]. As facilities used for proton and carbon therapy increase and the 3D RF simulation becomes reliable. IH DTL has been used widely in the injector of medical synchrotrons. A 216 MHz IH-DTL has been developed for HICAT (Heidelberg Heavy Ion Cancer Therapy) project. There are 4 KONUS (Kombinierte Null Grad Struktur) sections and three triplets in the tank. The proton beam can be accelerated from 0.4 MeV to 7 MeV in 3.76 m. The high effective gradient is 5.5 MV/m [3]. Another kind of proton IH DTL is developed via APF (Alternating Phase Focusing) beam dynamics. The length of this cavity is ~ 1.7 m. It can accelerate 10mA proton beam to 7.4 MeV at 200 MHz [4].

Considering the beam test on XiPAF (Xi'an Proton Application Facility) project, a 325 MHz IH-DTL is proposed and developing at Tsinghua University. The design parameters of this IH-linac is shown in Table 1.

The optimization of single cell geometry and the dynamics model is introduced in reference [5]. To get high accelerating gradient and high shunt impedance, there is no focusing elements in this 1 m cavity. The power loss of the cavity is 145 kW and the average accelerating gradient is 5.45 MV/m. While the peak surface electric field is 2.25 kV, which seems a little higher [6].

For both APF and KONUS beam dynamics design, it needs the approximation of E field distribution (or voltage versus gaps) at first. And the synchronous phase calculated by beam dynamics at each cell determines the cell length which changes the E field distribution meanwhile. Thus, an IH-DTL design needs the co-

BEAM DYNAMICS DESIGN

To design an IH-DTL, the gap voltage and the transit time factor (TTF) for different cell is necessary. The TTF of cell is determined by interpolation with some typical cells like Parmila code. The gap voltage is given by designers at first which is shown in Fig. 1. The code and model of the dynamics design is introduced in reference [5].

This 325MHz IH-DTL is divided into 3 sections: bunching, acceleration, de-bunching. There are 4 gaps used for bunching which's synchronous phase is -80 deg. The phase spread of the beam becomes bigger than ± 20 deg because of a long MEFT after RFQ. This bunching section can bunch this beam without big distortion in longitudinal phase space. The acceleration section is designed in a KONUS way [7]. The structure is designed with 0 deg synchronous phase and the designed injecting energy is a little lower than the real bunch central energy. The injecting phase is 8 deg. As the real bunch central energy is bigger than the synchronous energy, the RF phase of bunch center decreases as shown in Fig. 2. The synchronous phase at de-bunching section is 10 deg and there are 5 gaps. This section are used to suppress the beam envelop growth as there is no focusing elements in the cavity. Meanwhile, this positive synchronous phase design can defocusing beam at longitudinal phase space. The energy spread is too big for injection and a de-buncher is needed after the DTL. This de-bunching section makes the beam spread at the exit of IH-DTL widely, which decreases the drift length between the DTL and the de-buncher. There are 21 gaps for this design and the total length is 1m. The phase space evolution is shown in Fig. 3. The blue lines are the bucket plot. The red

[†] tang.xuh@tsinghua.edu.cn

MULTI-BEND ACHROMAT LATTICE WITH INTERLEAVED DISPERSION BUMPS FOR A DIFFRACTION-LIMITED STORAGE RING

Zhenghe Bai[†], Derong Xu, Penghui Yang, Lin Wang^{*}
National Synchrotron Radiation Laboratory, USTC, Hefei, China

Abstract

In this paper, we propose a new lattice concept of multi-bend achromat (MBA) for designing a diffraction-limited storage ring, which is inspired by the hybrid MBA concept proposed by ESRF EBS and the locally symmetric MBA concept recently proposed by ourselves. In this new MBA concept, two pairs of dispersion bumps are created in each cell, which accommodate sextupoles to correct chromaticities. For each pair of dispersion bumps, from the point of view of two different representations of a cell, many nonlinear effects caused by itself are cancelled out within one cell. For the two pairs of dispersion bumps, from the nonlinear cancellation point of view, they are interleaved. Compared to the hybrid MBA where only one pair of dispersion bumps is created in each cell, this new MBA can provide more knobs so as to better control tune shift terms, which is especially beneficial for enlarging dynamic momentum aperture.

INTRODUCTION

In the recent two years the MAX IV light source has opened the door to the next-generation synchrotron radiation sources, the so-called diffraction-limited storage rings (DLSRs). Today many advanced light sources are being constructed or designed around the world towards lower emittances than MAX IV, even on the order of tens of pm-rad. Following MAX IV, these DLSRs adopt multi-bend achromat (MBA) lattices to reduce the emittance. Lower emittance generally means stronger nonlinear dynamics. For DLSRs with emittances of about one hundred or tens of pm-rad, the nonlinear dynamics is extremely strong, which is a big challenge for lattice designers.

To combat the very serious nonlinear dynamics in DLSRs with even lower emittances, some MBA lattice concepts with different nonlinear cancellation schemes have been proposed. PEP-X proposed a fourth-order geometric achromat MBA concept, in which the nonlinear cancellation was done over some cells. There are many knobs (i.e. families of nonlinear multipoles) in this concept so that tune shift terms and higher-order resonance driving terms can be well controlled. ESRF EBS proposed a hybrid MBA concept [1], in which the nonlinear cancellation was done within one cell that can be more effective than the cancellation over some cells due to interleaved sextupoles. However, it is hard to control tune shift terms in the hybrid MBA concept due to limited knobs. For the APS-U and HEPS lattices that adopt the hybrid MBA concept but have lower emittances than ESRF EBS, the tune shift with momentum is large and half-integer resonance line will be crossed for particles with relative momentum deviation of about 2~3%.

Recently we proposed a locally symmetric MBA (LS-MBA) concept by making the beta functions locally symmetric about two mirror planes in each cell [2], in which the nonlinear cancellation was done within one cell and also many knobs could be used. The LS-MBA concept was applied to the design of Hefei Advanced Light Source (HALS), and the designed lattices with emittances of tens of pm-rad had excellent on- and off-momentum nonlinear dynamics, especially the dynamic momentum aperture being larger than 7% or even 10%.

In this paper, we develop a new MBA concept following the same philosophy as for the LS-MBA, i.e. doing nonlinear cancellation within one cell and having many knobs to be used. In this new MBA concept, the dispersion in the arc section will have several bumps as in the hybrid MBA so as to reduce the strengths of sextupoles. We will first give a description for this new MBA concept and then apply it to the design of HALS.

MBA LATTICE WITH INTERLEAVED DISPERSION BUMPS

In the hybrid MBA one pair of dispersion bumps is created at both ends of the arc section with a separation of $-I$ transformation, which is very effective for nonlinear cancellation and also can reduce the strengths of sextupoles. However, for each cell there can be placed only three families of sextupoles at most in the dispersion bumps. Due to that two knobs have to be used for correcting horizontal and vertical chromaticities, it is very hard to well control tune shifts with amplitude and momentum simultaneously using the other knobs (including one family of octupole). Our idea is to create an additional pair of dispersion bumps in each cell to increase the number of knobs. However, the problem for this idea is how to make a nonlinear cancellation for the additional pair of bumps. Inspired by the LS-MBA of the second kind that we proposed, the nonlinear cancellation for the additional pair of bumps can also be realized within one cell from the point of view of an unusual representation of a cell.

In the usual representation, we can write a cell as $ABBA$, where A represents one half of the long straight section and B one half of the arc section. In an unusual representation, we can also write it as $BAAB$. Using these two representations, we have classified the LS-MBA lattices into two kinds. For the hybrid MBA lattice, the nonlinear cancellation between the pair of two dispersion bumps is referred to using the representation of $ABBA$. For a MBA lattice, like the hybrid MBA lattice, with one pair of dispersion bumps satisfying the condition of nonlinear cancellation, if we create a second pair of dispersion bumps, generally the phase advance between the two bumps of the second pair

[†] baizhe@ustc.edu.cn
^{*} wanglin@ustc.edu.cn

OPTIMIZATION OF CLOSED ORBIT CORRECTION USING ANT COLONY ALGORITHM IN HALS

Derong Xu, Zhenghe Bai, Gangwen Liu, Hongliang Xu*, Lin Wang†
National Synchrotron Radiation Laboratory, USTC, Hefei 230029, China

Abstract

In this paper, we present a method using correctors as few as possible while controlling the residual closed orbit within an acceptable level based on ant colony optimization algorithm instead of the ideal optical properties. We prove that this method works well with HALS.

INTRODUCTION

The Hefei Advanced Light Source (HALS) project [1], as a soft X-ray diffraction limited storage ring (DLSR), was proposed by National Synchrotron Radiation Laboratory with a beam energy around 2.4 GeV and the detailed lattice design is in progress.

To reduce the emittance of a DLSR, multi-bend achromat (MBA) lattices have been adopted. The main method to reduce emittance is to employ many strong quadrupoles which depress dispersion function and introduce chromatic aberrations that must be corrected with strong sextupoles [2]. In our first version lattice, the ring consists of 32 identical 6BAs with a nature emittance of $26.5 \text{ pm} \cdot \text{rad}$ [3]. The strong quadrupoles and sextupoles make the lattice sensitive to closed orbit distortion. Therefore, the closed orbit correction plays an important role in HALS's design.

Ant colony optimization (ACO) is a heuristic technique for optimization that was introduced in the early 1990's [4]. ACO, which is inspired by the ants' foraging behavior, is very suitable for combinatorial optimization problem. A scientific description for ACO algorithm can be found in [5].

In this paper, we develop a method to correct the closed orbit using Rank-based Ant System (RAS) – a variant of ACO [6]. The goal is to apply correctors as few as possible while controlling the residual closed orbit within an acceptable level.

ERROR ESTIMATION AND BPMs LAYOUT OF HALS

The magnet elements of a storage ring can never be placed at their ideal positions. To simulate a real machine, we have to assume a statistical variation of their positions. The orbit distortion is caused by dipole errors which can be produced by bending magnets tilt, bending magnets strength or length error and transverse misalignment of quadrupoles etc. In addition, the orbit at quadrupoles or sextupoles concern with a closed orbit a lot in DLSR. If the closed orbit without correction exceed the vacuum chamber

aperture limits, the orbit correction is impossible. Tracking the closed orbit with elegant [7] for 10,000 seeds, we find that the misalignment should be less than $8 \mu\text{m}$ which is impossible technically. Tab. 1 shows the dipole error in the following simulations.

Table 1: Error Sheet for Magnets. All values are rms, and the truncation is 2σ .

dipole	misalignment	$5 \mu\text{m}$
	rotation error	0.2mrad
	strength error	5×10^{-4}
quadrupole	misalignment	$5 \mu\text{m}$
	strength error	10^{-3}
	multipole error	[8]
sextupole	misalignment	$5 \mu\text{m}$
	strength error	10^{-2}
	multipole error	[8]

Once a closed orbit is established, the position of this closed orbit is measured by a large number of Beam Position Monitors (BPM) and small corrector magnets are used to correct the closed orbit towards the ideal orbit. There are several guidelines to place BPMs along the ring.

- BPMs should be spaced by 90° in phase advance.
- The orbit at light source points should be stable enough. So both sides of radiation elements must be measured by BPMs.
- Maximum position measured by BPMs (MAX-BPM) have to approximately equal to the maximum closed orbit distortion (MAX-COD).
- BPMs are close to the sextupoles. In theory, the dynamic aperture can be restored if the beam pass through the center of the sextupoles.

In accordance with the above principles, we place 17 BPMs per cell in HALS as shown in Fig. 1. We also compare MAX-BPM with the MAX-COD for 10,000 seeds in Fig. 2. From the figure, we know that there is 93% possibility at least when the tolerance is 10%. That is

$$P\left(\left|\frac{u_c - u_b}{u_c}\right| < 10\%\right) > 93\%, \quad (1)$$

where u_c is MAX-COD and u_b is MAX-BPM. So our BPMs system is reasonable that the BPM measured value can reflect the real closed orbit.

ALGORITHM DESCRIPTION

Tab. 2 summarizes all elements contained in the HALS lattice cell. Every drift line is a possible position to place a corrector. Because the last drift is connected to the first line

* hlxu@ustc.edu.cn

† wanglin@ustc.edu.cn

RF EXCITATION PARAMETERS IN RESONANT EXTRACTION*

J. Li[†], Y. J. Yuan, Institute of Modern Physics, CAS, Lanzhou, China

Abstract

Ion beam resonant slow extraction from synchrotron is extensively used in experimental nuclear and particle physics, material radiation science, and deep-seated malignant tumours radiotherapy. In this paper, the ion motion of resonant extraction under RF excitation are discussed. The expression for sweeping frequency waveforms used in tracking code for resonant extraction are presented.

INTRODUCTION

The transverse excitation or RF-Knockout resonant extraction has been developed in the last twenty years as a popular method in slow beam extraction from synchrotron [1]. It also promotes the application of heavy ion radiotherapy due to the advantages of quick response on beam start and cut-off, and simple operation in controlling beam at therapy terminals [1]. The domestic heavy-ion synchrotron in operation e.g., CSRm and HIMM take this method to realize the slow extraction for experimental research and radiotherapy [2].

The process of RF transverse excitation is described as below. During the storage beam being accelerated to the energy for extraction, the betatron tune of synchrotron is adjusted to be closer to the third order resonance and synchronously introduced sextuple fields help to produce three separatrices in phase space and confine the stored beam inside the stable region that is larger than transversal beam emittance. The RF excitation heats the circulating stored beam at horizontal plane, so that the transverse emittance blows up rapid until some ions escape away the stable region along the separatrices and jump into the gap of electrostatic septum for extraction. To suppress the beam loss along the synchrotron, the electrostatic spectrum is required that further limits the dynamics aperture and deflects lost beam away from close orbit for those that jump into the septum gap. The extraction beam intensity is controlled by the RF excitation parameters. This method features fixed stable area in phase space or unchanged sextuple fields and synchrotron lattice parameters during the RF excitation process at extraction plateau. In additional, a orbit bump system upstream the electron spectrum and longitudinal RF capture are helpful to improve the extraction efficiency.

ION MOTION UNDER RF EXCITATION

The ion motion equation under sextuple field and RF transverse excitation is written as:

$$\begin{aligned} X''(\mu) + X(\mu) + \frac{1}{2}\beta_x^{5/2}k_2X^2(\mu) \\ = \beta_x^{3/2}\frac{\beta c}{B\rho}\sum_{n\geq 0}E_x\delta(\mu - 2\pi Q_x m - \mu_k) \end{aligned} \quad (1)$$

in which μ_k and μ are the Betatron phases of RF exciter and ions respectively, Q_x is the horizontal working point, k_2 is the field strength of sextuple, β_x is Twiss parameter, m is any integer greater than 0, $E_x = E_{x0} \sin(2\pi f_k t)$ represents the transverse excitation strength of RF electric field, δ at the right denotes Dirac function. If we replace the variable μ with revolution turn number n , i.e. $d\mu/dn \approx \Delta\mu/1 = 2\pi Q_x$ then equation (1) is rewritten as

$$\begin{aligned} X''(n) + (2\pi Q_x)^2(X(n) + \frac{1}{2}\beta_x^{5/2}k_2X^2(n)) \\ = (2\pi Q_x E_x)\frac{\beta_x^{3/2}\beta c}{B\rho}\sum_{n,m}\cos(2\pi\frac{f_k}{f_{rev}}n)\delta(n-m) \end{aligned} \quad (2)$$

with f_k is the RF excitation frequency, f_{rev} is the revolution frequency of ion beam in synchrotron. The homogeneous solution of equation (2) can be expressed as

$$X(n) = a \cos(2\pi q_x n + b) \quad (3)$$

where q_x is fraction part of the horizontal working point Q_x , a and b represent any constants. The summation part at the right side of equation (2) is further written as

$$\sum_n \cos(2\pi \frac{f_k}{f_{rev}} n)$$

In comparison with the right side of equation (3), we find that the horizontal excitation works only when the RF frequency satisfies the following relationship

$$\frac{f_k}{f_{rev}} = Integer \pm q_x \quad (4)$$

This is required by applying RF excitation to the circulating ion beam.

The betatron amplitude of 10 ions under influence of sextuple and RF excitation is shown in Fig. 1, in which, sextuple field is applied after 500 revolution turns, and RF excitation starts up at the 1000th turn.

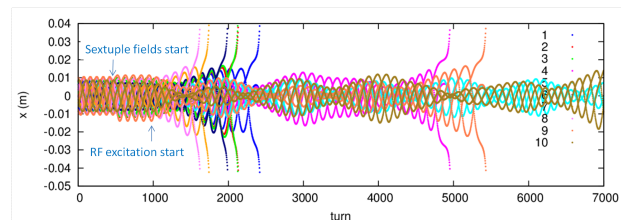


Figure 1: The betatron amplitude under influence of sextuple fields and RF excitation.

Because the betatron tune of ion also depends on momentum spread, betatron amplitude, and the magnetic field deviation and ripple etc., thus the circulated beam has a

* Work supported by NSFC (Grant No. 11475235, 11375245, 11575264)
[†] lijie@impcas.ac.cn

SIMULATION OF BEAM INTENSITY LIMITATIONS UNDER SPACE CHARGE EFFECTS AT BRING OF HIAF *

J. Li[†], J. C. Yang, HIAF design group, Institute of Modern Physics, CAS, Lanzhou, China

Abstract

The booster ring (BRing) of the new approved High Intensity heavy-ion Accelerator Facility (HIAF) in China is designed to stack $^{238}\text{U}^{35+}$ ions at the injection energy of 17MeV/u and deliver $1.0 \cdot 10^{11}$ of uranium ions at 800MeV/u. Two injection modes, with or without the electron cooling, are introduced. The transverse emittance evolution and beam lifetime are investigated by simulation of RF capture process for the fast cycle mode.

INTRODUCTION

HIAF Layout

The High Intensity heavy-ion Accelerator Facility (HIAF) is a new heavy ion accelerator complex under detailed design by Institute of Modern Physics [1]. Two typical particles of uranium and proton is considered in the design. The beam is generated by a Superconducting Electron Cyclotron Resonance (SECR) ion source or an intense proton source, and accelerated mainly by an ion linear accelerator (iLinac) and an booster ring (BRing). The iLinac is designed to deliver H_2^+ at 48 MeV and $^{238}\text{U}^{35+}$ at 17 MeV/u. Before entrancing into the BRing, H_2^+ is stripped to proton, then accumulated by two-plane painting and accelerated to 9.3 GeV. The $^{238}\text{U}^{35+}$ is injected by multi-turn two-plane painting scheme, after accumulation or cooling by an electron cooler at the BRing, then accelerated to 0.2-0.8 GeV/u for extraction. After being stripped at the HIAF FRagment Separator (HFRS), the secondary beam like $^{238}\text{U}^{92+}$ is injected to the Spectrometer Ring (SRing) for the high precision physics experiments. Besides, five external target stations of T1 - T5 is planned for nuclear and atomic experimental researches covering the energy range from 5.8-800 MeV/u for uranium beam. The global layout of the HIAF complex is illustrated in Fig. 1.

Overview of the BRing

The BRing is designed to accumulate beam intensity up to the space charge limit at injection energy and deliver over $1.0 \cdot 10^{11}$ $^{238}\text{U}^{35+}$ ions or $1.0 \cdot 10^{12}$ protons in extraction. Two operation modes of fast and slow are considered. The fast mode feathers multi-turn two-plane painting injection within around 120 revolution turns whereas the slow one by over 10 s injection time for electron cooling helped accumulation. Main parameters of the BRing are listed in Table 1. The BRing has a three-folding symmetry lattice around its circumference of 549.45 m. Each super-period consists of an eight-FODO-like arc and an over 70 m long dispersion-free straight section featured with length of 15.7 m drift reserved

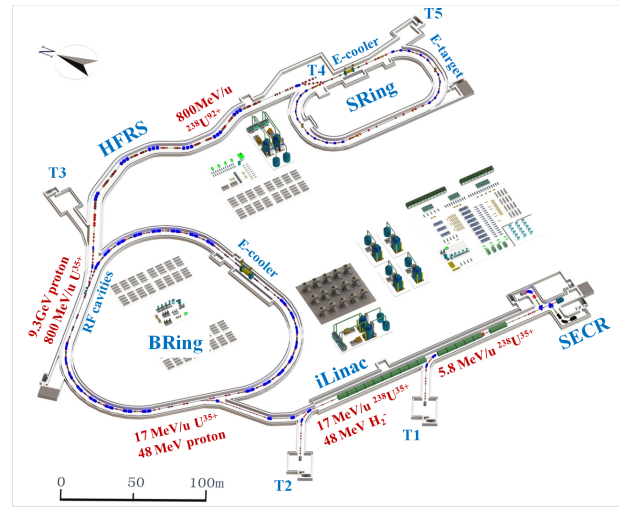


Figure 1: General layout of the HIAF complex.

for electron cooler, two-plane painting injection, or RF cavities. Lattice layout of the BRing for one super-period is shown in Fig. 2.

Table 1: Main Parameters of the BRing

Parameter	Proton	$^{238}\text{U}^{35+}$
Injection energy	48 MeV	17 MeV/u
Injection mode	EX ^a +PT ^b	PT, PT+EC ^c
Betatron tune	-	(8.45,8.43)
Circumference	549.45 m	
Max. magnetic rigidity	34 Tm	
Super-periodicity	3	
Bunching factor	0.2~0.4	
Acceptance ($H/V, \delta p/p$)	200/100 π mmmrad, $\pm 5.0\%$	

^a Charge exchange.

^b Two-plane painting.

^c Electron cooling.

Factors Concerning to Space Charge Effect

Space charge effect induced resonances dominate the limit on beam intensity and density especially at low energy heavy-ion synchrotron. Factors concerning to this effect at the BRing are list below.

Painting Injection Two-plane painting multi-turn injection scheme is adopted to accumulate high intensity beam. The injected storage beam has a momentum spread $\pm 2.0\%$, and horizontal emittance 200 π mmmrad and vertical one of 100 π mmmrad with a quasi-uniform or Gaussian distribution in transverse phase space according to the simulation [2, 3].

* Work supported by NSFC (Grant No. 11475235, 11375245, 11575264)

[†] lijie@impcas.ac.cn

INVESTIGATION ON THE SUPPRESSION OF INTRABEAM SCATTERING IN THE HIGH INTENSITY HEAVY ION BEAM WITH THE HELP OF LONGITUDINAL DOUBLE-BUNCH OF ELECTRON*

X. D. Yang[†], L. J. Mao, J. Li, X. M. Ma, T. L. Yan, M. T. Tang, H. Zhao, G. H. Li
Institute of Modern Physics, CAS, Lanzhou, China

Abstract

Intrabeam scattering is the main reason of degradation of the beam brightness and shortening of brightness lifetime in the collider, light source and storage ring. The intrabeam scattering presents dissimilar influence in the different facilities. Electron cooling was chosen to suppress the effect of intrabeam scattering and another unexpected effect happened during the cooling. The distribution of ion beam quickly deviates from the initial Gaussian type, then form a denser core and long tail. The ions standing in the tail of beam will loss soon owing to large amplitude. This solution will focus on the investigation on the suppression of intrabeam scattering in the high intensity heavy ion beam in the storage ring with the help of longitudinally modulated electron beam. The stronger cooling was expected in the tail of ion beam and the weaker cooling was performed in the tail of ion beam. The particle outside will experience stronger cooling and will be driven back into the centre of ion beam during which the ion loss will decrease and the lifetime will increase. The intensity of ion beam in the storage ring will be kept and maintain for a long time.

INTRODUCTION

This solution will focus on the investigation on the suppression of intrabeam scattering in the high intensity heavy ion beam in the storage ring with the help of longitudinally modulated electron beam. The traditional DC electron beam in the electron cooler was modulated into electron bunch with different longitudinal distribution. The stronger cooling was expected in the tail of ion beam and the weaker cooling was performed in the tail of ion beam. The particle outside will experience stronger cooling and will be driven back into the centre of ion beam. The ion loss will lessen and the lifetime will be increased. The intensity of ion beam in the storage ring will be kept and maintain for a long time. Two functions will be combined into one electron cooler. The more short pulse, the more high intensity and more low emittance heavy ion beam was expected in the cooler storage ring. In the future, these results of this project will be constructive to the upgrade and improvement for existing machine and also be helpful to the design and operation for future storage and high energy electron cooler.

SOME CONSIDERATIONS

The final equilibrium transverse emittance and longitu-

* Work supported by The National Natural Science Foundation of China, NSFC (Grant No. 11375245, 11475235, 11575264)

[†] yangxd@impcas.ac.cn

dinal momentum spread were determined by the cooling effect and intra-beam scattering heating effect together in the case of fixed ion energy and particle number. If we want to get more particle number, in other words, more intensive ion beam, a new parameters configuration will be necessary in the new equilibrium state. In the absence of electron cooling, the transverse ion beam will be blown-up due to not suppression intra-beam scattering effect. The transverse dimension and longitudinal length of ion beam will increase with time, as a result, some ion will loss and the lifetime of ion beam will become short.

LIFETIME AND INTENSITY OF ION BEAM

The ion beam of $^{238}\text{U}^{92+}$ with population $1 \cdot 10^{11}$ particle was required in the high energy high intensity accelerator facility [1]. In this situation, the final emittance and momentum spread were the key parameters which the physics experiments concerned, more important parameters of ion beam were lifetime and the ion number in the detectors.

MOTIVATION

Two essential questions should be certainly answered and clearly described in advance.

The first question concerned by physics experiment is that whether enough particle [2] be provided to the experiments terminals.

The second one concerned the lifetime [3] of the ion beam with so high intensity whether enough to satisfy the requirements of physics experiments, because it determines the efficiency of experiments.

NEW SOLUTION PROPOSED

There are three points in this solution. The first point, the intensity of electron bunch presents certain distribution according to the ion bunch distribution in the longitudinal direction. The second point, the electron bunch distribution will change actively according to the ion beam distribution in the cooling process. As a result, the electron beam will provide different strength cooling in the different periods. The third point, the transverse intensity distribution can change also, the electron beam can present different transverse distribution according to the transverse distribution of ion beam in the cooling process. The purpose of this solution will aim to suppress the effect of IBS, increase the lifetime of ion beam and reduce the ion loss during cooling [4].

SIMULATION OF ELECTRON COOLING ON BUNCHED ION BEAM

H. Zhao¹, L. J. Mao[†], X. D. Yang, J. C. Yang, J. Li, M. T. Tang,
 Institute of Modern Physics, Chinese Academy of Sciences, Lanzhou, China
¹also at University of Chinese Academy of Sciences, Beijing, China

Abstract

A combination of electron cooling and RF system is an effective method to compress the beam bunch length in storage rings. A simulation code based on multi-particle tracking was developed to calculate the bunched ion beam cooling process, in which the electron cooling, Intra-Beam Scattering (IBS), ion beam space charge field, transverse and synchrotron motion are considered. In the paper, the cooling process was simulated for C beam in HIRFL-CSRm, and the result was compared with experiments, according to which the dependence of the minimum bunch length on beam and machine parameters was studied in the paper.

INTRODUCTION

Electron cooling is a powerful method for shrinking the size, the divergence and the momentum spread of stored charged-particle beams in storage rings for precision experiments [1]. It also supports beam manipulations involving RF system to provide beams with short bunch length. Short-bunched ion beam has a wide range of application in rare isotope production, high energy density physics experiment, collider and cancer therapy [2]. In order to study the cooling process of bunched ion beam, a simulation code was developed, in which the electron cooling, IBS and space charge effect are considered, and simulation of electron cooling with a sinusoidal wave RF field were carried out in CSRm under various intensities of cooled 6.9 MeV/u C⁶⁺ ion beams. The simulation results have also compared with the experiment in CSRm. The simulation results show a good agreement with the experiment. Meanwhile, the investigation about the limitation of the bunch length is give in the paper.

SIMULATION CODE

The simulation code is developed based on multi-particle tracking, in which the ion beam is represented by a number of model particles and the beam dynamics is calculated by statistical method. In the code, a certain number of charged particles are generated according to the initial beam emittance, momentum spread and bunch length. Particularly, it assumes that the initial ion beam distribution is Gaussian in transverse and longitudinal. Each particle is presented as a six-coordinate vector: $(x, x', z, z', \varphi, \Delta v)$, where x and z are the horizontal and vertical coordinates, x' and z' are the corresponding angles in horizontal and vertical, φ is the phase angle with respect to the ring, and

Δv is the relative velocity of particle in Laboratory Reference Frame (LRF). For each turn, the coordinate of model particle will be tracked and the beam dynamics is based on the synchrotron and transverse motion [3].

The calculation of electron cooling is based upon the energy exchange between ions and electrons, which can be described in terms of a velocity-dependent friction force. In the simulation, the Parkhomchuk force formula was used to calculate the friction force on each particle at Particle Reference Frame (PRF) [4]. Additionally, the longitudinal velocities of electrons at a certain radius due to space charge effect should be corrected by

$$\frac{\Delta V_e}{V_e} = \frac{I_e}{4\pi\epsilon_0\beta^3\gamma^3 c} \frac{e}{m_e c^2} \frac{r^2}{r_b^2} \quad (1)$$

where ϵ_0 is the vacuum permittivity, I_e is the electron beam current, β, γ and c are Lorentz factors and r_b the radius of electron beam.

On the other hand, the heating effects which can induce beam blows up should be analysed seriously. However, the IBS effect is the most important effect, which is a multiple Coulomb interaction of the charged particles within the beam. In the code, the Martini IBS model was applied in the calculation, in which the growth rates are calculated from a complicated integration that connected the 6-dimensional phase space density of the beam with the optics of the storage ring [5].

The ion beam density will increase as it was cooling down, during which the space charge effect becomes much stronger to prevent the cooling effect on bunch length and beam profile accordingly. In the code, the space charge effect is considered only in longitudinal and this effect is represented by a potential applying to particles which is similar to the RF voltage, the space charge potential is given by [6].

$$V_{SC} = \frac{gh^2}{2R\epsilon_0\gamma^2} \frac{d\rho(\phi)}{d\phi} \quad (2)$$

in which ρ is the linear charge density of ion beam, h is the harmonic number, R the radius of the ring. The geometric factor $g=1+2\ln(b/a)$ depends on the radio of beam radius a to pipe radius b . The change of particle velocity caused by the space charge potential together with the RF voltage for each turn is applied based on the synchrotron motion.

[†] maolijun@impcas.ac.cn

RADIATION EFFECTS STUDY FOR BEAM LOSSES ON THE ELECTRO-STATIC DEFLECTOR IN HUST SCC250

S. W. Hu, K. J. Fan[†]

Institute of Applied Electromagnetic Engineering, Huazhong University of Science and Technology, Wuhan, China

Abstract

China has paid comprehensive attention to the study of proton therapy in recent years. Radiation effects induced by beam losses in compact, high energy superconducting cyclotrons are being taken into crucial considerations. The proton beam is extracted out of HUST SCC250 superconducting cyclotron by electrostatic deflectors. The fierce impinging between proton beam and the deflector septum is the main cause of beam losses, which will bring about radiation effects leading to activations in devices and coil quenching. This paper presents the simulation result of radiation effects between beam and septum by utilizing Geant4 code based on Monte Carlo method. The energy deposition of beam losses is figured. Meanwhile, the yields and energy distributions of secondary particles are investigated. The result focused on radiation effects will provide us with valuable implications for the design of this superconducting cyclotron.

INTRODUCTION

HUST SCC250, being developed for/at Huazhong University of Science and Technology, is a superconducting cyclotron applied for proton therapy. The extracted proton beam is expected to be 250MeV and the beam current is about 800nA. The electrostatic deflector in this cyclotron is the research subject of this paper, whose structure has been introduced in [1]. In real operation conditions, the deflector undergoes intense interactions with beam that will directly influence the beam quality and extraction efficiency. These interactions subsequently trigger severe cooling problem and radiation effects affecting the operating performance of the cyclotron. The cooling problem has been discussed in [1], then the radiation effects will be studied in this paper.

Radiation effects mainly exerts considerable influences on the operation of superconducting cyclotron from the following two aspects: the nuclear heating of the cryogenic magnet and radiation damage or activation of certain materials [2]. To gain a deeper insight into radiation effects, Geant4 toolkit has been used to simulate the radiation with the septum after impacted by proton beam. The energy deposition and secondary particles have been analysed which gives a reference to the future study and configuration of the cyclotron.

This paper is structured as follows: Section 2 introduces details on the simulation model and parameters employed in Geant4 toolkit, Section 3 presents results and discussion and then the conclusion is proposed in Section 4.

[†] kjfan@hust.edu.cn

MATERIAL AND METHODS

Geant4 Toolkit

Geant4 is a software toolkit for the simulation of the passage of particles through matter [3]. It is applied in a variety of domains including high energy physics, space applications, medical physics and radiation shielding. Geant4 code, which is written in C++ programming language, earns much favour from a large number of researchers whereby its abundant particle data libraries and open-source capability. Since plenty of examples adapted to various occasions contains in Geant4 data package, the users can modify the example codes as they need to satisfy their applications. Moreover, self-defining simulation models and physics lists give users much more setting options.

It is noted that Geant4 10.1.2 edition is employed in this study and the application platform is Win10 x64 system.

Incident Beam Properties

As the proton beam is propagated down the +Z axis into the deflector, its transverse motion can be represented by two ellipses in the phase spaces [4] (X, X_p) and (Y, Y_p) , where $X_p = P_x/P_z$, $Y_p = P_y/P_z$, represent respectively the beam angular divergences θ and φ , and P_x, P_y, P_z stand for the three components of the beam momentum. The phase ellipse is defined with Twiss parameters and beam emittance. The beam emittance is 1mm·mrad. Twiss parameters taken from beam dynamics calculation are tabulated in Table 1

Table 1: Margin Specifications

X planar	Y planar
$\alpha_x = -0.533862$	$\alpha_y = 0.219913$
$\beta_x = 1.303566$	$\beta_y = 0.668318$
$\gamma_x = 0.985764$	$\gamma_y = -1.568657$

Subsequently, the respective phase ellipse in X, Y directions and the beam profile in X-Y cross-section are plotted in Figure 1.

It is noteworthy to mention that Geant4 code package doesn't contain beam phase ellipse defining class so that users can only achieve this by employing mathematic manipulation. To define the phase space, the users should specify the four variables X, Y, X_p , Y_p into random Gaussian distribution respectively. Geant4 code provides the function--SetParticleMomentumDirection() for users to set the momentum direction of particles. The proton beam energy in our study is set to be monoenergetic 250 MeV.

Content from this work may be used under the terms of the CC BY 3.0 licence (© 2017). Any distribution of this work must maintain attribution to the author(s), title of the work, publisher, and DOI.

PRIMARY DESIGN OF 4 A S-BAND LINAC USING SLOTTED IRIS STRUCTURE FOR HOM DAMPING*

J. Pang[†], S. Chen, X. He, IFP, CAEP, Mianyang, China
 S. Pei, H. Shi, J. Zhang, IHEP, Beijing, China

Abstract

A S-band LINAC with the operating frequency of 2856MHz and beam current of 4 A was designed for flash X-ray radiography for hydrodynamic test. The optimization of the parameters of the LINAC was processed to achieve the minimum beam radius and the proper energy efficiency. For the purpose of reducing the beam orbits offset at the exit of LINAC, a slotted iris accelerating structure would be employed to suppress the transverse Higher Order Modes (HOMs) by cutting four radial slots in the iris to couple the HOMs to SiC loads. In this paper, we present the design of the LINAC and the results of beam dynamic analysis.

INTRODUCTION

Linear induction accelerators were used in large-size or full-size radiographic hydrodynamic test with dose of hundreds of Rad by accelerating several-kA electron beam to tens of MeV. In addition, small machine, such as pulsed X-ray machine with several hundreds kV and anode-pinch diode, was used in small-size hydrodynamic subdivision experiments for dynamic material characteristic study, micro jetting diagnosis, et al.

In the past twenty years, intense-beam normal conducting RF accelerator has been developed with great achievement due to the development of large collider technology. The CLIC Test Facility, CTF3, has accelerated the beam with current of up to 5A to 150MeV with full beam loading [1-2]. The HOM was damped by using slotted iris constant aperture (SICA) accelerating structures. The 100MeV/100kW linac, constructed by IHEP and used as a driver of a neutron source in KIPT, Ukraine, has accelerated a beam of 2A to 100MeV by using detuning accelerating tubes [3-5].

The great progress in intense-beam linac motivates the compact radiographic facility driven by a 4A 30MeV linac, which might be utilized for multi-pulse radiographic with the material planar density of several to tens g/cm². The most considered parameter, FWHM of transverse distribution of electron beam, should be limited less than 1 mm. A radiographic system has been discussed before [6]. The Monte Carlo codes, Geant4, has been used to simulate bremsstrahlung characteristic, such as exposure dose, energy deposit in target and increment of X-ray spot size by electron scatter, with 30 MeV electron beams bombarding tantalum target with various thickness in a certain radiography layout. Simulation results showed that the exposure dose 1 m away from the target right

ahead was about 9.1 R and the X-ray spot sizes were not increased with the increment of the thickness of target material. The results also shown that pulse number was limited by temperature rise in target, which was increased intensely with a very tiny beam transverse size.

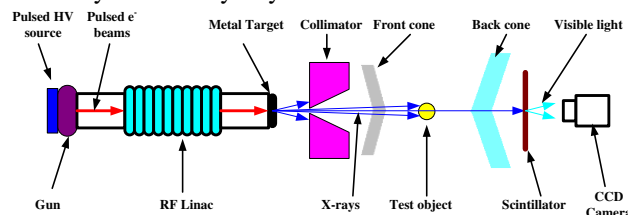


Figure 1: Layout of a typical flash X-ray radiography system using RF accelerator.

In this paper, the design of accelerator was described. A beam dynamic analysis was carried out with the primary design of the accelerating structure. BBU effect calculation was also carried out.

GENERAL DESCRIPTION OF THE ACCELERATOR

Layout of the accelerator, which consists of a DC gun, 3 accelerating tube, a chicane and matching beam line, was shown in Fig. 2. The total length is about 14m and could be reduced by farther optimization. Table 1 lists main parameters.

Table 1: Main Linac Parameters

Parameter	Value
RF frequency	2856MHz
Energy	>30MeV
Beam current (max)	4A
Energy spread (FWHM)	<1%
Emittance (RMS)	<50mm mrad
Beam pulse length	100ns
Number of pulses in a train	4-8
RF pulse duration	10μs
Pulse repetition rate	10Hz
Klystron power	65MW
Number of klystron	3
Number of ACC. structure	3
Gun voltage	~120 kV
Gun beam current	10A

ACCELERATING STRUCTURE

The goal of the design of accelerating structure is to achieve a high RF-beam power efficiency with short length as much as possible. Two type of structure was considered: the conventional disk-load structure and

* Work supported by Key Laboratory of Pulsed Power, CAEP (Contract NO. PPLF2014PZ05) and Key Laboratory of Particle Acceleration Physics & Technology, IHEP, CAS (Contract Y5294109T2D)

[†] email address j pang@caep.cn

STUDIES ON THE S-BAND BUNCHING SYSTEM WITH THE HYBRID ACCELERATING STRUCTURE*

S. Pei[†], B. Gao, Key Laboratory of Particle Acceleration Physics & Technology, Institute of High Energy Physics, Chinese Academy of Sciences, Beijing, China

Abstract

A standard bunching system is usually composed of a SW PB, a TW B and a standard accelerating structure. In the industrial area, the bunching system is usually simplified by eliminating the PB and integrating the B and the standard accelerating structure together to form a β -varied accelerating structure. The bunching efficiency for this kind of simplified system is lower than that for the standard one. The HB has been proved to be an innovative attempt to reduce the cost but preserve the beam quality as much as possible. Here, the HAS is proposed by integrating the PB, the B and the standard accelerating structure together to exclusively simplify the standard bunching system. Compared to the standard bunching system, the one with the HAS is more compact, and the cost is lowered to the largest extent without fairly degrading the beam performance. The proposed HAS can be widely applied in the industrial area.

INTRODUCTION

Generally, a standard bunching system is composed of a standing wave (SW) pre-buncher (PB), a travelling wave (TW) buncher (B) and a standard accelerating structure; all of them operate at the same radio frequency (RF) and are powered by one single klystron. However, for various reasons and different applications, the bunching system can be complicated or simplified. The complicated bunching system is always happened in the scientific area, and it is usually accompanied with better beam performance and higher construction cost. One typical example is the BEPCII sub-harmonic bunching system. Two sub-harmonic bunchers (SHB) were used to replace the PB [1]. In the industrial area, the usual way to simplify the bunching system and lower the cost is to eliminate the PB and integrate the B and the standard accelerating structure together to form a β -varied accelerating structure. However, the bunching efficiency will be lowered.

The hybrid buncher (HB) has been proved to be an innovative attempt to reduce the bunching system construction cost [2-4], and it is a combined structure of the PB and the B. Using the HB to replace the PB and B can simplify the bunching system to certain extent but not exclusively, it has been proved that the beam performance can be preserved as much as possible [4]. In this scenario, further simplification of the standard bunching system by integrating the PB, the B and the standard structure to form a hybrid accelerating structure (HAS) is proposed. It is worth to note that this paper focuses on the simplification studies of the standard bunching system operating at one single S-band

frequency (2856 MHz). The bunching system with the β -varied structure was studied first, and then that with the HAS was investigated.

BUNCHING SYSTEM LAYOUTS

Figure 1 shows the layouts of the standard bunching system applied in the linac of the NSC KIPT (National Science Center, Kharkov Institute of Physics and Technology, Ukraine) [5], the bunching system with the β -varied structure and that with the HAS. For both the simplified bunching systems, although the total linac length for S-band can only be shortened by several to twenty centimeters, but all the RF devices connected with the PB and B can be completely removed, this is more exclusive than the one with the HB [4]. Simplifying the bunching system with the HAS can lower the construction cost, facilitate the mechanical design and the tunnel installation, and less parameters need to be adjusted in the beam tuning process, while relatively accurate HAS design is needed, which depends on the gun emitted beam energy.

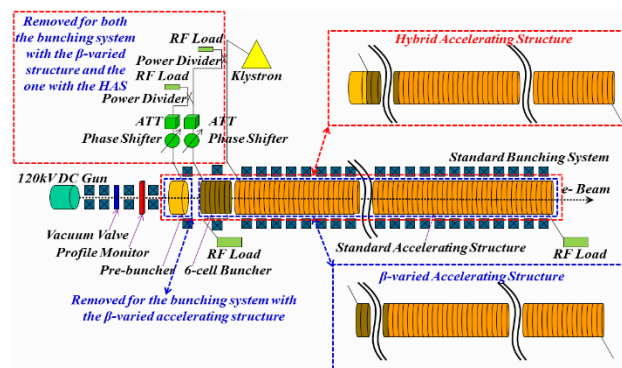


Figure 1: The bunching system layouts.

To easily compare the beam performance, the bunching system with the HAS was introduced into the KIPT linac [5] to replace the standard one. EGUN [6] and PARMELA [7] were used for the beam dynamics study. The RF power fed into the bunching system was all fixed to be 14.4 MW. The solenoid field distribution along the bunching system and the parameter setup for the chicane system were also adjusted to get the best beam quality at both the bunching system and the linac exits. At the bunching system exit, the higher the efficiency the better, and the energy spectrum should also be appropriate for the collimation process realized by a chicane system with a collimator deployed [8]. For the collimated beam, the RF phase for each accelerating structure downstream the chicane was optimized to minimize the energy spread at the linac end. At the linac exit, the more the particles within $\pm 4\%$ peak-to-peak (p-to-p) energy spread the better. This is demanded by the energy

* Work supported by the National Natural Science Foundation of China (11475201) and the Youth Innovation Promotion Association of Chinese Academy of Sciences, China.

[†] email address: peisl@ihep.ac.cn.

ELECTROMAGNETIC AND MECHANICAL DESIGN OF HIGH GRADIENT S-BAND ACCELERATING STRUCTURE IN TTX

Cao Dezhi^{1†}, Shi Jiaru¹, Zha Hao¹, Du Yingchao¹,
 Tang Chuanxiang¹, Huang Wenhui¹, Chen Huaibi¹, Wei Gai²

Department of Engineering Physics, Tsinghua University, Beijing, China

¹also at Key Laboratory of Particle and Radiation Imaging of Ministry of Education,
 Tsinghua University, Beijing, China

²also at High Energy Physics Division, Argonne National Laboratory, USA

Abstract

Thomson scattering x-ray source is an essential scientific platform and research tool in x-ray imaging technology for various fields. Upgrading plan that replacing the 3-meter S-band old linac with shorter high-gradient structure in Tsinghua Thomson scattering X-ray source (TTX) is undergoing so far, aiming to enhance accelerating gradient from 15 MV/m to 30 MV/m. Detailed parameters of couplers and electromagnetic simulation results of whole acceleration structure are presented in this paper. Finally, mechanical structure and further upgrading research on energy with X-band structures are also discussed.

INTRODUCTION

The Advanced X-ray sources, including X-ray free-electron-lasers facilities and Thomson scattering facilities, are widely used in molecular biology and material sciences research area. In Tsinghua University, we have built the compact Thomson x-ray scattering source, which is specialized in hard x-ray generating in china firstly [1]. The current beam line layout of TTX is presented in Fig. 1 (a).

In the latest proposal, we are planning to add two X-band accelerating structures and replace the S-band travelling wave (TW) tube with a shorter one in 1.5-meter, maintaining high-energy x-ray photos generation meanwhile. The layout of beam line after the upgrading is showed in Fig. 1(b).

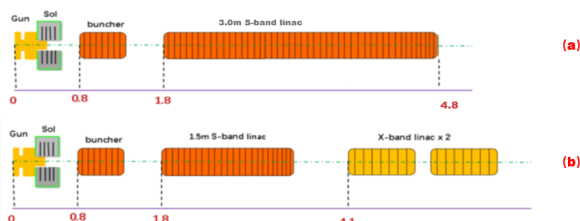


Figure 1: Present linac layout and upgrade proposal.

In the new acceleration structure, we have adopted the constant gradient design in chambers to achieve a higher acceleration gradient as well as a shorter distance. The S-band TW tube are supposed to working in $3\pi/4$ mode through electromagnetic simulation. The method and the concrete parameters of the design of the cavity structure has been demonstrated previously [2-3]. The following

section we will present input/output couplers design parameters and the whole integrated structure with acceleration chambers. The completely electromagnetic structure and mechanical structure of the S-band TW tube are also showed here.

ELECTROMAGNETIC DESIGN

Completely single-cell design procedure of S-band TW tube has finished [2]. Continuous feedback brings adjustments dynamically between the electromagnetic design and realistic mechanical manufacturing procedure.

The simulated parameters of S-band TW tube without couplers are updated in Table 1.

Table 1: Completely Parameters of S-band TW Tube

Parameters	Value
Frequency	2856.00 MHz
Phase advance per cell	$3\pi/4$
Length	1.456 m
Cell numbers	37
Period	39.36 mm
Iris half aperture	10.22 mm~8.13 mm
Cell radius	42.53 mm~42.17 mm
Elliptical iris long axis	9.54 mm
Elliptical iris thickness	5.3 mm
Filling time	999 ns
Group velocity (v_g/c)	0.00724~0.00302
Shunt impedance	66.2 MΩ/m~72.0 MΩ/m
Input power	30 MW
Gradient	31.5 MV/m~29.9 MV/m

Separate design process of dual-feed coupler was simulated in working frequency of 2856MHz to match the chambers as microwave input/output port.

Coupler Design

The input and output couplers have been designed in order to implement the power feeding into structure. Dual-feed coupler structure and its separated model with four cells are showed in Fig. 2 [4]. One fourth of side coupler are showed in Fig.3 [4].

[†] cdz16@mails.tsinghua.edu.cn

DEVELOPMENT OF LLRF SYSTEM FOR TSINGHUA X-BAND HIGH POWER TEST FACILITY

M. Peng[†], J. Shi^{*}, P. Wang, Department of Engineering Physics,
 Tsinghua University, Beijing, China

also at Key Laboratory of Particle & Radiation Imaging, Tsinghua University,
 Ministry of Education, Beijing, China

Z. Sun, D. Zhang, HZCY Technologies Co., Ltd., Beijing, China

Abstract

Tsinghua X-band high power test stand is under construction. A new LLRF system based on the original S-band LLRF system has been designed and tested. A 1 U chassis called X-Adapter was constructed, which has the ability of up-converting and down-converting the signals between 2.856 GHz and 11.424 GHz. The goal of the LLRF system development is to modulate and measure the phase and amplitude of the RF signals. The test results are presented and analysed.

INTRODUCTION

Tsinghua has been preparing for a high power test stand based on the 50 MW klystron. The 50 MW CPI klystron and ScandiNova modulator will be installed in this September, and then are the waveguides, cooling system, and RF load. Some tests of RF components and high power experiments are under planning. To do these experiments, one or more amplitude and phase tunable RF signals are required.

There are basically two ways to approach this goal. One is to quadruple the frequency of the 2856 MHz signal directly to 11.424 GHz. The other one is to triple the 2856 MHz signal and then multiply it with the original one. The first method has been tested on CERN's Xbox 2 [1]. Since the limited input power range of quadrupler, the output power of 11.424 GHz can only vary in a very small range, which is not suitable for some RF tests. So we chose the second way.

All the components used in the X-Adapter are small in size. So this adapter can be packaged in an individual 1 U chassis or assembled with the S-band LLRF chassis by adding 1 U in height. For preliminary research on the feasibility of the X-Adapter, we packaged the RF circuits on a plate. The test results show that the X-Adapter can generate RF signal with modulated phase or amplitude, which is enough for the experiments of the high power test stand in the early stage. More functions of the X-Adapter will be added in the future.

SCHEMATIC DESIGN

The signal flow of the X-Adapter is shown in Fig. 1. The whole adapter has at most seven connectors, three S-band input signals for three phase and amplitude modulated X-

band outputs, one X-band input signal for S-band output to be measured in S-band LLRF.

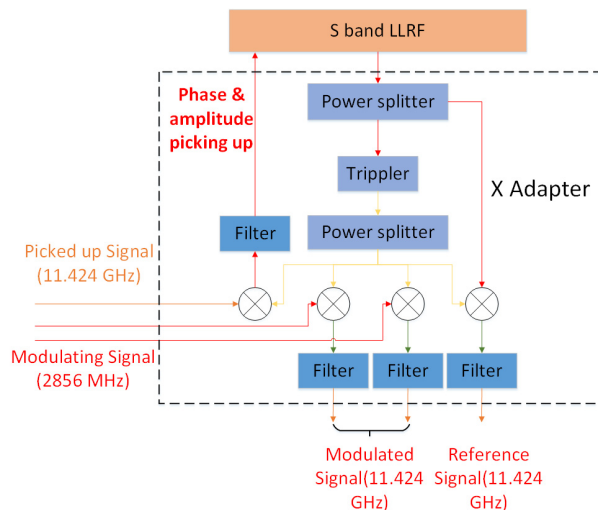


Figure 1: Schematic diagram of the X-Adapter.

Generation of RF Signal

The generation of X-band signal is achieved by the up conversion of S-band RF signal. A prerequisite signal $\cos(\omega_0 t + \varphi_0)$ from S-band LLRF, named input reference signal, first split into two same one by the power splitter. One of them then becomes $\cos(3\omega_0 t + 3\varphi_0)$ after the Tripler, as the LO of the four frequency mixers, the other one becomes the IF of one frequency mixer. It is obvious that the RF of this frequency mixer is $\cos(\omega_0 t + \varphi_0) \times \cos(3\omega_0 t + 3\varphi_0) = \frac{1}{2} [\cos 4(\omega_0 t + \varphi_0) + \cos 2(\omega_0 t + \varphi_0)]$. At the output of the filter, we have the reference X-band RF signal $\cos 4(\omega_0 t + \varphi_0)$, named output reference signal. The phase and amplitude of the reference signal is only depending on the input reference signal of S-band LLRF.

Two alternative modulated X-band signals are provided by inputting modulating S-band signals. For modulating signal $A\cos(\omega_0 t + \varphi_1)$, the modulated X-band signal is $\frac{1}{2} A\cos(4\omega_0 t + \varphi_0 + \varphi_1)$ after frequency the mixer and filter. The input S band signals and output X band signals are called modulating signal and modulated signal. The relative phase and amplitude of the modulated signals are alterable by changing A and φ_0 .

[†] pmm15@mails.tsinghua.edu.cn
^{*} shij@tsinghua.edu.cn

CEPC LINAC DESIGN AND ERROR STUDY*

C. Meng[†], Y. Chi, X. Li, G. Pei, S. Pei, D. Wang, J. Zhang
 Institute of High Energy Physics, Beijing, China

Abstract

Circular Electron-Positron Collider (CEPC) is a 100 km ring $e^+ e^-$ collider for a Higgs factory, including the double ring for collider and the injector. The injector is composed of the linac and booster. The linac of CEPC is a normal conducting S-band linac with frequency in 2856.75 MHz and provide electron and positron beam at an energy up to 10 GeV with bunch charge in 1.0 nC and repetition frequency in 100 Hz. The linac scheme will be detailed discussed. The beam dynamic results with short-range Wakefields and detailed error study including misalignment errors and field errors also be presented.

INTRODUCTION

With the discovery of the Higgs particle at the Large Hadron Collider at CERN in July 2012, further re-search and measurement in Higgs is very important for particle physics. In September 2012, Chinese scientists proposed a Circular Electron Positron Collider (CEPC) in China at 240 GeV centre of mass for Higgs studies [1]. It could later be used to host a Super proton proton Collider (SppC) in the future as a machine for new physics and discovery. After that a great effort have been made in parameter choice and physics design [2][3]. With the deep study and more consideration in CEPC the scheme has several versions compared with the pre-CDR [4]. The latest scheme has some updates, the baseline design of main ring is double ring with circumference 100 km and the linac energy is 10 GeV and also some more detailed optimizations.

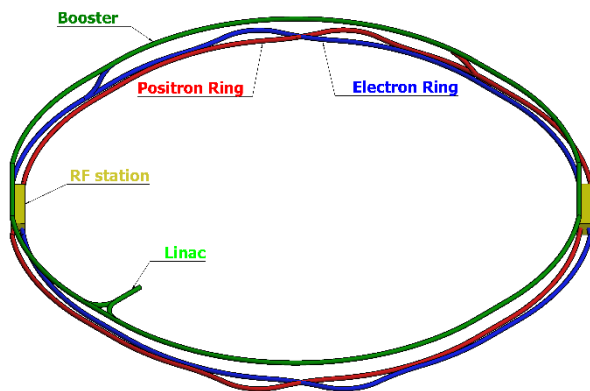


Figure 1: Layout of CEPC.

CEPC is composed of double ring for collider and the injector including linac and booster. The Booster provides

120 GeV electron and positron beams to the CEPC collider and is installed above the collider in the same tunnel, which is shown in Fig.1. Considering the very low magnetic field at the injection of booster, one pre-booster with energy in 45 GeV given consideration to Z study have been proposed.

The first part of the injector is a normal conducting S-band linac with frequency in 2856.75 MHz and provide electron and positron beam at an energy up to 10 GeV. The main parameters are shown in Table 1. With the study of CEPC booster and injection scheme, one-bunch-per-pulse mode is considered and the bunch charge is decreased to 1.0 nC from 3.2 nC at pre-CDR, however we also keep the ability to provide a 3.2 nC bunch beam by now. In the baseline design a 4 GeV primary electron beam with bunch charge in 10 nC hit a tungsten target to obtain a 3.2 nC positron beam.

Table 1: Main Parameters of CEPC Linac

Parameter	Unit	Value
e^- / e^+ beam energy	GeV	10
Repetition rate	Hz	100
e^- / e^+ bunch population	nC	1.0
Energy spread (e^- / e^+)		$< 2 \times 10^{-3}$
Emittance (e^- / e^+)	mm-mrad	< 0.3
e^- beam energy on Target	GeV	4
e^- bunch charge on Target	nC	10

Based on a lot of discussions of linac scheme, we choose the linear scheme as the baseline design, which is shown in Fig.2 and composed of electron source and bunching system (ESBS), the first accelerating section (FAS) where electron beam is accelerated to 4 GeV, positron source and pre-accelerating section (PSPAS) where positron beam is accelerated to 200 MeV, and the second accelerating section (SAS) where electron and positron beam are accelerated to 10 GeV. The electron bypass method, electron transport line bypass or target bypass, have not yet been determined. The beam dynamics will be presented. The errors study has been considered carefully, including the misalignment errors of magnets and accelerating tubes, correction scheme, filed errors and accelerating gradient errors of accelerating tube.

* Work supported by National Key Programme for S&T Research and Development (Grant NO.: 2016YFA0400400) and National Natural Science Foundation of China (NO. 11505198)

[†] mengc@ihep.ac.cn

Content from this work may be used under the terms of the CC BY 3.0 licence (© 2017). Any distribution of this work must maintain attribution to the author(s), title of the work, publisher, and DOI.

DESIGN STUDIES ON AN S-BAND HYBRID ACCELERATING STRUCTURE*

B. Gao†, S. Pei, Y. Chi, Key Laboratory of Particle Acceleration Physics and Technology, Institute of High Energy Physics, Chinese Academy of Science, Beijing, China

Abstract

In an electron linac, the composition of the bunching system is determined by the synthetical consideration of the beam performance and the construction cost. In the industrial area, the bunching system is usually simplified to reduce the construction cost by eliminating the PB and integrating the B and the standard accelerating structure to form the β -varied structure. The bunching performance for this kind of system is relatively worse than that for the standard one. To keep the beam performance of the standard bunching system and reduce the construction cost as much as possible, the HAS is proposed by integrating the PB, the B and the standard TW accelerating structure together. The HAS can be widely applied in the industrial area to enhance the beam performance of the industrial linac but not increase the cost. In this paper, the design studies on an S-band (2856 MHz) HAS is presented. The HAS studied here is composed of 2 SW cells, 40 TW cells and 2 coupler cells. The on-axis electric field amplitude distribution simulated by HFSS can fully meet the beam dynamics requirement.

INTRODUCTION

The standard bunching system consists of a standing wave (SW) prebuncher (PB), a traveling wave (TW) buncher (B) and a TW accelerating structure in an electron liner accelerator. Inspired by the ingenious idea of the hybrid photo-injector developed by the INFN-LNF/UCLA/ SAPIENZA collaboration [1], we successfully built the hybrid buncher (HB) [2]. It has been proved that the HB is an innovative attempt to reduce the construction cost of the standard bunching system but preserve the beam quality as much as possible [3]. In this scenario, to exclusively simplify the standard bunching system, the hybrid accelerating structure (HAS) shown in Fig. 1 is proposed by integrating the PB, the B and the standard accelerating structure together [4]. Compared to the standard bunching system, the one with the HAS is more compact, and the cost is lowered to the largest extent without fairly degrading the beam performance.

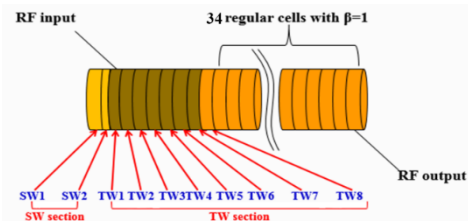


Figure 1: The schematic layout of the HAS.

Supported by the National Natural Science Foundation of China and the Youth Innovation Promotion Association of Chinese Academy of Sciences, China, we are building an S-band (2856 MHz) HAS prototype. The HAS prototype is composed of 2 SW cells, 40 TW cells and 2 coupler cells. The 2 SW cells operate at $\pi/2$ mode, while the 40 TW cells operate at $2\pi/3$ mode. The SW section of the HAS is generally the same as that of the HB [2, 3], while the iris apertures between the SW cells and the input RF coupler cell need to be adjusted carefully to obtain the appropriate field distribution. Beam dynamics study on the bunching system with the HAS has been done, it is shown that the HAS bunching system can keep the beam performance of the standard one as much as possible [4].

In this paper, the RF design of the HAS prototype is presented. Initially, 2D code SUPERFISH [5] was used to determine the dimensions of all the cells. Secondly, 3D code HFSS [6] was used to optimize the input and output RF coupler cells. Finally, the on-axis RF field distribution of the whole HAS prototype was calculated, which can fully meet the beam dynamics requirement determined by PARMELA [7].

INITIAL 2D DESIGN

The initial 2D design for the SW and the TW sections of the HAS were performed separately in SUPERFISH by setting appropriate boundary conditions and material properties. Table 1 lists the basic design requirement of the HAS [4],

In the TW section, the 1st and 42nd cells correspond to the RF input and output coupler cells respectively. The 2nd to 6th are β -varied cells and the rests are regular cells.

*Work supported by the National Natural Science Foundation of China (11475201) and the Youth Innovation Promotion Association of Chinese Academy of Sciences, China.

† email address: gaobin@ihep.ac.cn.

COMMISSIONING OF THE 2×4-CELL SUPERCONDUCTING ACCELERATOR FOR THE CAEP THz-FEL FACILITY *

K. Zhou, X. Luo[†], C. L. Lao, D. Wu, J. X. Wang, D. X. Xiao, L. J. Shan
 T. H. He, X. M. Shen, S. F. Lin, H. B. Wang, X. F. Yang, M. Li
 Institution of Applied Electronics, CAEP, Mianyang, China
 X. Y. Lu Peking University, Beijing, China

Abstract

The CAEP THz-FEL facility is the first high average power THz radiation user facility in China. The superconducting accelerator including double 4-cell superconducting radio frequency (SRF) cavities is one of the most important components for this facility. The construction and horizontal test of the superconducting accelerator have been finished. At 2K state, the effective gradients of both cavities have reached our designed goal, 10 MV/m. This paper mainly presents the commissioning results of the superconducting accelerator. In the commissioning experiments, the kinetic energy of 5mA electron beams can be accelerated to 8 MeV successfully, with the energy spread less than 0.2%, much better than our design goal. Further beam loading experiments are in progress.

INTRODUCTION

At present, China Academy of Engineering Physics (CAEP) is developing a THz radiation facility (THz-FEL), which is the first high average power THz user facility in China based on SRF driven oscillator type free electron laser [1]. The THz-FEL facility consists of a high-brilliance electron gun, a superconducting accelerator, a high-performance undulator and so on, as shown in Fig. 1. The designed frequency of the THz radiation is 1-3 THz with the average output power beyond 10 W. Correspondingly, the superconducting accelerator is expected to provide 6-8 MeV quasi-CW electron beams with the average current of 1-5 mA.

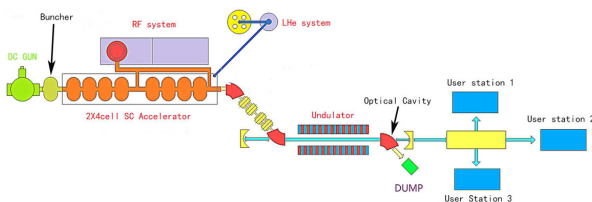


Figure 1: General layout of the CAEP FEL-THz facility.

The superconducting accelerator is one of the most important components for this facility, which contains a cryostat, double 4-cell TESLA SRF cavities, double tuners, double

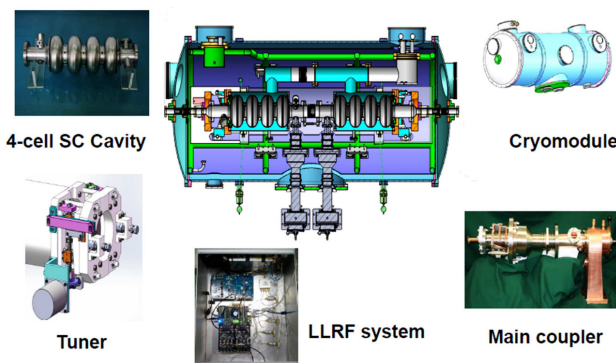


Figure 2: The cross-section and components of the superconducting accelerator [2].

Table 1: Designed Parameters of the 2×4-cell Superconducting Accelerator.

Parameters	Designed value
Frequency	1.300 GHz
Q_0	$\geq 5 \times 10^9$
Q_e	$8 \times 10^5 - 5 \times 10^6$
E_{acc}	8-10 MV/m
I_b	1-5 mA
Repetition rate	54.17 MHz
Energy gained	6-8 MeV
Energy spread	0.75%
2 K heat loss	≤ 20 W
Magnetic field @ central axis	≤ 20 mGs

main couplers and some auxiliary systems, including the microwave system, the cryogenic system and the low level RF control system, as shown in Fig. 2. The design and fabrication of these subsystems have been finished [3]. All these components have reached their designed goals and the linac module has also finished its assembling and horizontal test at Chengdu. At 2 K state, the whole superconducting accelerator works well and stably. The effective field gradients of both cavities have achieved 10 MV/m [4]. This paper mainly presents the commissioning results of the 2x4-cell superconducting accelerator, including some beam loading experiments and the measurement of energy and energy spread of the electron beams.

BEAM LOADING EXPERIMENTS

The superconducting linac module has been connected with the beam line after the horizontal test. Figure 3 shows

* Work supported by China National Key Scientific Instrument and Equipment Development Project (2011YQ130018), National Natural Science Foundation of China with grant (11475159, 11505173, 11576254 and 11605190).

[†] Email address: luox8688@163.com

FRINGE FIELD OVERLAP MODEL FOR QUADRUPOLES

Huan Jia, Institute of Modern Physics, CAS, Lanzhou, China
Michael Plum, Oak Ridge National Laboratory, Oak Ridge, USA

Abstract

In the large aperture-to-length ratio quadrupoles, there will be long fringe field. When putting three of this type quadrupoles next to each other, the field will overlap and change the beam dynamics of “hard-edge” model. By numeric integration, we find that the transfer matrix difference is quite significant at the first part of MEBT of CADS Injector II. By re-exploring the “hard-edge” model, the traditional definition of quadrupole’s effective length and effective gradient are found to be just rough approximations and not right in this condition. The finding explains the good prediction of beam dynamics model of MEBT by emittance measurements with different current settings of the triplet quadrupoles, and may be also helpful in explaining some discrepancies in beam lines around the world

INTRODUCTION

At the MEBT of CADS Injector II, quadrupoles have very large bore aperture to bore length ratio, i.e. 54 mm/52 mm for QL80 and 54 mm/ 74 mm for QL100 [1]. At the same time, due to the strong focusing properties at MEBT, the distance between quadrupoles is quite near. The distance between the first three adjacent quadrupoles is 180 mm, which is smaller than the sum of quadrupole bore length and 3 times of apertures.

Thus, the fringe field is quite significant for the quadrupoles at MEBT, and the overlap effect between adjacent quadrupoles is also significant. This effect is analysed by comparison of beam properties after tracking through both the hard-edge model and fieldmap overlap model.

In the past, people try to treat the field overlap problem by multiplying some factors for the three quadrupoles [2]. But our finding is that such a method is not right, because it is not the effective length or effective gradient making effect. It is the total transfer matrix integration making change, and the change is different in horizontal and vertical plane.

The emittance measurement at MEBT of CADS Injector II shows good agreement to multi particle tracking simulation, with 1-D fringe field overlap model [3]. The new finding in the paper explains the agreement between simulation and measurement.

HARD EDGE MODEL

The hard edge model has been prompted for the quadrupoles for many years. The “hard edge” means that quadrupole’s gradient is a square-like waveform, with two step-function “edges” in both sides, as shown in Fig. 1.

The transfer matrix of “hard edge” model is that:

$$R_{xx} = \begin{bmatrix} \cos(k\Delta s) & \frac{\sin(k\Delta s)}{k} \\ -k\sin(k\Delta s) & \cos(k\Delta s) \end{bmatrix}. \quad (1)$$

$$R_{yy} = \begin{bmatrix} \cosh(k\Delta s) & \frac{\sinh(k\Delta s)}{k} \\ k\sinh(k\Delta s) & \cosh(k\Delta s) \end{bmatrix}. \quad (2)$$

Where $k = \sqrt{\frac{G}{B\rho}}$ is the focusing strength, $G = \frac{\partial B_y}{\partial x}$ is the quadrupole gradient. $B\rho$ is the magnetic rigidity.

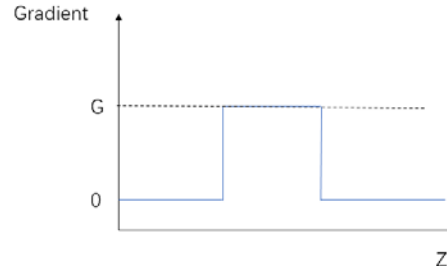


Figure 1: “hard edge” gradient along the quadrupole.

In reality, there is no quadrupole that is “hard edge”. The model is right for “thick” quadrupoles, which means that quadrupole has small aperture-to-length ratio. But for “thin” quadrupoles, which means that quadrupole has large aperture-to-length ratio, the model is not right and need to be re-investigated.

For example, because of the large aperture-to-length ratio, the QL80s in MEBT of CADS Injector II can be regard as “thin” quadrupoles, as shown by field gradient simulation and measurements in Fig. 2.

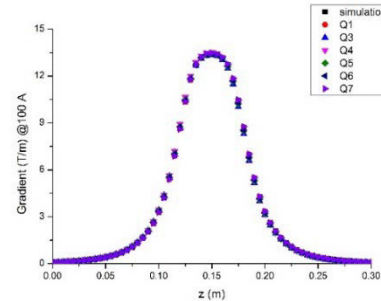


Figure 2: Simulated (black) and measured gradient along axis for six QL80 at MEBT of CADS Injector II [1].

If we treat the quadrupole with “hard edge” approximation, the effective length and effective gradient will be

$$L_{eff} = \int_0^{300} \frac{G \cdot dL}{G_{z=150 \text{ mm}}} = 80 \text{ mm} \quad (3)$$

$$G_{eff} = G_{z=150 \text{ mm}} = 13.5 \text{ T/m} \quad (4)$$

FRINGE FIELD MODEL

For the same quadrupole field distribution, we integrate the transfer matrix by sliced pieces M_i , where each M_i is treated as “hard edge” quadrupole, then,

$$M = \prod_{i=1}^n M_i \quad (5)$$

Here we define the new effective length as l and effective gradient as k , thus, the new transfer matrix is [4],

BEAM PARAMETER RECONSTRUCTION AT THE INPUT OF LEBT OF C-ADS INJECTOR II*

W. L. Chen, W. S. Wang, Y. S. Qin, S. H. Liu, W. P. Dou, C. Wang, Z. J. Wang, Y. He
 Institute of Modern Physics (IMP), Chinese Academy of Sciences, Lanzhou, China

Abstract

The Injector II for the C-ADS is designed to accelerate a proton beam to 10 MeV in continuous wave (CW) mode with beam current up to 10 mA, which is the demonstration of the key technologies for CiADS. The LEBT section physical length and dynamic lattice is calibrated recently, and the more receivable beam parameters has been reconstructed at the input of LEBT. AS the transport of high current beams at low energies is critical, for at kinetic energies of a few MeV, the beams are space charge dominated. This paper will introduce beam parameters reconstruction based on emittance measurement experiment and PIC code TraceWin to reconstruct with space charge considered.

INTRODUCTION

A project named China Accelerator Driven Sub-Critical System (C-ADS) has been proposed to treat the spent nuclear fuel and began construction since 2011 [1]. Under six years commissioning, the demo facility had accelerated 12.6 mA Pulse proton beam to 26.06 MeV, 170 uA CW proton beam had accelerated up to 25 MeV, and recently the project of C-ADS demo facility just has completed the acceptance. The layout of the demo facility is shown in Figure 1.

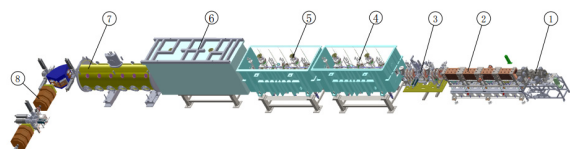


Figure 1: The layout of the demo facility of C-ADS.

- ① LEBT section
- ② RFQ
- ③ MEBT section
- ④ CM1(HWR010)
- ⑤ CM2(HWR010)
- ⑥ CM3(Taper HWR015)
- ⑦ CM4 (Spoke021)
- ⑧ HEBT section

The LEBT is designed by Y.Yao [2], the Layout of the LEBT is shown in Figure 2. As the project tasks arranged so compact, the beam parameters had not measured so clear at the beginning of the LEBT commissioning. The LEBT beam parameters of injector II are copied by injector I at IHEP, for the two LEBT designed all by IMP is very similar.

The LEBT physical length has been alignment recently by machinery group, but the collimation error is far away from the dynamic length. Using the initial beam parameters and the actual solenoid magnetic field values for beam transport simulation and tracking, the beam parameters at the end of the LEBT cannot match well with the download

section (RFQ). Figure 3 is the beam phase space out of RFQ tracking by matched beam. But for the mismatched beam the transmission of the RFQ is about 98%, and the beam emittance growth is almost 47%. Table1 shows the comparison of these.

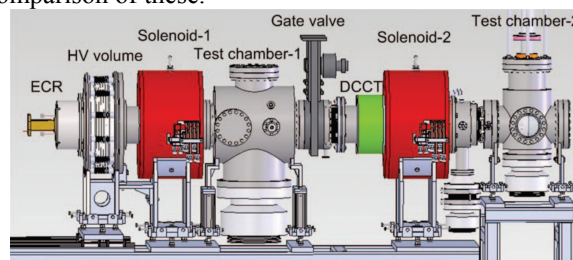


Figure 2: The layout of the LEBT of C-ADS.

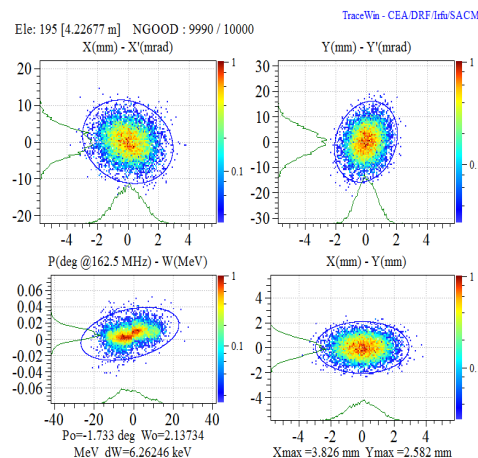


Figure 3: Phase space out of the RFQ.

For getting the real beam initial parameter at the LEBT input, a beam dynamic code named TraceWin combined with python is used for beam parameter reconstruction.

Table 1: Comprision of the Match or Mismatch Beam Parameters out of RFQ

	α_x	β_x	E_x (RMS)	α_y	β_y	E_y (RMS)
LEBT Input	0	0.16	0.189	0	0.16	0.189
Matched beam	0.1551	0.2646	0.2257	-0.1945	0.1316	0.2229
Mismatched beam	0.1554	0.2574	0.2916	-0.2294	0.1312	0.2767

*Work supported by National Science Foundation of China (Grant No. 91426303 and No.11525523)

BEAM OPTICS VERIFICATION FOR A QWR*

Y. S. Qin[†], Z. J. Wang, H. Jia, Y. He, S. H. Liu, W. L. Chen, C. Wang, Y. Z. Jia, P. H. Gao
Institute of Modern Physics (IMP), Chinese Academy of Sciences, Lanzhou, China

Abstract

Quarter-wave resonators (QWRs) are being widely used in linear accelerators (linac) for acceleration of ions with low- β velocity. Two effects of this kind of cavities are the beam steering effect and RF defocusing effect caused by geometric asymmetry and the offset of input beam. Measurement for these two effects has been conducted by beam position monitors (BPM) and wire in a QWR type buncher whose frequency is 162.5 MHz at Institute of Modern Physics (IMP), Chinese Academy of Sciences (CAS). Since the experimental result and simulation result matches well, beam optics has been verified, such that beam central position and beam envelope could be predicted in simulation and an online orbit correction program will be developed in the future.

INTRODUCTION

QWRs, being widely studied and built in many laboratories for accelerating of ions in the velocity range from $0.01c$ to $0.3c$ [1], are cylindrical and coaxial cavities who have an up-down asymmetry with respect to the beam axis. Because of lacking of symmetry, QWR will lead to beam steering and RF de-focusing. Both horizontal magnetic field and vertical electric field will produce steering in the direction of the resonator axis. The beam deflection, moreover, depends on the particle position, which will create emittance growth and beam spill, especially in high intensity proton linac[2]. Beam envelope will also increase because of RF defocusing effect.

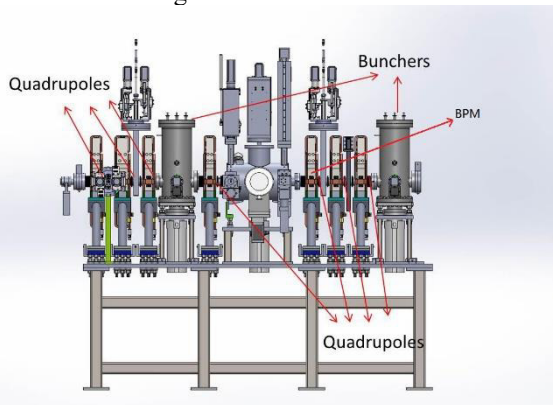


Figure 1: Layout of MEBT of C-ADS Injector II.

Based on the initial simulation and beam experiment, QWR will lead to considerable beam deflection and beam envelope increase. Beam optics verification for the QWR has been carried out based on beam experiment which is conducted on the MEBT of C-ADS injector II. In the experiment, the first buncher and the BPM are used as shown

in Figure 1[3]. By comparing the experimental result with the simulation result, beam steering effect and RF defocusing effect could be calculated.

The simulation code we used is TraceWin.

BEAM STEERING EFFECT IN QWR

Figure 2 shows the QWR buncher cavity and the electromagnetic field distribution. The blue line presents the longitudinal electric field E_z along the cavity axis, the red line presents the vertical electric field $E_y \times 10$, and the black line presents the horizontal magnetic field cB_x . Compared with the accelerating component E_z , the transverse electric field E_y and the horizontal magnetic field B_x will cause dipole component field. Thus, both horizontal magnetic field and vertical electric field will produce beam steering in the vertical direction and RF defocusing in transverse direction[4].

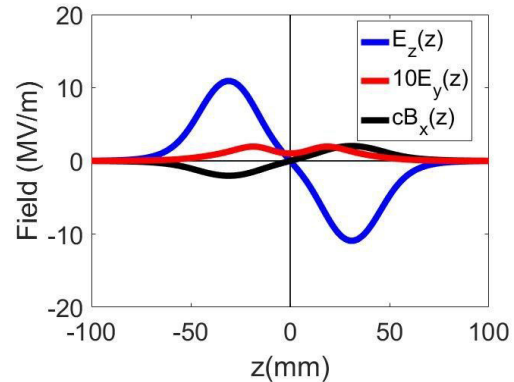


Figure 2: QWR field distribution.

In a RF cavity, beam energy gain is associated with the cavity voltage V_0 and the RF phase ϕ as shown in the following equation:

$$\Delta U = qV_0 T L \cos \phi$$

Considering the asymmetrical electric and magnetic field, beam steering effect will vary with the voltage and RF phase:

$$\Delta y' = -\frac{\Delta U}{\gamma m c^2 \beta} \tan \phi \left[\frac{\cos\left(\frac{\pi d_y}{\beta \lambda}\right)}{\beta \sin\left(\frac{\pi d_y}{\beta \lambda}\right)} K_{E_y}(y) + K_{B_x}(y) \right]$$

where $\Delta y' \approx \Delta p_y / p$ is the deflection angle produced by the QWR, and $\Delta U, m, \phi, \lambda$ are the particle energy gain, rest mass, RF phase and RF wavelength respectively. While d is the gap-to-gap distance, d_y is an effective gap-to-gap distance for the transverse electric field E_y . The

* Supported by the National Natural Science Foundation of China (Grant No. 91426303 and No. 11525523)

[†] E-mail: marshal@impcas.ac.cn

BEAM DYNAMICS DESIGN OF CIADS SUPERCONDUCTING SECTION *

Shuhui Liu, Zhijun Wang, Yuan He, Insitution of Modern Physics, China

Abstract

China Initiative Accelerator Driven system (CiADS) is a strategic plan to solve the nuclear waste problem and the resource problem for nuclear power plants in China, and it aims to design and build an ADS demonstration facility with 500 MeV in energy and 5mA in beam current. CiADS contains driver linac, target and reactor. In this paper, the beam dynamics philosophy applied to the design of the superconducting part of the linac as well as the beam dynamics performance of this structure are focused on.

INTRUDUCTION

The CiADS linac, to be built in Huizhou, Guangdong, is a CW proton accelerator. The driven linac will deliver a 500 MeV, 5 mA proton beams in CW operation mode. The general layout is shown in Figure 1. The driver linac is composed of two major sections. One is the normal conducting section and the other is the superconducting (SC) section. The normal conducting section is composed of an electron cyclotron resonance (ECR) ion source with frequency of 2.45 GHz, a low energy beam transport (LEBT) line, a four-vane type copper structure radio frequency quadrupole (RFQ) with frequency of 162.5 MHz and a medium energy beam transport (MEBT) line. The normal conducting section will accelerate proton beam to 2.1 MeV. The SC section as the main accelerating section will accelerate the proton beam from 2.1 MeV up to 500 MeV. Then, the beam is transported to the beam dump going through the high energy beam transport (HEBT) line.

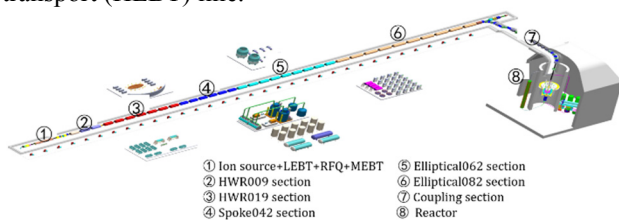


Figure 1: General layout of the CiADS linac.

In this paper, the design considerations of the superconducting section with different types cavity is discussed and the multi-particle simulation results are also presented.

GENERAL CONSIDERATION AND PHILOSOPHY ON SC SECTION DESIGN

Hands on maintenance and machine protection set strict limits, 1 W/m and 0.1 W/m respectively, on beam losses and have been a concern in high power linacs [1]. Therefore, it is crucial to design a linac, which does not

excite beam halo and keeps the emittance growth at a minimum level to avoid beam loss. Given the demands of stability and reliability, some guidelines are required to be considered in the design process. Although a lot of the design philosophy for the linac has been addressed in previous literature, we still consider some of them so important to be stated here, and the most important factors in designing our machine are the following [2]:

- (1) Transverse period phase advances for zero current beams should be below 90° to avoid the structure resonance.
- (2) Wave numbers of oscillations need change adiabatically along the linac, especially at the lattice transitions with different types of focusing structure and inter-cryostat spaces.
- (3) Avoid strong space charge resonances through the judgment of Hofmann's Chart.
- (4) Minimize the emittance growth and beam halo formation caused by mismatching in the lattice transition section.
- (5) Enough redundancy to avoid the beam loss along the linac.

LATTICE DESIGN

Five types cavities are adopted in SC section based on the analytical results of optimization code. The general parameters of these cavities are determined through optimization as shown in table1. For beam dynamics design and simulation, Epeak is 75% of designed performance, and another 25% is used for element failure compensation, and this redundancy also benefits the cavity reliability.

Table 1: Parameters of the Cavities in the SC Section

Cavity type	β_g	Frequency MHz	E _{max} MV/m	B _{max} mT
HWR	0.10	162.5	28	56.75
	0.19	162.5	32	58.24
Spoke	0.42	325	35	65.91
Elliptical	0.62	650	35	67.34
	0.82	650	35	68.30

The optimized lattice structures for each section of the SC segment are shown in Figure 2. In the first segment with HWR010 cavity, in order to overcome the emittance growth and beam loss caused by strong space charge effect and nonlinear effect, short and compact structure is used, which is also beneficial to raise the accelerating efficiency and increase the longitudinal acceptance for the RFQ output beam. The output energy is about 8MeV. In

*Work supported by National Science Foundation of China (Grant No.91426303 and No.11525523)

ORBIT CORRECTION STUDY BASED ON SIMULATION FOR INJECTOR II

W.S.Wang, Z.J.Wang, C.Jin, Y.He, S.H.Liu, P.Y.Jiang, W.P.Dou, W.L.Chen, Y.S.Qin
Institute of Modern Physics (IMP), Chinese Academy of Sciences, Lanzhou, China

Abstract

Orbit correction is one of the most fundamental processes used for beam control in accelerators. The CADS is a CW machine and a few particle loss will cause serious damage to the machine. Therefore, the quality of the orbit control is an essential component towards the efficiency in operation, flexibility in machine studies. This paper describes an orbit correction implementation using singular value decomposition (SVD) of the response matrix and the simulation of its application to the CIADS injector II. This effort was achieved by exploiting the capabilities of Python, which provided the hands-on modules to develop the GUI code easily. Also involved in this effort was the code TraceWin, which was used to construct the virtual machine by providing the parameters of the Linac optics. Several iterations of the orbit correction may be required in order to obtain a satisfactory control of the orbit, because the the response matrix changes with iteration in an attenuating mode. After appropriate removal the redundancy steerers, a promising result of the orbit control was achieved.

Introduction

The CIADS project aims to deliver high power proton beams for nuclear transmutation. The neutrons created in the target from a spallation reaction between protons and heavy elements drive the subcritical reactor for sustained chain reaction. CIADS will be a continuous wave (CW), proton RF superconducting linear accelerator with current (10mA) and final energy 1.5GeV. The pre-feasibility study facility, injector II established mainly by IMP, was successfully commissioned in June 2017 with the jointed efforts of IMP and IHEP. The overall architecture of injector II is shown in Fig. 1. The chosen sequence of accelerating sections is quite standard for modern pulsed linac designs. The ion source is followed by a Radio Frequency Quadrupole (RFQ), a MEBT and the superconducting accelerating structures. Four cryomodules of the accelerating structures bring the energy from 2.1MeV at the exit of RFQ up to 25MeV: the first three cryomodules and the last one are fabricated by IMP and IHEP respectively.

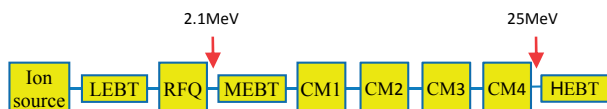


Figure 1: Scheme of Injector II.

CIADS is designed to enable hands-on maintenance and minimize the performance deterioration of superconducting cavities caused by particle loss, which means that its beam loss will be below 1 W/m for the entire accelerator. These specifications will place CIADS in line with the next generation of accelerators worldwide. In real life errors will be present: misalignments, incorrect field settings, magnetic field inhomogeneities, etc. These errors can cause unacceptably large deviation of the orbit. Usually the distorted orbit can be corrected using the dipole correctors and BPMs. In this paper, we select a partial section of injector II, consisting of MEBT and the first three cryomodules, to conduct the correction study. The distribution of correctors and BPMs is shown in Fig. 2. MEBT includes 7 quadrupoles, each of which contains a pair of horizontal and vertical steerers, and there are 4 BPMs separately installed at the center of 1th, 4th, 5th and 7th quadrupoles. Each cryomodule consists of a series of periods and there are a magnet assembly of focusing solenoid and corrector coils, a cavity and a BPM cell in each period.

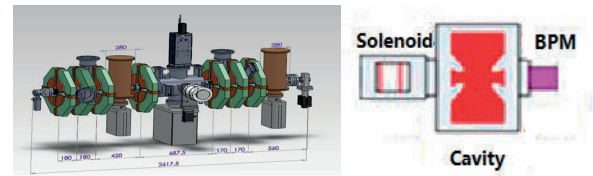


Figure 2: The layout of MEBT and a cryomodule period

In the orbit correction study, we use TraceWin to simulate the behaviour of proton beams in the accelerator and displace the central orbit at the accelerator entrance in the transversal direction to introduce an artificial orbit deviation. As a preliminary attempt, a well-known orbit correction approach using SVD of the response matrix was implemented on the accelerator to estimate the correction effect on bringing back the beam orbit.

Orbit Correction Method

According to accelerator theory the transfer matrix R between positions 1 and 2 is given by [1]:

$$R = \begin{bmatrix} R_{11} & R_{12} \\ R_{21} & R_{22} \end{bmatrix} \quad (1)$$

The elements of the matrix are as follows:

$$R_{11} = \sqrt{\beta_2/\beta_1} (\cos\Delta\psi + \alpha_1 \sin\Delta\psi)$$

$$R_{12} = \sqrt{\beta_1\beta_2} \sin\Delta\psi$$

$$R_{21} = -[(1 + \alpha_1\alpha_2) \sin\Delta\psi + (\alpha_2 - \alpha_1) \cos\Delta\psi] / \sqrt{\beta_1\beta_2}$$

$$R_{22} = \sqrt{\beta_2/\beta_1} (\cos\Delta\psi - \alpha_1 \sin\Delta\psi)$$

where β_i and α_i ($i=1, 2$) are the machine functions; $\Delta\psi$ is the phase difference between positions 1 and 2.

* Work supported by National Science Foundation of China (Grant No.91426303 and No.11525523)

† email address: wwshunan@impcas.ac.cn

THE PROGRESS OF THE CHINA MATERIAL IRRADIATION FACILITY RFQ*

Weiping Dou[†], Zhijun Wang, Chenxing Li, Yuan He, Fengfeng Wang, Xianbo Xu, Shuhui Liu, Zhouli Zhang, Institute of Modern Physics, Lanzhou, China

Abstract

The design and low power RF measurement of the radio frequency quadrupole (RFQ) for the front end of China Material Irradiation Facility (CMIF), which is an accelerator based neutron irradiation facility for fusion reactor material qualification, has been completed. The RFQ, which operated under CW mode, is specified to accelerate 10 mA deuteron beam from the energy of 20 keV/u to 1.5 MeV/u. To reduce the possibility of beam loss in superconducting section, the output longitudinal emittance need be optimized. The idea of “Kick-drift” is adopted in beam dynamic design. The challenge for CW RFQ is not only the beam dynamic design but also in the design of cavity structure and cooling of structure. With the experience obtained in the design of the RFQ for CIADS injector II, the structure design and cooling design have been finished. The results of low power RF measurement show the flatness and asymmetry are below 4% for each module.

INTRODUCTION

The China Material Irradiation Facility (CMIF) will be established by the Institute of Modern Physics (IMP), Chinese Academy of Science. CMIF is a new compact neutron source with less cost and low level risk than the project IFMIF. The schematic diagram of CMIF is illustrated in Fig. 1. It consists of ion source, LEBT, RFQ, MEBT, superconducting section, HEBT, and granular beryllium alloy particle target [1]. The RFQ operated under CW mode, as a key equipment of the CMIF linac, is specified to accelerate deuteron beam with intensity high to 10mA from the energy of 20 keV/u to 1.5 MeV/u.

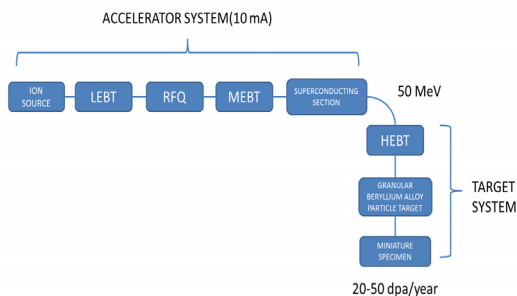


Figure 1: The schematic diagram of CMIF.

BEAM DYNAMIC DESIGN

The main RFQ parameters are shown in Table 1.

Table 1: CMIF RFQ Design Parameters

Particle	Value	Unit
Beam current	10	mA
I/O energy	0.02-1.5	MeV/u
Vane voltage	65	kV
Vane length	526.43	cm
Max.surface filed	19.01	MV/m
Transmission rate	98.2	%
Tr.n.r.emittance	0.203	pi.mm.mrad
99.99%	3.5	pi.mm.mrad
long.emittance		

These goals of RFQ beam dynamic studies usually are minimize the vane length, beam loss and emittance growth. For CMIF RFQ, two special goal are optimized Kilpatrick factor and output longitudinal emittance. PARMTEQM code [2], which was developed at Los Alamos National Laboratory, is used to generate RFQ parameters. The Kilpatrick factor was optimized to 1.4 computed by PARMTEQM code, which is small enough for avoiding any possible breakdown and reducing time of conditioning of the resonator. The output longitudinal emittance need be optimized to 3.5 pi.mm.mrad to reduce the possibility of beam loss in superconducting section. The idea of “kick-drift” and Four-Section Procedure are adopted in beam dynamic optimized design. The “kick-drift” act as internal bunch system to bunch beam in short distance. The longitudinal emittance growth and bunch efficient with different electrode modulation factor and drift length have been studied in Fig. 2. The results show when max electrode modulation is 1.02 and the distance is appropriate, the longitudinal emittance growth is smaller and the phase spread is about ± 30 deg.

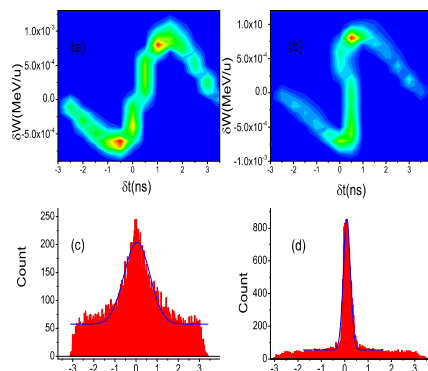


Figure 2: The evolution of longitudinal phase space with different electrode modulation factor and drift length.

* Work supported by National Science Foundation of China (Grant No.9142603) and National Magnetic confinement Fusion Science Program of China (Grant No.2014GB104001)

[†] email address: douweiping@impcas.ac.cn

CALIBRATION OF THE BPM OFFSETS IN CRYOMODULE AT CIADS INJECTOR II

C. Feng*, Z. J. Wang, W. S. Wang, Y. He

Institute of Modern Physics (IMP), Chinese Academy of Sciences, Lanzhou, China

Abstract

China Initiative Accelerator Driven System (CiADS) project is a strategic plan to solve the nuclear waste problem and the resource problem for nuclear power plants in China. For CiADS driven linac, which has a long superconducting accelerator section, traditional ways to calibrate the Beam Position Monitor (BPM) are not always available. In order to calibrate the BPM offsets in cryomodule so as to adjust the beam orbit effectively and accurately, we have tried to scan the superconducting solenoid's current, read the BPM values, and fit the data to get BPM offsets.

INTRODUCTION

The Injector Scheme II which is being built at IMP is composed of an ion source, a low energy beam transport line (LEBT), a 162.5 MHz radio frequency quadrupole accelerator (RFQ), a medium energy beam transport line (MEBT) and a superconducting Half Wave Resonator (HWR) accelerator section. In superconducting accelerator section, beam loss is particularly deleterious. Large beam orbit excursion is one of the major reasons causing beam loss. In order to align the beam orbit accurately to the centroid of the accelerator components, calibration of the BPM offsets is essential.

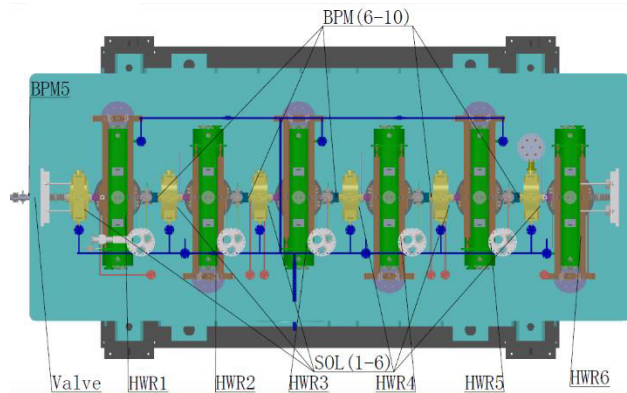


Figure 1: Layout of CM1 of C-ADS Injector II.

Traditional methods of calibrating BPM offsets always need quadrupoles [1]. But in cryomodule, such as CM1 shown in Fig. 1, there is no quadrupole. On this occasion, solenoid may be a substitute. In this report, the formulations of calibration of the BPM offsets with solenoid will be briefly described in the second section. The experiment

designs and results are demonstrated in the third section. Finally, the summary of the studies will be given and some ideas for further studies will also be discussed in the last section.

MATHEMATICAL THEORY

Let $x, x', y,$ and y' be coordinates of the particle and the subscript 0 and 1 denote the beginning and ending point of the lattice, we get

$$\begin{pmatrix} x_1 \\ x'_1 \\ y_1 \\ y'_1 \end{pmatrix} = M \cdot \begin{pmatrix} x_0 \\ x'_0 \\ y_0 \\ y'_0 \end{pmatrix}, M = \begin{bmatrix} m_{11} & m_{12} & m_{13} & m_{14} \\ m_{21} & m_{22} & m_{23} & m_{24} \\ m_{31} & m_{32} & m_{33} & m_{34} \\ m_{41} & m_{42} & m_{43} & m_{44} \end{bmatrix}$$

where M is the total transfer matrix which can be calculated by [2]

$$R_{drift} = \begin{bmatrix} 1 & L & 0 & 0 \\ 0 & 1 & 0 & 0 \\ 0 & 0 & 1 & L \\ 0 & 0 & 0 & 1 \end{bmatrix}$$

$$R_{solenoid} = \begin{bmatrix} \cos^2(kL) & \frac{1}{2k} \sin(2kL) & \frac{1}{2} \sin(2kL) & \frac{1}{k} \sin^2(kL) \\ -\frac{k}{2} \sin(2kL) & \cos^2(kL) & -k \sin^2(kL) & \frac{1}{2} \sin(2kL) \\ -\frac{1}{2} \sin(2kL) & -\frac{1}{k} \sin^2(kL) & \cos^2(kL) & \frac{1}{2k} \sin(2kL) \\ k \sin^2(kL) & -\frac{1}{2} \sin(2kL) & -\frac{k}{2} \sin(2kL) & \cos^2(kL) \end{bmatrix}$$

Define x_{off} and y_{off} as offsets of the BPM next the solenoid, there are

$$\begin{aligned} \langle x_1 \rangle &= m_{11} \langle x_0 \rangle + m_{12} \langle x'_0 \rangle + m_{13} \langle y_0 \rangle + m_{14} \langle y'_0 \rangle - x_{off} \\ \langle y_1 \rangle &= m_{31} \langle x_0 \rangle + m_{32} \langle x'_0 \rangle + m_{33} \langle y_0 \rangle + m_{34} \langle y'_0 \rangle - y_{off} \end{aligned}$$

Respectively, the following equations can be obtained:

$$\begin{pmatrix} \langle x_1 \rangle \\ \dots \\ \langle x_N \rangle \\ \langle y_1 \rangle \\ \dots \\ \langle y_N \rangle \end{pmatrix} = A \cdot \begin{pmatrix} x_0 \\ x'_0 \\ y_0 \\ y'_0 \\ x_{off} \\ y_{off} \end{pmatrix},$$

$$A = \begin{bmatrix} m_{11}^{(1)} & m_{12}^{(1)} & m_{13}^{(1)} & m_{14}^{(1)} & -1 & 0 \\ \dots & \dots & \dots & \dots & \dots & \dots \\ m_{11}^{(N)} & m_{12}^{(N)} & m_{13}^{(N)} & m_{14}^{(N)} & -1 & 0 \\ m_{31}^{(1)} & m_{32}^{(1)} & m_{33}^{(1)} & m_{34}^{(1)} & 0 & -1 \\ \dots & \dots & \dots & \dots & \dots & \dots \\ m_{31}^{(N)} & m_{32}^{(N)} & m_{33}^{(N)} & m_{34}^{(N)} & 0 & -1 \end{bmatrix}$$

With enough measured $\langle x_i \rangle$ and $\langle y_i \rangle$ values, the quantity of x_{off} and y_{off} can be fitted by using the least square method, which can be simplified as [3]

* E-mail: fengchi@impcas.ac.cn

USING A BESSEL LIGHT BEAM AS AN ULTRA-SHORT PERIOD HELICAL UNDULATOR

B. C. Jiang, Q. L. Zhang, J. H. Chen and Z. T. Zhao, Shanghai Institute of Applied Physics, Chinese Academy of Sciences, Shanghai, China

Abstract

An undulator is a critical component to produce synchrotron radiation and free electron laser. When a Bessel light beam carrying the orbit angular momentum co-propagates with an electron beam, a net transverse deflection force will be subjected to the latter one. As a result of dephasing effect, the deflection force will oscillate and act as an undulator. For such a laser based undulator, the period length can reach sub-millimeter level, which will greatly reduce the electron energy for the required X-ray production.

INTRODUCTION

A magnetostatic undulator is in periodic structures of dipole magnets [1, 2]. The static magnetic field of the undulator is perpendicular to the electron beam trajectory, and periodically changes its directions, which causes an electron beam bunch to follow an undulating trajectory, hence the energy radiations. The radiation brightness from an undulator at the resonance wavelength is N^2 times higher than that from a single bending magnet, where N is total period number of the undulator.

The radiation wavelength can be calculated by Eqs. (1) and (2) [2, 3]:

$$\lambda_{\text{rad}} = \frac{\lambda_u}{2\gamma^2} \left(1 + \frac{K^2}{2} + \gamma^2\theta^2\right), \quad (1)$$

$$K = \frac{eB\lambda_u}{2\pi m_e c} = 0.934B(T)\lambda_u(\text{cm}), \quad (2)$$

where, λ_u is period length of the undulator; B is peak magnetic field of the undulator; λ_{rad} is the radiation wavelength; θ is the radiation angle; γ , e and m_e are the Lorentz factor, charge and rest mass of electron, respectively; and c is the speed of light.

An important direction of the undulator improvement is to decrease the period length. The shorter is the period length of undulator, the lower is the electron energy required for a desired X-ray, hence a great reduction of the facility scale and cost.

For a practical configuration, K value of an undulator should be in order of 1. To this end, the shorter the period length, the higher the peak magnetic field should be. This prevents the undulator period from being ultra-short. In-vacuum undulator was developed for short period approach [4, 5]. In this type of undulator, the permanent magnets are installed in a vacuum tank, thus the undulator pole gap can be much smaller, the peak field can be increased, and the period length can be reduced.

The discovery of increasing remanent field and coercivity of the permanent magnet at low temperatures provides the possibility of building cryogenic permanent magnet undulator (CPMU) [6, 7] with a shorter period, a little bit, though, at the cost of an additional liquid nitrogen cryogenic system. The superconducting technology helps to

build undulators of even shorter periods [8, 9]. However, even for the state-of-the-arts technology, the period length of a magnetostatic undulator is beyond 1 mm [10]. It is possible for an RF undulator [11, 12] to achieve period length of shorter than 1 mm. However, for lacking of high power THz source, it is still hard to realize a millimeter-period undulator.

Optical undulator has been proposed for compact FEL purpose for years. When an intense and long enough laser pulse counter-propagates with the electron beam, the laser may act as an undulator [13–16]. The period length of optical undulator is in micron range. This requires that the electron beam is orders of magnitude brighter than the existing electron source for FEL generation. Laser plasma undulator [16, 17] was just proposed to build sub-millimeter period undulator, but the fact that the electrons do not pass through free space may prevent its use in storage rings.

In the following sections we will show that a Bessel light beam can be used for undulating relativistic electrons when it is co-propagating as shown in Figure 1. With the advent of high power laser, it is possible to achieve K value of around 1 for Bessel light beam undulator (BLU) with period length approaching sub-millimeter.

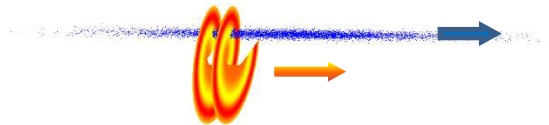


Figure 1: Sketch of Bessel light beam (red-orange vortex) interaction with electron beam (blue dot).

TRANSVERSE FORCE OF BESSEL LIGHT BEAM TO THE RELATIVISTIC ELECTRON

For a monochromatic Bessel light beam, in the dimensionless system ($c=1$), the electric and magnetic fields of the wave in the Cartesian coordinate for paraxial approximation can be expressed as [18]:

$$\begin{pmatrix} \mathcal{E}_x \\ \mathcal{E}_y \\ \mathcal{E}_z \end{pmatrix} = \begin{pmatrix} \kappa_- C_{M+1} + \kappa_+ C_{M-1} \\ \kappa_- S_{M+1} - \kappa_+ S_{M-1} \\ 2S_M \end{pmatrix}, \quad (3-a)$$

$$\begin{pmatrix} \mathcal{B}_x \\ \mathcal{B}_y \\ \mathcal{B}_z \end{pmatrix} = \begin{pmatrix} \kappa_- S_{M+1} + \kappa_+ S_{M-1} \\ -\kappa_- C_{M+1} + \kappa_+ C_{M-1} \\ 2C_M \end{pmatrix}, \quad (3-b)$$

$$C_M = \cos(k_{\parallel}z - \chi\omega t + M\phi) J_M(k_{\perp}\rho), \quad (4-a)$$

$$S_M = \sin(k_{\parallel}z - \chi\omega t + M\phi) J_M(k_{\perp}\rho), \quad (4-b)$$

where, z is the light propagation direction, $\rho = \sqrt{x^2 + y^2}$ is the transverse distance to the z axis, ϕ is the azimuthal phase to the z axis, M is the order of Bessel beam, and

PIC SIMULATION OF THE HIGH CURRENT BEAM FOR THE LIA

Liao Shuqing, He Xiaozhong, IFP, CAEP, Mianyang, China
 Liu Shuang, DEP, TSINGHUA. Beijing, China

Abstract

High current beams emitting and transport of the linear induction accelerator (LIA) injector are simulated by a PIC code. And then beam transport and accelerated with space charge from injector exit to the LIA exit is simulated by another PIC simulation code and the slice beam parameters variability are also presented by this paper.

INTRODUCTION

The new type linear induction accelerator DRAGON-II is performed a multi-pulse x-ray flash radiography. The accelerator is delivered several about 20MeV (about 2% over the flattop), 2.0kA, 90ns(FWHM), 2000mm.mrad beams. To achieve the radiographic performance specifications, the time integrated beam spot size on the target should be less than 2mm. However, the interactions between the high energy intensity beams with the target may disrupt the beam spot size. These beam parameters make the new accelerator transport system the complicated system ever designed to transport a high current, high energy and long pulse beam. And designing the new accelerator transport system is challenging.

The DRAGON-II consists of pulse power system (triggering synchronizer, Marx generators and Blumlein lines), accelerator platform (injector, accelerator modules, beam transport system, beam downstream system), auxiliary system (vacuum system, isolated gas supply and water-cooling device). The pulse system that powers the injector for the new accelerator is capable of producing a 2.5-3 MV output pulse that is 90ns (FWHM). With the 2.5-3 MV diode voltage the cathode emits an about 2.0-2.5 kA pulse electron beam with more than 90ns (FWHM) current/energy “flat-top”. After leaving the diode, the beam is accelerated by induction cells to 2.5-3MeV. Following the injector, these are a series of accelerator cells which consist of four accelerator cells and a vacuum cell. At the accelerator exit the beams are accelerated by all cells to about 20MeV. The beam downstream system focuses the high energy beams to target less than 2mm for the x-ray flash radiography.

The accelerator transport system consists of three sections. The first, a solenoid transport system consists of several large size solenoids which diameter are about 450mm. Namely the first transport system is the injector beam transport system. The second section consists of a series of solenoids which named accelerator cell solenoid. The second system transports the beam between the injector and the accelerator exit. The third transport system is the beam downstream system, the target beam line. In this paper we discuss the model of the transport sections; from the cathode to the accelerator exit.

THE INJECTOR

A particle simulation code named CHIPIC [1] is utilized to model the transport of a 90ns pulse beam from the cathode emitting, through the anode hole, and to the injector exit. Particle simulations can provide additional information on the performance of the beam line, for example the beam slice emittance. Figure 1 shows the geometry for the PIC simulation and the transport solenoids.

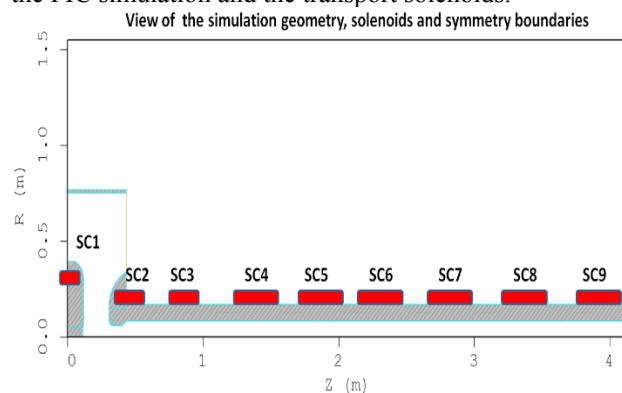


Figure 1: The geometry for the Injector simulation.

By the POSSION/SUPERFISH code, we obtain the injector axial magnetic field that Figure 2 shows. All the solenoids are designed at a lower tilt/offset that about 1mrad/0.5mm for the corkscrew control.

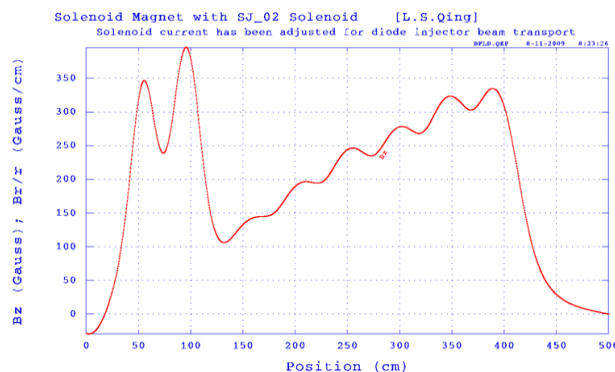


Figure 2: The axial magnetic field of the Injector.

A voltage pulse $V(t)$ is applied to the injector. The different voltages lead to the different emit beam currents and the different cathode-anode gaps also lead to the different beam currents that Table.1 shows.

Table 1: Emit Beam Currents with the Voltages

Voltage Mv	Emit current A
1.2	738
2.4	1893
3	2543
3.6	3231
4.8	4679

Content from this work may be used under the terms of the CC BY 3.0 licence (© 2017). Any distribution of this work must maintain attribution to the author(s), title of the work, publisher, and DOI.

CENTRAL REGION DESIGN OF THE HUST SCC250 SUPERCONDUCTING CYCLOTRON *

Z. J. Zeng[†], K. J. Fan, Huazhong University of Science and Technology, Wuhan, China

Abstract

A superconducting cyclotron based proton therapy system is being developed at Huazhong University of Science and Technology (HUST). The compactness of superconducting cyclotron imposes a challenge to the central region design. This paper describes beam dynamic studies in the central region. Beam performance at the initial 4 or so turns is crucial that determines the beam emittance, energy divergence and extraction efficiency. Therefore, considerable efforts have been made to the central region design and optimization. The electric and magnetic field distribution are numerically calculated by the program OPERA. Particle trajectories are simulated by means of the computer code Z3CYCLONE and the track command in OPERA. Finally, an optimum central region configuration is obtained which meets the stringent requirements and further studies is carried out about the beam radial and axial motion based on the designed central region.

INTRODUCTION

Proton therapy has shown advantages in treating several kinds of cancer and has become a favorable treatment option for patients, which shows considerable advantages over conventional photon therapy. In recent years, there has been a massive growth in the development of proton therapy centers in the world particularly in China. The cancer incidence in China is the greatest in the world, and cancer is the leading cause of death, which has become a major public health problem in China. In order to meet the fast growing demand for proton therapy, Chinese government decided to support the development of a superconducting cyclotron based proton therapy facility in the National Key Research and Development Program at 2016. This project is being taken by several institutes and Huazhong University of Science and Technology (HUST) plays a crucial role in this program.

The superconducting cyclotron HUST-SCC250 has the advantage of minimizing the size, however, it has as a drawback of difficult to design a very compact central region. The central region uses an internal cold cathode PIG source to simplify the structure. The configuration of the central region is optimized by using the OPREA code, which can numerically simulate the electric and magnetic field distribution exactly. The beam dynamics studies in the central region are carried out using the beam tracking codes Z3CYCLONE and the track command in OPERA.

* Work supported by national key R & D program, 2016YFC0105303
[†] zengzhijie@hust.edu.cn

CENTRAL REGION DESIGN

One of the challenging design tasks of a superconducting cyclotrons is the central region, where the initial proton orbits are crucial in determining the properties of the final beam.

To study the beam dynamics in the central region, considerable efforts have been made to optimize the central region geometry. The optimum central region design could be achieved using iterative process. Two main problems concerning the central region are the axial motion and radial motion [1]. The main parameters of the central region are listed in Table 1.

Table 1: Basic Parameters

Parameters	Value
DEE width	50°
DEE voltage	60 kV
Harmonic mode	2
RF frequency	75.52 MHz
Injection radius	1.18 cm
Injection angle	122°
Central magnetic field	2.476 T

The design process of central region is illustrated as follows,

- 1) Assuming a uniform magnetic field in the central region, the initial condition of the beam after circulating one turn is obtained based on the ideal energy gain. Then, the initial condition is revised in order to make beam be centered.
- 2) Using backward algorithm to determine the position of the ion source.
- 3) Beam forward tracking algorithm is again used to optimize the electrode structure.

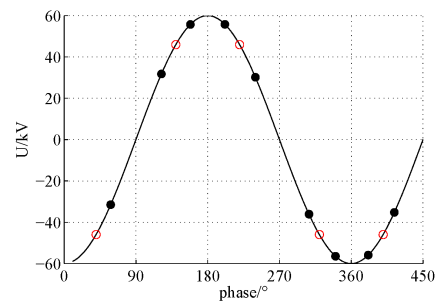


Figure 1: RF phase of the proton crossing the DEE boundary.

Ignoring the transition effect of the accelerating gap, the maximum energy gain on certain RF phases can be obtained, which is shown in Fig. 1 marked as the hollow circles.

INCOHERENT TRANSVERSE TUNE SHIFT CAUSED BY SPACE-CHARGE EFFECTS IN HEPS STORAGE RING AND BOOSTER

Chongchong Du[†], Jiuqing Wang, IHEP, Beijing, China

Abstract

In cases of low beam energy and high particle densities, space-charge effects become necessary discussions on transverse beam dynamics. It may cause a big enough tune shift in a circular accelerator moving the beam onto a resonance. In this paper, the transverse tune shift in High Energy Photon Source (HEPS) storage ring and booster ring caused by space-charge effects is firstly estimated based on the existing theory. Since the tune shift is at the level of 0.2, it may move the beam onto a resonance in the operation mode with high bunch charges. Then some simulations are made by tracking particles with elegant in the HEPS storage ring and booster including the space-charge effects. During the tracking, some particles are lost in HEPS booster ring with bunch charge of 14.4nC for the so called “swap-out” mode. Further simulation shows that no particles would be lost if the charge of single bunch was less than 8.6nC in HEPS booster.

INTRODUCTION

The High Energy Photon Source (HEPS), with a beam energy of 6 GeV, a natural emittance of 59.4 pm-rad and a storage ring circumference of 1295.6m, is a diffraction-limited storage ring to be built in Beijing [1]. The beam current is 200mA, and currently two filling patterns are under consideration. One is the high brightness mode with 648 bunches and the other one is the timing mode with 60 bunches.

The space-charge effect forces the beam to defocus transversely to produce tune shift, which may cause the particles to cross the resonance lines during the accumulation and acceleration process, resulting in loss of the beam or deterioration of the beam quality. Although space-charge effects is often overlooked in the discussion of high-energy accelerators, it must be taken into account in the case of low energy and high particle density. Considering the ultra-low-emittance and the mode of 60 bunches with single bunch charge 14.4 nC in HEPS storage ring, space-charge effects may result in deterioration of the beam quality. Also, the booster is ramping from low energy 300 MeV, and the single bunch charge is large with “swap-out” mode, space-charge effects may result in loss of the beam. So we study the transverse tune shift in HEPS storage ring and booster ring caused by space-charge effects.

In this paper, based on current parameters [2], the transverse tune shift in HEPS storage ring and booster ring caused by space-charge effects is firstly estimated based on the existing theory. Some simulations are made by tracking particles with elegant [3] in HEPS storage ring and booster ring including the space-charge effects.

[†] ducc@ihep.ac.cn

TUNE SHIFT THEORY

Due to the nonuniform charge distribution within a beam, tune shifts are not the same for all particles. Only particles close to the beam center suffer the maximum tune shift, but less affect betatron oscillation amplitudes. The space-charge effects therefore introduces a tune spread rather than a coherent tune shift and we refer to this effect as the incoherent space-charge tune shift.

The incoherent space-charge tune shift is [4]

$$\Delta\nu_{x,y} = -\frac{\lambda r_c}{(2\pi)\beta^2\gamma^3} \left[\oint \frac{\beta_{x,y}}{\sigma_{x,y}(\sigma_x+\sigma_y)} dz + 2(1 + \beta^2\gamma^2 B) \int_0^{L_{vac}} \frac{\varepsilon_1 \beta_{x,y}}{b^2} dz + 2\beta^2\gamma^2 B \int_0^{L_{mag}} \frac{\varepsilon_2 \beta_{x,y}}{g^2} dz \right] \quad (1)$$

where $\lambda = \frac{N_{tot}}{n_b l_b} = \frac{N_{tot}}{n_b \sqrt{2\pi} \sigma_l}$ is the linear particle density, N_{tot} is the total number of particle in the circulating beam, n_b is the number of bunches, σ_l is the standard bunch length for a Gaussian distribution, $r_c = \frac{q^2}{4\pi\epsilon_0 mc^2}$ is the classical particle radius, $\sigma_{x,y}$ is the beam size, $B = \frac{n_b l_b}{2\pi R}$ is the bunch occupation along the ring circumference, b is the vertical half axis of an elliptical vacuum chamber, a is the horizontal half axis, as shown in Fig. 1, ε_1 and ε_2 are the Laslett form factors, $\varepsilon_2 = \frac{\pi^2}{24}$, ε_1 is compiled in Table 1.

Table 1: Laslett Incoherent Tune Shift form Factors for Elliptical Vacuum Chamber[4,5]

a/b	1	6/5	5/4	4/3	3/2	2/1	∞
ε_1	0	0.065	0.09	0.107	0.134	0.172	$\frac{\pi^2}{48}$

In equation (1), the loop integral is equal to the total length of the ring, the integration length L_{vac} is equal to the total length of the vacuum chamber, L_{mag} is the total length of magnets along the ring circumference.

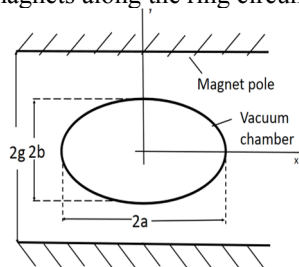


Figure 1: Metallic vacuum chamber and ferromagnetic boundaries.

TUNE SHIFT IN STORAGE RING

The main parameters of the HEPS storage ring used for

MEGA-ELECTRON-VOLT ULTRAFAST ELECTRON DIFFRACTION AND MICROSCOPE AT TSINGHUA UNIVERSITY*

Z. Zhou, Y.C. Du, L.X. Yan, W.H. Huang[†] and C.X. Tang

Department of Engineering Physics, Tsinghua University, Beijing, China

Abstract

Photocathode gun enabled high brightness, relativistic electron beams with femtoseconds to picosecond tuneable time structure are powerful tools for structural dynamics study. A prototype MeV UED system has been built and operated at Accelerator laboratory of Tsinghua University since a decade ago. Experiments of high quality single-shot static diffraction as well as pump-probe based dynamical process have been successfully conducted, especially the pump-probe experiment in continuously-time resolved mode to achieve better temporal resolution. These studies demonstrated the sub-picosecond timescale and atomic length resolving capabilities of our UED facility. To meet the growing interest of ultrafast sciences based on MeV UED facility, we are upgrading it to a user facility. Meanwhile the concept design of ultrafast electron microscope is proceeding. The current status of UED/UEM facility will be reported in this paper.

INTRODUCTIONS

High brightness electron beams with ultrashort pulse duration are suitable probes for observing structural changes with ultrahigh spatiotemporal resolution. Compared to X-ray probes, electrons serve several unique advantages: 10^4 - 10^6 times larger scattering cross sections, 10^3 times less radiation damage and much easier manipulability [1]. Moreover, electrons are sensitive to both electrons and nuclei in material, thus making it an ideal complementary tools for understanding ultrafast structural dynamics.

In 1980s, the concept of ultrafast electron diffraction (UED) was proposed and demonstrated by G. Mourou et al [2], based on pump-probe method, where the electrons are generated by high voltage photocathode DC gun, and then probe the laser pumped sample structures on the atomic level and ps time domain. Following this novel and powerful technique, numbers of UED facilities have been constructed and many remarkable experimental results have been generated [3]. However, the temporal resolution of DC-based keV UED facility is limited to picosecond scale because of the strong space charge effect, which causes severe pulse elongating with increasing charge density and drift length. To overcome these barriers, photocathode rf gun was proposed to serve as the high brightness beam source for UED facility [4], in which the electrons are quickly accelerated to a few MeV and space charge force is dramatically suppressed since it scales as γ^{-3} , where γ is the Lorentz factor. Meanwhile, utilization of MeV electron probes also solves the problems of velocity mismatch,

where electron travels slower than light in sample, especially in gas sample or surface. Since then, intensive efforts have been devoted to development of MeV UED facilities [5-9], including machine performance, methodology and science application.

On the other hand, diffraction patterns are the Fourier transformation of the nuclei and electrons density distribution of the sample, thus no spatial resolution is achievable is UED. Therefore, to observe directly the image of the sample with sub-angstrom space resolution and sub-ps time resolution is indispensable, which is the main purpose of ultrafast electron microscope (UEM). Currently, most widely used UEM facility are based on photocathode DC gun, where the electron energy is limited to hundreds of keV due to the limited accelerating gradient. Problems of strong space charge effected are also encountered in keV UEM, resulting in pulse duration and energy spread increasing during propagations.

To overcome these problems, a S-band photocathode rf gun based UED prototype has been constructed in Tsinghua university since 2008, both high quality static diffraction and pump-probe experiments were successfully conducted. Now we are upgrading it to a user facility using a more flexible and versatile beamline design and a state-of-art new power source. Meanwhile, the design of UEM is ongoing, where a set of permanent magnet quadruplets (PMQs) are employed as a single imaging unit, different to the commonly used superconducting solenoids. The summary of previous work and the current status of the UED/UEM facility in Tsinghua will be present in this paper.

UED RESEARCH AT THU

The schematic of the prototype UED instrument is shown in Fig.1 [10], where the electrons are generated by a S-band photocathode rf gun and focused by a magnetic solenoid. The collimator located just before the sample is used to select a small portion of electrons to improve diffraction pattern quality. A plug-in Faraday cup is to measure the bunch charge. A pair of steering coils are used to correct possible misalignments and fine tune the beam trajectory. Bunch duration is measured by the deflecting cavity, which also enables the UED system working on the so-called "continuously time resolved (CTR)" mode. The diffraction patterns are captured by the detector system, comprised of a phosphor screen, a 45-deg mirror and an EMCCD perpendicular to the beamline.

A set of machine parameters are optimized by thorough, start-to-end simulations, under the guidance of which a high quality single-shot diffraction pattern of a ~ 200 nm polycrystalline aluminium foil is gained, as shown in Fig.2. It is easy to see that the (111) ring and (200) ring are clearly

* Work supported by NSFC Grants No. 11375097 and No. 11435015.

[†] huangwh@mail.tsinghua.edu.cn

ELECTRON OSCILLATIONS IN THE INTENSE LASER PRODUCED THREE-DIMENSIONAL POST-SOLITON ELECTROMAGNETIC FIELD

Dongning Yue, Xiaohui Yuan, Min Chen[†]

Key Laboratory for Laser Plasmas (Ministry of Education), School of Physics and Astronomy,
Shanghai Jiao Tong University, Shanghai, China

Collaborative Innovation Center of IFSA, Shanghai Jiao Tong University, Shanghai, China

Abstract

Electron oscillations in the three-dimensional post-soliton electromagnetic field generated by ultrashort intense laser in near-critical density plasma were studied using 3D particle-in-cell (PIC) simulations. Two types of post-solitons were observed. We found that unlike the ions, which are expelled from the centre of post-soliton, electrons oscillate around the centre of a post-soliton and the resultant poloidal electric vector field behaves like an oscillating electric dipole. The toroidal magnetic field also oscillates along with electrons. On the timescale of ω_{pi}^{-1} , where ω_{pi} is the ion plasma frequency, protons have evolved into multi-shell structures due to Coulomb explosion in the post-soliton. The polarization of the post-soliton is found to be different from that of the driver laser beam.

INTRODUCTION

Nonlinear localized coherent electromagnetic (EM) modes have been found in the interaction of ultra-intense ($I \geq 10^{18}$ Wcm⁻²) laser pulse with underdense plasma ($\omega_{pe} < \omega_L$, where ω_L is the laser frequency, $\omega_{pe} = \sqrt{4\pi n_e e^2 / m_e}$ is the electron plasma frequency, n_e is the electron density). A laser pulse depletes its energy into plasma on a spatial scale of the order of $l_{depl} \approx l_{pulse} (\omega_L / \omega_{pe})^2$ during propagation, where l_{pulse} represents the laser pulse length [1]. With the laser energy loss, the laser frequency undergoes a redshift. The laser experiences locally overcritical density plasma and is trapped in the plasma cavity. This coherent structure shows excellent stability in one-dimensional PIC simulation and propagates with a velocity that is well below the speed of light or almost equal to zero in homogeneous plasma [2]. Since the low frequency EM wave confined inside the slowly expanding plasma cavity is normally generated in the wake of the driver laser pulse, it is therefore denoted as “post-soliton”.

A model called “snowplow” has been proposed to explain the generation and evolution of the two-dimensional s-polarized post-soliton [3, 4]. Experimental and PIC simulation results show that the structure of the three-dimensional post-soliton is anisotropic like a prolate spheroid [4, 5] and depends on the plasma parameters [6].

In this paper, the EM field structure of the three-dimensional post-soliton, electron oscillations in this field and multi-shell like structure of protons will be presented.

The polarization of post-soliton is different from that of laser, which has not been reported before as far as we know.

SIMULATION RESULTS

Three-Dimensional Particle-In-Cell (3D-PIC) code OSIRIS was used in this study [8]. In the simulation, the laser pulse propagates along x_1 direction and is linearly polarized along x_2 axis. The normalized electric vector is $a = eE / (m_e \omega c) = 1$ with pulse duration of 40 fs corresponding to $15 T_0$ which $T_0 = \lambda_0 / c$ and laser wavelength λ_0 is $0.8 \mu\text{m}$. The laser pulse has a transversely Gaussian envelope and its focal plane is at a distance of $20 \mu\text{m}$ from the back of plasma slab. The laser pulse starts at $x_1 = 15 \mu\text{m}$ (the front of the plasma slab). The plasma slab is $30 \mu\text{m}$ thickness and the homogenous density is $n_e = 0.28 n_{cr}$. The simulation box is $x_1 \times x_2 \times x_3 = 45 \mu\text{m} \times 14 \mu\text{m} \times 14 \mu\text{m}$ and is divided into $900 \times 280 \times 280$ cells. Protons are set to be mobile in the simulations.

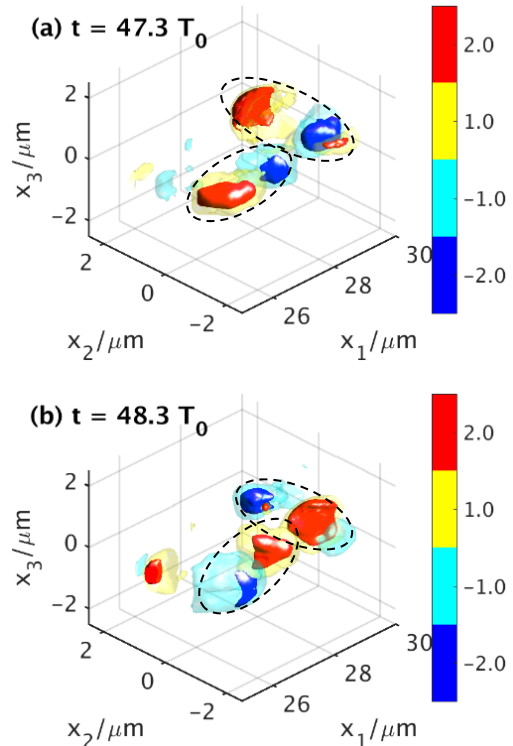


Figure 1: Distributions of transverse electric field E_2 at $t = 47.3 T_0$ (a) and $t = 48.3 T_0$ (b), respectively. Dotted line areas highlight the electric fields that are trapped inside the post-soliton structure.

[†] minchen@sjtu.edu.cn

2 σ SIGNALS FOR THE ELECTRO-GRAVITATIONAL INDUCTION BASED ON BEAM INSTABILITY IN CHARGED PARTICLE STORAGE RINGS *

Dong Dong †

Institute of High Energy Physics, Chinese Academy of Sciences, Beijing, China

Abstract

Changes in beam position within charged particle accelerator storage rings have been observed due to changes in gravity caused by the moon and sun. The terrestrial tidal model has been used to explain this type of beam instability. Further analysis reveals that these instabilities arise from changes in the electron beam energy, that may not only come from movements of the accelerator components due to terrestrial tidal forces, and may be caused by the unsighted process. We try to induce an electromotive force along the ring, referred to as electro-gravitational induction (EGI). The circular motion of the charged particles causes the accumulation of the EGI in the storage ring, turn by turn. We used existing data from storage ring beam signals to estimate the maximum value of the gravity coefficient of the induced electromotive force.

INTRODUCTION

LEP and Spring8 have observed COD changes, the period of 12 hours, comes from the gravity changes, the change of acceleration of gravity g , Δg caused by the moon and sun moving relative to the earth [1-2]. See the Figure 1 and 2.

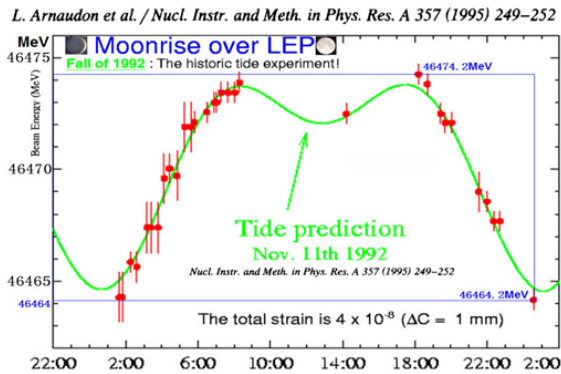


Figure 1: LEP Observation, see reference [1].

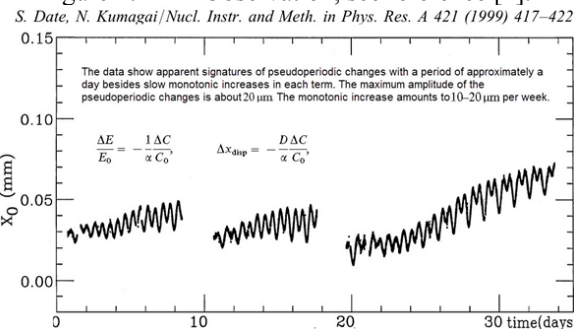


Figure 2: SPrng8 observation, see reference [2].

Phenomenology, we would assume that the gravity changes caused by the moon and sun moving at the storage ring have caused the beam energy changes in the storage ring [3].

$$\Delta E = \xi \cdot \Delta g \quad (1)$$

Which ΔE is the beam energy changes, caused by gravity changes Δg . If it is true, then it may be the electro-gravitational induction (EGI). We have discussed the possibility of EGI, and estimate the maximum value of the gravity coefficient of the induced electromotive force by using the existing beam data from the storage rings.

The EGI coefficient ξ is found to be less than $3.78 \text{ statcoul}^{-1} \cdot \text{m}^{-1} \cdot \text{kg} \cdot \text{sec}$. There is still a question of whether the value ξ actually exists or zero; we may be able to obtain a more accurate measurement from a setup with no feedback systems in place, that is, no beam energy compensation systems, beam orbit correction systems, and so on.

Furthermore, the EGI coefficient $\xi \leq 3.78 \text{ statcoul}^{-1} \cdot \text{m}^{-1} \cdot \text{kg} \cdot \text{sec}$ can also be formulated using the existing constants, G and κ_e :

$$\xi \leq 9.7 \times 10^{-4} \left(\frac{1}{c} \sqrt{\frac{\kappa_e}{G}} \right) \quad (2)$$

where G is the gravitational constant, κ_e is the dielectric constant, and c is the speed of light in a vacuum. From equation (6), we see that the resulting value of ξ would be less than that obtained above, if the EGI does in fact exist.

DISCUSSION

The changes of COD predicts by the EGI is in a same-phase transformation with the changes caused by the Newton tidal force. However, EGI, if exist, will affects the positive charged particle and negative charged particle in opposite way, one is accelerated and another is decelerated at same time, in same place. For example, if we have two same size rings, located in the same site of ground, one is electron ring another is positron ring, moving in same direction; we can measure the COD of these two similar storage rings respectively at same time, and noted as $\text{COD}_+(t)$ for the closed orbit distortion of the positive particles beam, $\text{COD}_-(t)$ for the negative particles beam, respectively. So we can obtain the $\Delta\text{COD}(t)$, $\Delta\text{COD}(t) = \text{COD}_+(t) - \text{COD}_-(t)$, see the Figure3. Therefore, $\Delta\text{COD}(t)$ signals will be independent on the terrestrial tidal force. So the effect of the EGI model will be $\Delta\text{COD}(t)/2$. Here, we must consider all the influence

* Work supported by the National Natural Science Foundation of China under Grant No. 11575215, partly.

† email address dongd@ihep.ac.cn

A PROPOSAL OF USING IMPROVED RHODOTRON AS A HIGH DOSE RATE MICRO-FOCUSED X-RAY SOURCE*

Xiaozhong He†, Liu Yang, Shuqing Liao, Wei Wang, Jidong Long, Jinshui Shi, Institute of Fluid Physics, Chinese Academy of Engineering Physics, Mianyang, China

Abstract

High energy X-ray computer tomography has wide application in industry, especially in quality control of complicated high-tech equipment. In many applications, higher spatial resolution is needed to discover smaller defects. Rhodotron have been used to produce high power CW electron beam in hundreds of kilowatts level. In this paper, we propose to use an improved Rhodotron to generate high brightness electron beam with high average power. Beam dynamics study shows that when producing tens of kilowatts electron beam, the normalized RMS emittance can be lower than 10 μm , and the relative RMS energy spread can be lower than 0.2%. The beam can be focused to a spot size of about 100 μm , and converted to X-Ray by using a rotating target within several kilowatts beam power. Improved Rhodotron proposed in this paper is a good candidate of X-ray source for high resolution high energy industrial CT systems.

INTRODUCTION

High energy industrial CT has shown to be of great value in the research and development of the high-end equipments (large locomotives, engines, nuclear weapons, etc.). But it is still urgent need for higher resolution to detect smaller defects in high-end equipments. To meet the needs, a micro-focused accelerator with high dose rate will be needed.

Traditional used accelerator used for this purpose is RF traveling or standing wave linear accelerator. There are many commercial companies such as VARIAN in American, GUHONG in China, providing linear accelerators for high energy CT inspection. The typical beam energy for high energy CT inspection is 9-15MeV, the dose rate for 9MeV is about 3000 Rad/min, and the X-ray spot size is about 1-2mm. There are also many micro-focused X-ray source products using a DC acceleration tube and a rotating target, the X-ray spot-size can be small as 0.2mm at the electron beam power of 750W and the beam energy of 750kV. For the CT inspection of large equipment with large aerial density, especially in the case of high resolution is needed, one need a X-ray source with high energy (not less than 9MeV), and with high dose rate (not less than 3000 Rad/min), and a very small spot size (not more than 0.2mm).

To generate micro-focused high dose rate X-ray, high brightness electron beam is needed. More specific, electron beam with high average power, low emittance and low energy spread is needed, so one can use a not so complicated focus system to get a small spot size such as 0.2mm. On other side, one should deal with the target

temperature rise when producing high dose rate X-ray at a very small spot size. Even use the rotating target system, high duty factor accelerator is needed to avoid the target melting problem.

Some type of accelerators such as Rhodotron [1-8], Rdigetron [9], Fabitron [10], can accelerate electron beam many times using the same RF structure, and can work at very high duty factor, and sometimes work at continuous wave mode. In this paper, it is proposed that using Rhodotron and a rotating target to generate a high dose rate micro-focused X-ray. A layout is shown in Figure 1. The Rhodotron is designed to produce high power electron beam with high brightness.

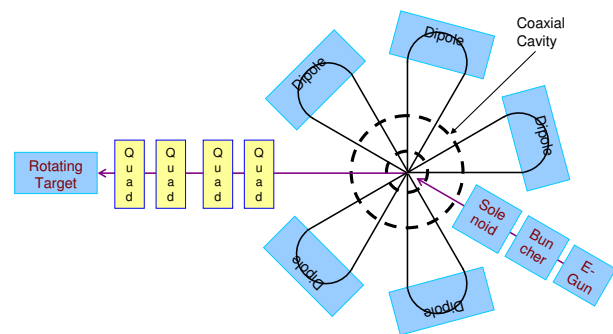


Figure 1: Layout of the proposed micro-focused X-ray source.

Main specification of the proposed micro-focus X-ray source is listed in Table 1.

Table 1: Main specifications of the proposed X-ray source.

Parameters	Value
electron beam energy	9 MeV
dose rate of X-ray at 1m from target	≥ 3000 Rad/min
X-ray spot size (FWHM)	$\leq 0.2\text{mm}$
time structure	10% duty factor, and at 100 Hz

PRELIMINARY BEAM DYNAMICS DESIGN

To generate the proposed dose rate, the needed average power of the electron beam is about 1kW. This value is far less than that has been achieved at high power Rhodotron, in which several hundreds of kW electron beam was produced. So the beam current in our design is relatively low, and the electron beam can be bunched to shorter phase width to acquire high brightness, and a smaller cathode can be used to archive smaller emittance. Additional to the buncher used in low energy section, the acceleration phases in the RF cavity are also chosen to

* Work supported by R&D PROJECT OF IFP/CAEP

† hexiaozhong@caep.cn

SPONTANEOUS RADIATION OF HIGH-ORDER MAGNETIC FIELD UNDULATOR

Tao Wei[†], Peng Li, China Academy of Engineering Physics, Mianyang, China
Joachim Pflueger, Yuhui Li, European XFEL GmbH, Schenefeld, Germany

Abstract

Based on the purpose of concision, nearly all the undulator radiation formulas have made an assumption that the guiding magnetic field is a sinusoid wave. The assumption is consistent with the truth if the ratio of undulator gap to period length is large enough. However, high-order magnetic field exists widely in most undulators, especially those with long period length and short gap. This paper will derive the radiation output equations of high-order magnetic field undulator, what's more, the formulas are validated through numerical simulation with code SPECTRA.

INTRODUCTION

The undulators have been widely used as insertion devices in synchrotron sources and free electron laser (FEL) to generate magnetic field which is periodic along the electron beam direction. The simplest case is the planar undulator which presents a sinusoid field perpendicular to the electron beam path. It is the most popular undulator model, the characteristic of its radiation have been discussed in many references [1, 2].

Taking into account a practical undulator, high-order magnetic field exists more or less. This paper will derive the far-field radiation of high-order planar undulator and discuss the influence of high-order magnetic field.

SPONTANEOUS RADIATION EQUATION

The magnetic field of planar undulator should be periodic along the beam direction, in addition, the integral of the magnetic field over a single period length vanished [3]. Without loss of generality, the planar undulator which contains high-order magnetic field can be described as

$$\vec{B} = \sum_{m=1}^{+\infty} B_m \sin(mk_u z - \delta\phi_m) \vec{e}_y. \quad (1)$$

In which $k_u = 2\pi/\lambda_u$, λ_u is the period length of undulator. To simplify the expression, the phase of fundamental magnetic field was chosen zero ($\delta\phi_1 = 0$).

The electron motion equation in the undulator can be described as

$$\gamma m_e \dot{\vec{v}} = -e\vec{v} \times \vec{B}. \quad (2)$$

This results in two coupled equations for the undulator with field distribution (1),

$$\dot{x} = \frac{e}{\gamma m_e} B_y \dot{z}, \quad \dot{z} = -\frac{e}{\gamma m_e} B_y \dot{x}. \quad (3)$$

In which m_e and e are the mass and charge of electron, γ

[†] email address: weitaocaep@qq.com

is the Lorentz factor, z-axis is the direction of electron beam moving forward. The formula (3) can be solved iteratively. To obtain the first-order motion solution we assume v_z keep constant ($v_z = \dot{z} \approx \bar{\beta}_s c$), in which $\bar{\beta}_s$ is the average velocity in the forward direction. For the case of high energy electron, $\bar{\beta}_s$ is infinitely close to 1, i.e. $\bar{\beta}_s \rightarrow 1$. Then $z \approx \bar{\beta}_s c t$ and the transverse component of electron trajectory is

$$x(t) \approx -\frac{ec}{\gamma m_e \omega_u^2} \sum_{m=1}^{+\infty} \frac{B_m \sin(m\omega_u t - \delta\phi_m)}{m^2}, \quad (4)$$

in which $\omega_u = \frac{k_u z}{t} \approx k_u c$. The relative transverse velocity is

$$\beta_x = \frac{v_x}{c} = \frac{\dot{x}(t)}{c} \approx -\frac{e}{\gamma m_e \omega_u} \sum_{m=1}^{+\infty} \frac{B_m \cos(m\omega_u t - \delta\phi_m)}{m}. \quad (5)$$

As the energy of the electron is fixed, the electron velocity β is also fixed. Therefore any variation in β_x must result in a corresponding change in β_s because of $\beta^2 = \beta_x^2 + \beta_s^2$. From this we have

$$\bar{\beta}_s \approx 1 - \frac{1}{2\gamma^2} - \frac{e^2}{4\gamma^2 m_e^2 c^2 k_u^2} \sum_{m=1}^{+\infty} \left(\frac{B_m}{m}\right)^2. \quad (6)$$

The fundamental radiation wavelength in the laboratory system [4] is thus

$$\lambda_r = \lambda_u (1 - \bar{\beta}_s \cos\vartheta) \approx \frac{\lambda_u}{2\gamma^2} \left\{ 1 + \frac{e^2}{2m_e^2 c^2 k_u^2} \sum_{m=1}^{+\infty} \left(\frac{B_m}{m}\right)^2 + \gamma^2 \vartheta^2 \right\}. \quad (7)$$

In which ϑ is the emission angle respect to the beam direction. Here we define the undulator parameter K as

$$K = \frac{e}{m_e c k_u} \sqrt{\sum_{m=1}^{+\infty} \left(\frac{B_m}{m}\right)^2}. \quad (8)$$

Then formula (7) returns to the familiar expression as

$$\lambda_r = \frac{\lambda_u}{2\gamma^2} \{1 + K^2/2 + \gamma^2 \vartheta^2\}. \quad (9)$$

Let's consider of the second-order motion solution,

$$\begin{aligned} \ddot{z} &= \frac{e^2 c}{\gamma^2 m_e^2 \omega_u} \sum_{j,k=1}^{+\infty} \frac{B_j B_k \sin(j\omega_u t - \delta\phi_j) \cos(k\omega_u t - \delta\phi_k)}{k} \\ &= \frac{e^2 c}{2\gamma^2 m_e^2 \omega_u} \left[\sum_{j,k} \frac{B_j B_k \sin(j\omega_u t + k\omega_u t - \delta\phi_j - \delta\phi_k)}{k} \right. \\ &\quad \left. + \sum_{j,k} \frac{B_j B_k \sin(j\omega_u t - k\omega_u t - \delta\phi_j + \delta\phi_k)}{k} \right]. \quad (10) \end{aligned}$$

ELECTRON COOLING OF BUNCHED ION BEAM IN STORAGE RING *

Lijun Mao[†], He Zhao, Meitang Tang, Jie Li, Xiaoming Ma, Xiaodong Yang, Jiancheng Yang
Insitute of Modern Physics, Lanzhou, China

Abstract

A combination of electron cooling and RF system is an effective method to compress the beam bunch length in storage rings. Bunched ion beam cooling experiments have been carried out in the main cooling storage ring (CSRm) of the Heavy Ion Research Facility in Lanzhou (HIRFL), to investigate the minimum bunch length obtained by the cooling method, and study the dependence of the minimum bunch length on beam and machine parameters. It is observed that the IBS effect is dominant for low intensity beams, and the space charge effect is much more important for high intensity beams. The experimental results in CSRm shown a good agreement with the analytical model in the IBS dominated regime. Meanwhile, the simulation work offers us comparable results to those from the analytical model both in IBS dominated and space charge dominated regimes.

INTRODUCTION

The HIRFL accelerator complex is a multipurpose research facility for nuclear physics, atomic physics and applied research in medicine, biology and materials science. It consists of two cyclotrons, two storage rings and several experimental terminals[1]. Two electron coolers installed in the storage rings CSRm and CSRe (experimental Cooling Storage Ring) are applied to the stored ion beams for the phase space compression. The electron coolers were designed and manufactured in the cooperation between IMP China and BINP Russian[2]. The layout of HIRFL accelerator complex is shown in Fig. 1.

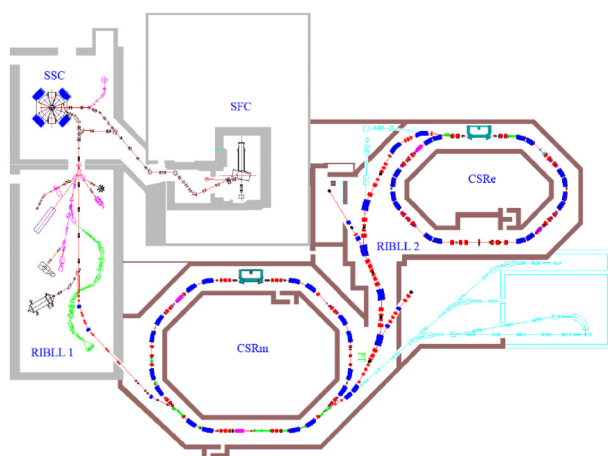


Figure 1: Layout of HIRFL accelerator complex.

Electron cooling is a powerful method for shrinking the size, the divergence and the momentum spread of stored charged-particle beams in storage rings for precision experiments. It also supports beam manipulations involving RF system to provide beam with short bunch length. Short-bunched ion beam has a wide range of application in rare isotope production, high energy density physics experiment, collider and cancer therapy. In order to study the cooling process of bunched ion beam, a series of experiments have been done in several cooling storage rings, such as HIMAC, ESR, IUCF and CSRe[3-5]. The results shown that the minimum bunch length of cooled-beam is affected by the equilibrium between electron cooling, IBS effect, ion beam space charge field and RF voltage, but the dependence of the minimum bunch length on the beam parameters has a slight difference in those experiments.

In this paper, we present the recent experimental results which was done at CSRm, and compare with the simulation results based on the multi-particle tracking method. Bothe experimental and simulated results shown a good agreement with the analytical model.

BUNCH LENGTH MEASUREMENT

The experiments were performed with $^{112}\text{Sn}^{36+}$ beam at the energy of 3.7 MeV/u and $^{12}\text{C}^{6+}$ beam at the energy of 6.9 MeV/u, respectively. The range of stored particle number was from 10^6 to 10^9 . A flat distribution electron beam with diameter around 50 mm was used for beam cooling. The electron beam current was set as 135 mA for $^{112}\text{Sn}^{36+}$ beam and 44 mA for $^{12}\text{C}^{6+}$ beam, respectively. A sinusoidal RF voltage from 0.2 to 2.3 kV was applied with the harmonic number of 2.

A typical experimental cycle is as follow: heavy ions are injected, accumulated and cooled with the help of continuous electron beam, and then a sinusoidal RF voltage is switched on with 2nd harmonic number of revolution frequency. The bunch length after 2 seconds of turning on the RF system is measured by a position pick up with the length of 150 mm and the capacitor of 120 pF. The voltage drop at a 50 Ohms resistor between the pick up and ground is amplified by a pre-amplifier with the gain factor of 54 dB. An oscilloscope with bandwidth of 1 GHz is used to read the signal from the pre-amplifier. A RMS bunch length value is evaluated from a Fokker-Plank fitting result of this voltage signal. As an example, a measurement of the voltage signal from pick up for $^{112}\text{Sn}^{36+}$ beam is shown in Fig. 2. In this case, the beam longitudinal linear charge density is obtained by the integration of the pick up voltage signal. The RMS bunch length σ_t is evaluated by the Fokker Plank fitting result of the bunch shape data.

* Work supported by National Natural Science Foundation of China No. 11575264, No. 11375245, No. 11475235 and the Hundred Talents Project of the Chinese Academy of Sciences
[†] email address: maolijun@impcas.ac.cn

RESONANCE STOP-BANDS COMPENSATION FOR THE BOOSTER RING AT HIAF*

J. Li[†], J. C. Yang, HIAF design group, Institute of Modern Physics, CAS, Lanzhou, China

Abstract

The Booster Ring (BRing) of the new approved High Intensity heavy-ion Accelerator Facility (HIAF) in China is designed to stack $1.0 \cdot 10^{11}$ number of $^{238}\text{U}^{35+}$ ions at the injection energy of 17 MeV/u and deliver over such intensity beam to SRing (Spectrometer Ring) at 800 MeV/u. However such intensity beam causes low-order resonances crossing during RF bunching. To keep a low beam loss, resonance stop-band compensation scheme is proposed covering the process from RF capture to the first stage of acceleration below 200 MeV/u.

INTRODUCTION

Layout of the HIAF

The High Intensity heavy-ion Accelerator Facility (HIAF) is a new heavy ion accelerator complex under detailed design by Institute of Modern Physics [1]. Two typical particles of $^{238}\text{U}^{35+}$ and proton is considered in the design. The beam is generated by a Superconducting Electron Cyclotron Resonance (SECR) ion source or an intense proton source, and accelerated mainly by an ion linear accelerator (iLinac) and an booster ring (BRing). The iLinac is designed to deliver H_2^+ at 48 MeV and $^{238}\text{U}^{35+}$ at 17 MeV/u. Before entering the BRing, H_2^+ is stripped to proton, and then accumulated by two-plane painting and accelerated to 9.3 GeV. The $^{238}\text{U}^{35+}$ is injected by multi-turn two-plane painting scheme, after accumulation or cooling by a electron cooler at the BRing, then accelerated to 0.2-0.8 GeV/u for extraction. After being stripped at the HIAF FRagment Separator (HFRS), the secondary beam like $^{238}\text{U}^{92+}$ is injected to the Spectrometer Ring (SRing) for the high precision physics experiments. Besides, five external target stations of T1 - T5 is planned for nuclear and atomic experimental researches with the energy range from 5.8-800 MeV/u for uranium beam.

Overview of the BRing

The BRing is designed to accumulate beam intensity up to space charge limit at the injection energy and deliver over $1.0 \cdot 10^{11}$ $^{238}\text{U}^{35+}$ ions or $1.0 \cdot 10^{12}$ proton to SRing in extraction. Two operation modes of fast and slow are considered. Fast mode features multi-turn two-plane painting injection within around 120 revolution turns whereas the slow one by over 10 s injection time for electron cooling helped accumulation. Main parameters of the BRing are listed in Table 1. The BRing has a three-folding symmetry lattice around its circumference of 549.45 m. Each super-period consists of

an eight-FODO-like arc and an over 70 m long dispersion-free straight section featured with a length of 15.7 m drift reserved for electron cooler, two-plane painting injection, or RF cavities. Lattice layout of the BRing for one super-period is shown in Fig. 1.

Table 1: Main Parameters of $^{238}\text{U}^{35+}$ at the BRing

Circumference	549.45 m
Max. magnetic rigidity	34 Tm
Periodicity	3
Injection energy	17 MeV/u
Betatron tune	(8.45, 8.43)
Acceptance ($H/V, \delta p/p$)	$200/100\pi\text{mmrad}, \pm 5.0\%$

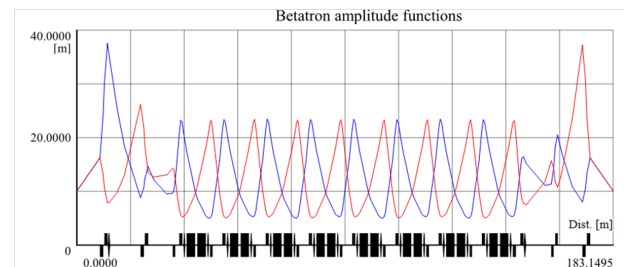


Figure 1: BRing lattice for one super-period.

RESONANCE AND STOP-BANDS

Betatron Resonances

The charged particle beam produces repulsive force and results in depressed tune distribution in tune diagram. During the injection and accumulation process of $^{238}\text{U}^{35+}$ beam at the BRing, the nominal working point is set as (8.45, 8.43) with safety distance from dangerous low order structure resonances e.g., $2Q_y - Q_x = 9$ and $2Q_x - Q_y = 9$. The only structure resonances appear in Fig. 2 are four 4th-order ones shown as pink lines. They will be ignored due to weak effect considering the operation experiences. Thus, no structure resonances will be considered at our case.

The tune spread of $^{238}\text{U}^{35+}$ at the design intensity of $1.0 \cdot 10^{11}$ is shown in Fig. 2 as the blue dots when the transverse emittance equals to acceptance. The red dots give the spread information of cooled beam when the emittance is decreased to $50/50\pi\text{mmrad}$ [2]. For the two cases above, the uranium beam has a momentum spread of $\pm 2.0\%$ and bunching factor of 0.4 after RF capture. The design intensity produces a vertical tune spread about 0.16 for $200/100\pi\text{mmrad}$ and 0.33 for the cooled beam. The figure also indicates an overlapping of tune spread with four 3rd-order betatron resonances and a linear coupling difference resonance at the both situation. The overlapping of tune

* Work supported by NSFC (Grant No. 11475235, 11375245, 11575264)

[†] lijie@impcas.ac.cn

Content from this work may be used under the terms of the CC BY 3.0 licence (© 2017). Any distribution of this work must maintain attribution to the author(s), title of the work, publisher, and DOI.

MAGNETIC MEASUREMENT OF THE UNDULATOR U38 FOR THz-FEL

L. G. Yan, D. R. Deng, P. Li, J. X. Wang, H. Zhang, M. Li, X. F. Yang

Institute of Applied Electronics, China Academy of Engineering and Physics, Mianyang, China

Abstract

The high average power terahertz free electronic laser facility (THz-FEL) has one undulator named U38. As one of the most important components, U38 has a significant effect on entire facility. So, we measure the magnetic field of U38 to confirm its field qualities using magnetic field measurement bench before installation. The measurement gaps include 19 mm, 21 mm, 24 mm, 25.6 mm and 28 mm, and the longitudinal distribution of magnetic field on five lines at transverse positions of -6 mm, -3 mm, 0 mm, 3 mm and 6 mm are scanned. Electronic trajectory, peak field vs gap curve and peak-to-peak error are calculated based on the longitudinal distribution of magnetic field. We also measure the transverse distribution of magnetic field to test the good field region. In this proceeding, the measurement method is described and the results are presented and discussed.

INTRODUCTION

The high average power terahertz source at CAEP (China Academy of Engineering Physics) is based on the routine of free electronic laser (FEL), which will output with the average power 10 W between the range of 100-300 μm . Undulator is one of the most important components in FEL and has a significant effect on spontaneous radiation, gain and saturation [1,2]. THz-FEL has one undulator named U38, which is manufactured by SINAP (Shanghai Institute of Applied Physics) at Shanghai. The magnetic structure of U38 consists of two standard Halbach-type permanent magnet arrays with period length 38 mm and gap range of 18-32 mm, which can generate max peak field of 0.55 T. Some errors must be decreased, such as peak-to-peak error (<1%), center trajectory deviation (<0.1 mm) and deviation error in 12 mm good field region (<0.5%) [3]. Before installation, it is indispensable to measure and characterize the magnetic field of U38 precisely in order to achieve high magnetic performances. In 2017, U38 is measured at Chengdu using magnetic field measurement bench. In this proceeding, the measurement method is described and the results are presented and discussed.

INSTRUMENT AND METHOD

A magnetic field measurement bench (MFMB) has been constructed to confirm the field qualities of U38, which transports Hall probe through the undulator straightly and precisely. The figure 1 shows the measure-

ment site. The total length of MFMB is 3 m, which is enough to measure 1.64-m-long U38. Positioning errors of MFMB are better than 10 μm in all three moving axis, which limits errors in the probe motion through the undulator and in turn decreases measurement errors. Before measurement, the rough alignment is done by laser tracker to parallel the three center planes of MFMB and U38, and then the fine alignment is done by measuring and analyzing the magnetic field in horizontal and vertical plane to fix the position of Hall probe in U38. MFMB works on go-stop mode with step length of 0.5 mm and pause time of 0.5 s. Local magnetic field is acquired by Bell 8030 that is a three dimensions Gaussmeter with accuracy of $\pm 0.05\%$. The room temperature is controlled within 23 ± 0.5 $^{\circ}\text{C}$ to minimize the field variation of U38 and ensure an acceptable stability of the MFMB.

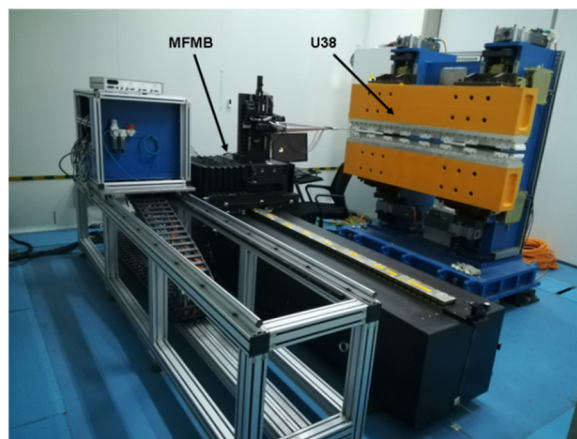


Figure 1: Measurement site.

RESULTS AND DISCUSSION

The vertical component of earth field in our lab is about 0.3 Gs. It is known a small field can influence undulating field obviously and then damage the straightness of trajectory. So, there is a long coil on both of upper and lower beam to cancel the residual dipole field and earth field in gap. In the following data, if not specified, the optimal current has been applied on the long coil.

The measurement gaps include 19 mm, 21 mm, 24 mm, 25.6 mm and 28 mm. We scan five lines in the transverse position from 6 mm to -6 mm with step length of 3 mm along the U38 at every gap. The total measurement points are 4600, which correspond to a measurement distance of 2.3 m. The margin length on both sides is 0.33 m.

BEAM LOSS SIMULATION AND GAS DESORPTION MEASUREMENT FOR HIAF*

P. Li, J[†]C. Yang, Z.Q. Dong, W.H. Zheng, W.J. Xie, J.J. Chang, X.J. Liu, M. Li, Y.J. Yuan,
 J. Meng, CH. Luo, R.S. Mao, W.L. Li

Institute of Modern Physics, Chinese Academy of Sciences, Lanzhou, China

Abstract

Large dynamic vacuum pressure rises of orders of magnitude which caused by the lost heavy ions can seriously limit the ion intensity and beam lifetime of the intermediate charge state heavy ion accelerator. The High Intensity heavy ion Accelerator Facility (HIAF) which will be built by the IMP will accumulate the intermediate charge state ion $^{238}\text{U}^{35+}$ to intensity 3×10^{10} ppp to different terminals for nuclear physics, nuclear astrophysics and so on. In order to control the dynamic vacuum effects induced by the lose beams and design the collimation system for the BRing of the HIAF, a newly developed dynamic vacuum simulation program is conducted to optimize the collimation efficiency. Furthermore, two dedicated desorption measurement setups have been established at the terminal of the CSRm and 320 kV HV platform to study the molecular desorption process and do the benchmarking of the simulation code. This presentation will describe the collimation efficiency optimization, measurement results with Sn beam at the CSRm and with the Xe beam in the HV platform.

INTRODUCTION

The HIAF project consists of ion sources, Linac accelerator, synchrotrons and several experimental terminals. The Superconducting Electron-Cyclotron-Resonance ion source (SECR) is used to provide highly charged ion beams, and the Lanzhou Intense Proton Source (LIPS) is used to provide H_2^+ beam. The superconducting ion Linac accelerator (iLinac) is designed to accelerate ions with the charge-mass ratio $Z/A=1/7$ (e.g. $^{238}\text{U}^{35+}$) to the energy of 17 MeV/u. Ions provided by iLinac will be cooled, accumulated and accelerated to the required intensity and energy (up to 3×10^{10} and 800 MeV/u of $^{238}\text{U}^{35+}$) in the Booster Ring (BRing), then fast extracted and transferred either to the external targets or the Spectrometer Ring (SRing) [1].

The intermediate charge state $^{238}\text{U}^{35+}$ has been chosen as the reference ion for the facility HIAF. Intermediate charge state particles are much easier lost when they collide with the rest gas atoms and change to other charge states. The resulting change in the mass over charge ratio m/q leads to modified trajectories in dispersive beam transport elements, and finally to the loss of the particle at the vacuum chamber. Secondary particles are produced at the impact position by ion-induced desorption and as a result the pressure in the vacuum chamber is increased locally. This local

rise in pressure enhances the charge changing processes, and at extremely bad conditions, it can cause an avalanche process resulting in a complete loss of the beam during a few turns in the synchrotron. The layout of the HIAF project is shown in Fig. 1.



Figure 1: Layout of HIAF project.

BRING COLLIMATION EFFICIENCY

The Booster Ring (BRing) of the HIAF project has a threefold- and mirror-symmetric lattice over its circumference of 530.8 m. Each super period consists of 8 DF structure arc and FODO straight sections. Beam loss distribution is calculated by the new developed simulation program.

In order to simulate the charge exchange driven beam loss and dynamic vacuum effects in heavy ion synchrotrons, a new program package (ColBeam) designed for optimizing the collimation efficiency is developed by taking different types of errors into account in the accelerator [2].

The particles can be tracked in a ring during multiple turns or in a beamline just one-pass. Firstly the software package must load a lattice file which contains essential element parameters of the ring or beamline, such as element type, length, strength, vacuum chamber aperture and so on. The lattice file with extension "LAT" for the simulation software Winagile [3] is used as the default input file.

More than thirty lattices for the BRing have been simulated and the collimation efficiency was optimized. Collimation efficiency is defined as the ration of the particles hitting the collimators N_c and the wall N_w .

$$\theta = \frac{N_c}{N_w + N_c} \quad (1)$$

The final accepted lattice is the DF structure and its collimation efficiency is 100% according to the simulation result. With a constant vacuum pressure around the ring, the

* Work supported by National Natural Science Foundation of China (11675235) and Youth Innovation Promotion Association of Chinese Academy of Sciences 2016364.

[†] Email address LIPENG@IMP.CAS.AC.CN

NUMERICAL ASSESSMENT OF BEAM DIAGNOSTIC CALORIMETER FOR EAST NEUTRAL BEAM INJECTOR*

Yongjian Xu, Chundong Hu, Yahong Xie, Yuanlai Xie, Ling Yu, Lizhen Liang†
Institute of Plasma Physics, Chinese Academy of Sciences, Hefei, China

Abstract

Neutral beam injection is one of the most effective means of plasma heating and has been also verified to be applicable for current driving. In order to support the physical research of EAST, two neutral beam injectors (NBI, 80keV, 4 MW) have been developed and constructed in Institute of Plasma Physics, CAS. In order to evaluate beam intensity distribution and divergence, a moveable sophisticated copper short-pulse beam diagnostic calorimeter is designed and installed on the NBI test stand. In this article, the structure of calorimeter, the operating parameters are introduced. The new diagnostic calorimeter plate bombarded by the beam adopts blocking design and there is no heat transfer between adjacent block. Thermocouples are installed into the block, so the temperature can be measured precisely. Based on the data obtained by thermocouples, the beam pattern can be plotted. In order to ensure the diagnostic calorimeter work safely, the operating parameters are explored using FEM. As a new beam diagnostic calorimeter, it solves the problem of mutual interference due to the heat transfer of each block, it can give more precise beam property comparing with the present calorimeter.

INTRODUCTION

Neutral beam injection is one of the most effective means of plasma heating and has been also verified to be applicable for current driving [1-5]. In order to support the physical research of the Experiment Advanced Superconductive Tokamak (EAST), two identical neutral beam injectors (NBI, 80 keV, 4 MW) have been developed and constructed in Institute of Plasma Physics, Chinese Academy of Sciences [6-11]. In order to evaluate more precisely the beam intensity distribution, divergence and uniformity [12-16], a moveable sophisticated copper short-pulse beam diagnostic calorimeter is designed and installed on the NBI test stand. The new diagnostic calorimeter plate bombarded by the beam adopts blocking design and there is no heat transfer between adjacent block. Thermocouples are installed into the block, so the temperature can be measured precisely. Based on the data obtained by thermocouples, the beam pattern, divergence can be obtained. Considering the limitation of the heat exchange capacity, the diagnostics calorimeter only works in short-pulse mode, in order to determine the operation parameter, the diagnostics calorimeter is analyzed by FEM. In this article, the structure of calorimeter, the pri-

mary simulation results are introduced. Simulation results give the maximum operation pulse length at different beam energy.

As a new beam diagnostic calorimeter, it solves the problem of mutual interference due to the heat transfer of each block. Comparing with the present calorimeter, it can give more precise beam property.

SIMULATION AND ANALYSIS

Layout and Design of Diagnostics Calorimeter

Short-Pulse beam diagnostic calorimeter is installed between the gas baffle and bending magnet. Diagnostic calorimeter can be moved left and right under the traction of steel cable (see Fig.1). The diagnostic calorimeter will be moved out of beam channel during long pulse beam extraction.

The diagnostic calorimeter is designed to be operated inertially. It is made of a cooling back plate with a cooling circuit and 5×19 copper blocks which are brazed on the "beam side". Each block is inertially cooled via small cooling channels in the back plate and through a small $\varnothing 10 \text{ mm} \times 2 \text{ mm}$ copper cylinder that acts as a thermal resistance between cooling plate and block. Each block has a surface of $30 \text{ mm} \times 30 \text{ mm}$ and a thickness of 25 mm. Each block is separated from adjacent blocks by a 2 mm gap (see Fig.2). With this solution the transversal heat transmission between blocks during the beam phase is practically negligible. 34 sheath thermocouples (K-Type) are used for temperature measure of the calorimeter (see Fig.3). The embedded thermocouples are positioned at half depth (12.5 mm) of a block (which is 25 mm thick) in order to provide a good assessment of the average block temperature. According to the temperature rise of the blocks, the beam profile in vertical and horizontal direction can be obtained.

FEM Analysis of Diagnostics Calorimeter

The incidence angle of the beam on the calorimeter is supposed to be 90° . The simulations have been performed with pulse length 1s, heat flux 10 MW/m^2 (uniform distribution). The flow rate of cooling water is 2m/s and the origin temperature is 293K. The thermal radiation between the adjacent blocks is ignored. The model is shown in Fig.4.

Relationship between Inclination Angle and Surface Temperature of Block In order to decrease thermal radiation between the adjacent blocks, the block is designed as regular hexahedron (see Fig.5a). For the difference of heat transfer path, there is a big gap between edge and center (see Figs.5b, 5c) with the change of inclination angle α . As the softening temperature of the material of

* Work supported by the National Natural Science Foundation of China (NNSFC) (Contract No. 11575240) and the Foundation of ASIPP (Contract No. DSJJ-15-GC03)

† Email: address: lzliang@ipp.ac.cn

ELECTROMAGNETIC, THERMAL, STRUCTURAL ANALYSIS FOR THE RF-CAVITY OF A RHODOTRON ACCELERATOR *

L. Yang[†], X. Z. He, H. Li, Institute of Fluid Physics, CAEP, Mianyang, Sichuan, China

Abstract

A Rhodotron-based electron accelerator served as micro-focused X-ray source at a high repetition rate of 10.75 MHz is proposed at IFP, CAEP. The RF-cavity, running in long pulse/ CW mode, will deliver 9 MeV energy gain to the charged beam at the exit by taking its advantage of multiple accelerations with the same field at a frequency of 107.5MHz. A substantial amount of power loss will be dissipated on the RF surface of the cavity within beam time. Further electromagnetic (EM) optimization was performed on a standard coaxial model with slight modifications aiming to achieve a higher shunt impedance, thus less power loss on surfaces. A proper water cooling design is still required to prevent large scale temperature rise on the cavity wall. The corresponding effects on cavity mechanical stability and resonant frequency shifting are concerned. This paper will present the details in the EM, thermal, structural analysis of the RF-cavity.

INTRODUCTION

Rhodotron, as a kind of compact electron accelerator with high efficiency of energy transfer to charged beams, has been widely employed to generate X-ray for industrial irradiation since the concept of multiple accelerations in the same field supplied by a half wave resonator (HWR) was raised by J. Pottier [1]. With several bend magnets azimuthally surrounding to an HWR, Electron beams could re-entry into the cavity and be re-accelerated at each time passing through a bend. A schematic view is shown in Figure 1. A high energy in the order of 10MeV which well meets the energy level of industrial irradiation sources, could be achieved with a relatively low field intensity. Hence long-pulse mode with large duty factor and fully continuous wave mode (CW) at an acceptable power loss level $\sim 100\text{kW}$ are applicable and not often seen in normal conducting electron accelerators. Variable designs but in the same principle could be referred in these literatures [2-5]. We propose a micro-focused X-ray source at a high repetition rate of 10.75 MHz by adopting a 107.5MHz Rhodotron being able to accelerate electron beams with initial energy 40keV up to 9 MeV after 10 times across. Great efforts have been put on the beam dynamics design to form a 0.2 mm beam spot at the target location other than a typical size of 2 mm for normal industrial CT machines, which in details is documented in the paper ([6] A proposal of using improved Rhodotron as a high dose rate micro-focused X-ray source) of this conference. This paper is focusing on some specific cavity design issues.

One important thing should be carefully concerned is water cooling for CW running mode or high duty cycle

mode. Large surface loss density in an order of 10^6 w/cm^2 is concentrated on the areas at the strong magnetic field zone considering OFC material being penetrated by RF field. Since the cavity body will be made out of stainless steel with OFC coated on the inner surface, the high surface loss density areas should be fully covered by forced water where efficient heat convection would occur. With the known heat convection status, one can perform the thermal analysis in those commonly used FEA codes to predict the steady temperature pattern over the cavity wall, which is of an important body load for the subsequent structural analysis and coupled thermal induced frequency drift estimation. The heat convection coefficient regarding to normal water cooling problems with regular meanders and uniform heat flux has been well developed in theory and usually adopted by the thermal simulations for normal conducting RF guns, cavities [7-8]. In our case, however, the heat convection highly depends on the local heat flux and varied fluid field due to the non-regular cavity geometry, therefore theoretical approximation is too roughly to calculate the distribution of heat convection coefficient. Thanks to the heat transfer enabled fluent package in ANSYS [9], the heat convection is internally computed and coupled with fluid calculation. The data mapping technology in Workbench allows load import between different physics fields that even don't share the same mesh and node pattern. By taking such advantages, we have done a complete coupled EM, thermal, fluid and structural simulation during the cavity design stage, which along with EM optimization will be presented in following sections.

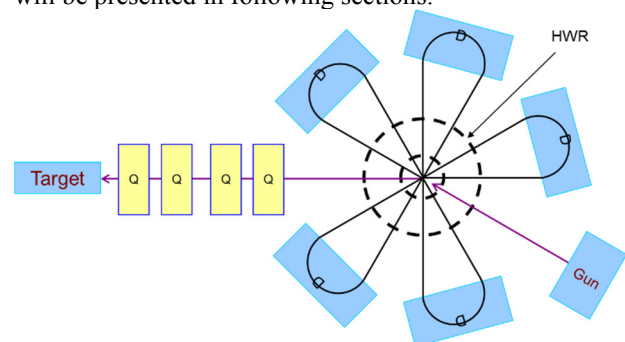


Figure 1: Layout of a Rhodotron.

EM OPTIMIZATION

EM optimization started with a standard initial coaxial line model resonating at the targeting frequency 107.5MHz. The outer conductor diameter D was set to 1.6m in order to keep an appropriate room for installing beam diagnostic elements on the beam line section between the cavity and the bend magnets. The inner conductor diameter d was defined to $0.25D$ where reaches the maximum shunt impedance by taking the transit time effect into account. A further optimization step with a

* Work supported by R&D project of IFP/CAEP

[†] yyperf57@163.com

REDUNDANCY ANALYSIS OF SOLID-STATE AMPLIFIERS FOR CIADS ACCELERATOR *

Penghui Gao[†], Zhijun Wang, Institute of Modern Physics, CAS, Lanzhou, China
Yi Xiong, Beijing BBEF Science and Technology Co., Ltd, Beijing, China
Yuan He, Yuanshuai Qin, Weiping Dou, Shuhui Liu, Wangsheng Wang, Weilong Chen, Huan Jia, Peiyong Jiang, Chi Feng, Yongzhi Jia, Chao Wang, Haoye Wang, Institute of Modern Physics, CAS, Lanzhou, China

Abstract

The solid-state amplifier(SSA) will be applied in China Initial Accelerator Driven System (CiADS) accelerator. 20KW SSA is the basis of RF power systems. With considering power loss redundancy of the main amplifier(MA) is analyzed by building k/N reliability model for various redundancy. 26/30 redundancy is optimal for 20KW SSA in term of reliability.

INTRODUCTION

The solid-state amplifier has proved to be quite reliable as well as easy maintenance compared to tetrode and klystron, so it will satisfy high availability of CiADS accelerator. CiADS amplifiers have four types: 20KW, 40KW, 60KW and 80KW [1] and they are combined by 20KW SSA.

Redundancy of SSA is analyzed by the fault tree(FT) model in IFMIF [2]. However, power loss is not considered and causes a large effect for availability analysis.

With considering power loss, k/n RBD model of MA is built and MTBF of various redundancy is calculated in this paper.

THE PRICIPLE OF 20KW SSA

20KW SSA is composed by RF chain, central control, the cooling system and power assembly. There are many components, such as limiter, attenuator, RF switch, 1:6 splitter, pre-amplifier which has six 50W-SSA, 6:1 combiner, 1:22 splitter, the main amplifier that has twenty-two 1KW-SSA, 22:1 combiner and coupler in RF chain. As is shown in Figure 1. The cooling system includes cooling pipe, pump and flowmeter. Central control is combined by an industrial computer and monitoring circuits.

Low level radio frequency(LLRF) transmit a signal to limiter which discriminates range of amplitude. Attenuator can amplifying signal and RF switch controls signal output. Small power amplifys to 20KW through the pre-amplifier and MA. The data that coupler monitors the power is transmitted to central control which gives commands to every component. The cooling system cools large-power components and power assembly complishes 220V or 380V conversion.

* Work supported by Strategic Priority Research Program-Future Advanced Nuclear Fission Energy (Grant No. Y102070ADS)

[†] gaoph2016@impcas.ac.cn

K/N RBD MODEL OF MA

Component Definition

Component definition is different between physical model and RBD model. 20KW SSA is composed by components such as input control, splitter, the pre-amplifier, combiner, equivalent splitter, 1KW SSA, equivalent combiner, the cooling system and central control in RBD model. Here concepts of equivalent splitter and combiner are put forward to solve redundancy analysis of MA. If one 1KW-SSA is wrong, 20KW SSA which has twenty-two 1KW-SSA can not output rated power. If MA has twenty-four 1KW-SSA, 20KW SSA can tolerate one 1KW-SSA is wrong. Styles of splitting and combining which are different for various redundancy are unified with concepts of equivalent splitter and combiner and it will not affect reliability analysis.

Redundancy Analysis of MA

Insertion loss of equivalent combiner and equivalent splitter is 0.4dB. If guaranteeing P_o of SSA output is 20 KW, P_m of the main amplifier must equal 21.93KW according to the equation(1).

$$10 * \lg(P_m/P_o) = 0.4 \quad (1)$$

(P_m-P_o) is insertion loss of equivalent combiner. If the power source outputs 20KW, MA at least needs twenty-two 1KW-SSA. This situation is no redundancy. Any amplifier which is fault can cause the fault of the power source. If applying more than 22 amplifiers, the power source could tolerate one or a few amplifiers which are fault. However, in this case inconsistency of amplitude and phase will bring about additional power loss. N represents the number of total amplifiers and n represents the most number of amplifiers that are wrong. And $k=N-n$. We can calculate P_m according to equation(2) and equation(3). P_i represents the power output of k amplifiers. Different redundancy is as followed table1.

$$P_i = P_o * (N/(N - n))^2 \quad (2)$$

$$10 * \lg(P_m/P_i) = 0.4 \quad (3)$$

In conclusion, 24 amplifiers can tolerate at most one which is fault. 26 amplifiers can tolerate at most two which are fault. 32 amplifiers can tolerate at most five which are fault. k/N RBD model of MA is as followed Figure 2.

Content from this work may be used under the terms of the CC BY 3.0 licence (© 2017). Any distribution of this work must maintain attribution to the author(s), title of the work, publisher, and DOI.

BUNCH LENGTH MEASUREMENT SYSTEM FOR 500 kV PHOTOCATHODE DC GUN AT IHEP

O. Z. Xiao¹, J. R. Zhang, X. P. Li, X.J.Wang, D.R.Sun

Institute of High Energy Physics, Chinese Academy of Sciences, Beijing, China

¹also at Key Laboratory of Particle Acceleration Physics and Technology, Institute of High Energy Physics, Chinese Academy of Sciences, Beijing, China

Abstract

In September of 2011, a 500 kV photocathode DC gun was proposed for FEL-ERL two purpose facility at Institute of High Energy Physics (IHEP). So far, the whole system has been installed and the preliminary high voltage conditioning has been carried out. Since the photocathode response time influence the beam quality, the bunch length measurement system is required, which consist of a solenoid, a 1.3 GHz standing wave deflecting cavity, a slit and a YAG screen. In this paper, the design of a deflecting cavity with TM₂₁₀ mode is presented. In addition, the beam dynamics study of the bunch measurement system is performed using ASTRA and the layout of the bunch measurement system is determined. The bunch length in simulation is in good agreement with theoretical calculation.

INTRODUCTION

High voltage DC electron guns based on GaAs photocathode are proposed for energy recovery linac and free electron laser in many laboratories around the world. Compared with RF guns, DC guns can produce high average current beam with low emittance and operate at CW mode. As a key technology for future advanced light source, the R&D of photocathode dc electron gun was supported at IHEP in 2012. So far, the construction of the DC gun had been completed and a preliminary high voltage conditioning was carried out up to 440 kV [1]. The performance of photocathode depends on many factors such as cathode material, the preparation and activation condition, which will influence the beam parameter. For example, the photocathode with slow response time will generate a long tail compared with laser pulse width, which will cause the emittance growth. For this reason, a bunch length and longitudinal profile measurement system based on deflecting cavity is essential to investigate cathode property.

BUNCH LENGTH MEASUREMENT SYSTEM DESIGN

To reduce the space charge effect in the gun region, the laser pulse illuminating the photocathode is necessary to shape and extend to tens of picoseconds. In our case, the laser pulse is like plateau distribution with flat top of 20 ps and rise and fall time each of 2 ps. The beam longitudinal distribution is almost the same as the laser pulse when the photocathode response time is rapid. In order to study the properties of photocathode, a bunch length measurement system is proposed, which includes a solenoid, a 1.3 GHz standing wave deflecting cavity, a slit and a YAG screen. The deflecting cavity is 1.15 m away from the cathode of

the electron gun. A YAG screen to measure the transverse beam profile is put at downstream of 1.4 m from deflecting cavity. To improve the resolution length of measurement, a solenoid after the gun and a slit before the deflecting cavity are used to reduce the horizontal beam size. The resolution length determine the measurement accuracy, which is defined as

$$L_{res_t} = \frac{\sigma_{x0}(E/e)}{wV_{def}L} \quad (1)$$

Where σ_{x0} is the horizontal beam size at screen with deflecting cavity turn-off, E is the beam energy, V_{def} is the deflecting voltage, w is the circular frequency of cavity. The layout of the bunch measurement system is shown in Fig. 1.

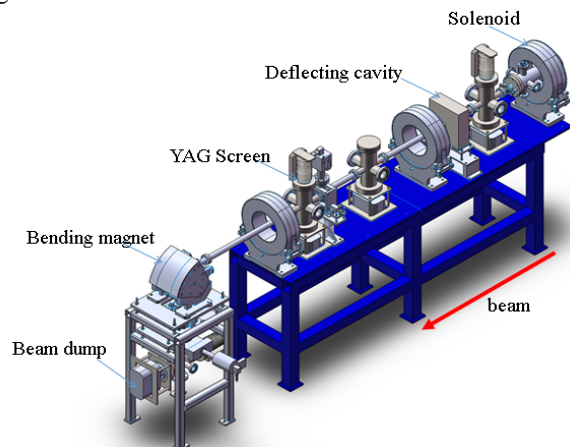


Figure 1: The layout of the bunch measurement system.

The parameters of the bunch measurement system are presented in Table 1. Using these parameters, the relation between the resolution length and the input power is shown in Fig. 2.

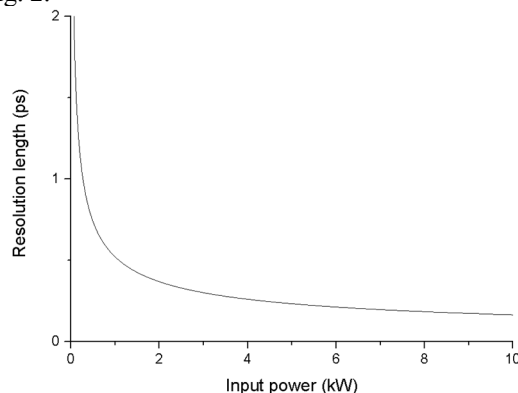


Figure 2: The relation between the resolution length and the input power.

EXPERIMENTAL POLARIZATION CONTROL OF THOMSON SCATTERING X-RAY SOURCE

Zhang Hongze[†]

Tsinghua University, Beijing, China

Abstract

Thomson scattering of intense laser pulses from relativistic electrons allows us to generate high-brightness and tunable-polarization X/ γ -ray pulses. In this paper, we demonstrate the polarization control of the Thomson scattering source experimentally. We control the incident laser polarization by rotating a quarter-wave plate, thus controlling X/ γ -ray polarization. In order to measure the polarization, we use Compton scattering method. Meanwhile, stokes parameters of X/ γ -ray whose energy varies between tens of keV and MeV are simulated. The simulation results show that with the increasing of X-ray Energy, X-ray polarization is a constant value in a small cone of motivation. According to modulation curves analysed from experiment results, we can get the conclusion that the polarization of Thomson scattering source is tunable and controllable.

INTRODUCTION

Polarized X/ γ -ray has been studied and widely used in various scientific field. Polarization of X/ γ -ray can provide unique information addition to X-ray imaging and analysis of spectroscopy for researchers. In astrophysics, polarimetric observations of neutron stars provide the information of the intensity and geometry of the magnetic field [1-4]. In material science and biology, polarized X-rays can enhance the sensitivity of X-ray fluorescence analysis [5]. In nuclear physics, polarized γ -rays plays an important role in studying nuclear property. We can study the structure of nuclear by nuclear resonance fluorescence with polarized X/ γ -ray (NFR) [6-9]. And the polarized state of γ -rays is also important for the measurements of the parity of the nuclear states [10], the investigation of giant resonances of nuclei and the scattering reactions between photons and nuclei [11,12].

Compton scattering is the elastic scattering of a photon from a free electron, for the low energy electron (~MeV), it is also called as Thomson scattering [13-15]. Compton(Thomson) scattering X-ray source has been studied and developed for decades [16-20]. Comparing to the mechanism of other radiation sources, it can produce ultrashort, energy continuously tunable, high brightness, well-collimate and high polarized X-ray beams by laser photons scattering from free relativistic electrons [21-24]. Because of the advantages in X-ray application, Thomson scattering X-ray source is utility in material, medical and biological areas [24-28]. In our experiment, we change the polarization of X-ray by adjusting the polarization of laser beams since the polarization of laser is directly transferred to the scattered photons.

EXPERIMENT

We carry out the X-ray polarization control and measurement experiment on Tsinghua Thomson scattering X-ray source (TTX) platform. TTX is set up with a linac system and a femtosecond laser system. The linac system consists of a S-band photocathode RF gun, a magnet compressor and two x-band harmonic structures to generate high brightness electron pulse. The laser system can generate 266-nm ultraviolet pulse for the photocathode and 800-nm infrared pulse for the scattering interaction. The energy of X-ray photons is 50-keV and the flux is about $10^7 s^{-1}$ [29]. In our experiment, laser photons track through the quarter-wave plate and have a head-on interaction with the high-quality electron beams in the vacuum interaction room. The polarization of scatted photons is determined by the incident laser beams, which are controlled by the quarter-wave plate precisely.

In our experiment, we use the Compton scattering method, a kind of polarization-sensitive process which is more accurate than before, to measure the polarization of X-ray beams. According to the Klein-Nishina formula [30], for linear incident X/ γ -ray photon, the azimuthal distribution of the scattered photons is strongly depended on the X-ray polarization. A target, made from polyethylene, is placed after the titanium window of the beam pipe. The size of the cylinder target is 5-cm in height and 0.75-cm in radius. X-ray pulses irradiate on the end of the cylinder and generate scattered photons. We use an image plate wrapping around the cylinder to record scattered photons (Figur 1). Meanwhile, we use two thin aluminium rings locked to both ends of the polyethylene cylinder to support the image plate. The curved image plate is 2.5-cm in radius.

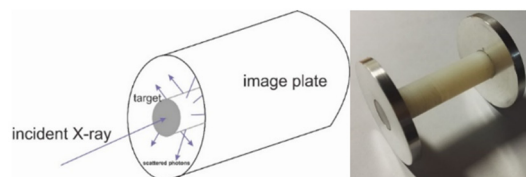


Figure 1: Schematic and real picture of target.

RESULTS

Figures 2-4 show the experiment results recorded by image plate and the simulation results done with Geant4.

[†] zhz16@mails.tsinghua.edu.cn

BEAM OPTIMIZATION AND MEASUREMENT OF CAEP FEL-THz INJECTOR*

D. Wu, D. X. Xiao, P Li, J. X. Wang[†], X. K. Li, X. Luo, K. Zhou, C. L. Lao,
Q. Pan, S. F. Lin, L. J. Shan, H. B. Wang, X. F. Yang, M. Li
Institute of Applied Electronics, China Academy of Engineering Physics (CAEP/IAE),
Mianyang, P. R. China

Abstract

The FEL-THz facility in Chinese Academy of Engineering Physics (CAEP) requires high brightness high repetition electron beam, which needs optimization of multi-parameter and multi-objective, such as emittance, energy spread, bunch length, etc. In this paper, some studies of beam optimization based on differential evolution (DE) algorithm and Astra code are shown. Dozens of the DC-SRF-injector parameters have been considered in the optimization. Some measurements of the electron beam are also introduced, including emittance measurement with the three-profile method, energy spread measurement with analyzing magnet and beam length diagnostics with zero-phasing method. These studies indicate that the injector beam quality satisfies the requirement of the FEL-THz facility.

INTRODUCTION

High average power high-brightness electron source plays a significant role in the path to the realization of the future high repetition short-wave free electron lasers (FELs) and energy recovery linacs (ERLs)[1, 2]. With the construction of European XFEL[3], and with some new projects put forward, such as LCLS-II[4] and MaRIE[5], the X-ray free electron lasers are moving in the direction of high repetition or even continuous-wave mode. These new developments have proposed some new requirements of the high brightness electron sources. The biggest challenge is to maintain the high brightness (electron charge ~ 200 pC, emittance < 0.5 mm-mrad, longitudinal length < 1 ps and energy spread $\sim 10^{-5}$) of the electron beams at high average current (\sim MHz repetition and ~ 100 mA average current).

High-voltage (HV) DC photocathode injector with superconducting RF accelerator could provide high brightness electron beams in CW mode, which makes it a hotspot in short-wave FEL research. One of the best results[6] is achieved by CLASS team in Cornell university, who has get a 0.3 mm-mrad emittance (95% core) at 100 pC CW mode with 1.3 GHz repetition. The dynamics design of the Cornell beamline is optimized by a multivariate genetic algorithm[7].

In China, the CAEP FEL-THz facility is the first high average Tera-Hertz source based on FEL, which is driven by

a DC gun with GaAs photocathode and two 4-cell 1.3 GHz super-conducting radio frequency (SRF) accelerator[8–12]. This is also the first DC-SRF-injector designed for high-Brightness electron beams In China. The repetition of FEL-THz is 54.167 MHz, one in twenty-fourth of 1.3 GHz. The effective accelerator field gradient is about 10 MV/m. The injector could provide high-brightness CW electron beam for the oscillator Tera-Hertz free electron laser. And the beam quality could be optimized better than the FEL-THz requirements. In this paper, an optimization with differential evolution genetic algorithm is discussed. And the beam measurement is shown, including emittance, energy spread and bunch length.

BEAM OPTIMIZATION

DE Algorithm

Differential evolution (DE) algorithm is a heuristic global optimization based on population, works on Darwin's concept of survival of the fittest[13, 14]. DE and other evolutionary algorithms are often used to solve the beam dynamic optimization[7, 15–17]

DE starts with a population of NP candidate solutions, which may be represented as $X_{i,G}$, $i = 1, 2, \dots, NP$, where i index denotes the population and G denotes the generation to which the population belongs. DE uses mutation, crossover and selection to solve problems, which are shown in Fig. 1.

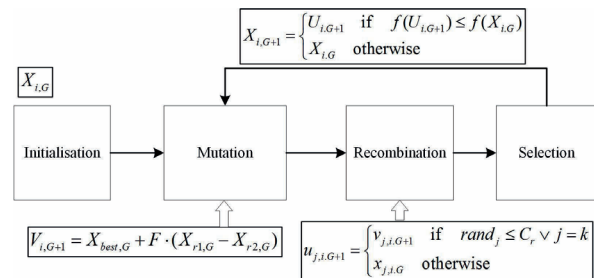


Figure 1: DE flow chart.

The mutation operator is the prime operator of DE. In this paper, a so-called 'best-strategy-type-1' is used[18], where $F \in [0, 1]$ is the control parameter. $r_i \in \{1, \dots, NP\}$ is a random selection and $r_1 \neq r_2$. The operator recombination and selection are also shown in Fig. 1 The crossover rate $C_r \in [0, 1]$ is the other control parameter of DE.

The most important part in the selection operator is the objective function f . In the one-objective situation, f is often as simple as normalized emittance or energy spread

* Work supported by China National Key Scientific Instrument and Equipment Development Project (2011YQ130018), National Natural Science Foundation of China with grant (11475159, 11505173, 11576254 and 11605190)

[†] jianxinwang1026@163.com

OVERALL DESIGN AND PROGRESS OF XiPAF PROJECT

S.X. Zheng, Q.Z. Xing, X.L. Guan, H.J. Yao, C. Cheng, T.B. Du, K.D. Man, H.Y. Zhang, G.R. Li, P.F. Ma, R.Tang, M.W. Wang, Y. Yang, H.J. Zeng, Q. Zhang, C.B. Bi, C.T. Du, Q.K. Guo, W.H. Huang, C.X. Tang, H.B. Chen, D. Wang, X.W. Wang[†], Key Laboratory of Particle & Radiation

Imaging (Tsinghua University), Ministry of Education, Beijing, China
 also at Laboratory for Advanced Radiation Sources and Application, Tsinghua University, Beijing, China

also at Department of Engineering Physics, Tsinghua University, Beijing, China

Z.M. Wang, C. Zhao, B.C. Wang, C.Y. Wei, Y.P. Wang, Y.H. Yan, H. Zhang, W.L. Liu, D. Wang, M.C. Wang, Y.M. Fu, E.Y. Qu, M.T. Qiu, W. Chen,

State Key Laboratory of Intense Pulsed Radiation Simulation and Effect (Northwest Institute of Nuclear Technology), Xi'an, China

W.Q. Guan, Y. He, J. Li, NUCTECH Co. Ltd., Beijing, China

Abstract

Xi'an Proton Application Facility (XiPAF) which consists of one 230 MeV proton accelerator and irradiation stations, will be constructed in Xi'an city, Shaanxi, China. The facility is composed of a 230 MeV synchrotron, a 7 MeV H-linac injector and two experimental stations. It can provide a flux of $10^5\sim 10^8$ p/cm²/s with the uniformity of better than 90% on the 10 cm×10 cm sample. The overall design of XiPAF accelerator is presented in this paper. And the progress of project is reported also.

INTRODUCTION

To fulfil the need of the experimental simulation of the space radiation environment, especially the investigation of the single event effect, the project of Xi'an Proton Application Facility (XiPAF) is under construction in Xi'an City, Shaanxi China. The facility is mainly composed of a 230 MeV synchrotron with a 7 MeV H⁺ linac injector and two experimental stations. A proton flux of $10^5\sim 10^8$ p/cm²/s with the uniformity of better than 90% on the 10 cm×10 cm sample is designed [1]. Table 1 shows the main parameters of the synchrotron and linac injector.

Table 1: Main Parameters of the XiPAF

Parameter	Injector	Synchrotron
Ion type	H ⁺	Proton
Output energy (MeV)	7	60~230
Peak current (mA)	5	
Repetition rate (Hz)	0.1~0.5	0.1~0.5
Beam pulse width	10~40 μs	1~10 s
Max. average current (nA)	100	30
Flux (p/cm ² /s) (10×10cm ²)		$10^5\sim 10^8$

The schematic layout of the XiPAF Accelerator system is presented in Fig. 1. The H⁺ beam is produced at the ion source (IS), accelerated to 7 MeV in linac injector, and then transferred to synchrotron through Medium Energy Beam Transport line (MEBT). This H⁺ beam is stripped by carbon foil in synchrotron and it is accelerated up to 230 MeV. Then the beam is extracted to experimental

station through High Energy Beam Transport line (HEBT). The HEBT have two beamlines, where T2 is used for 60 to 230 MeV proton application extracted from synchrotron directly, and the T1 can degrade the proton energy from 60 MeV to 10 MeV for low energy application. The lowest extraction energy from the synchrotron is 60 MeV.

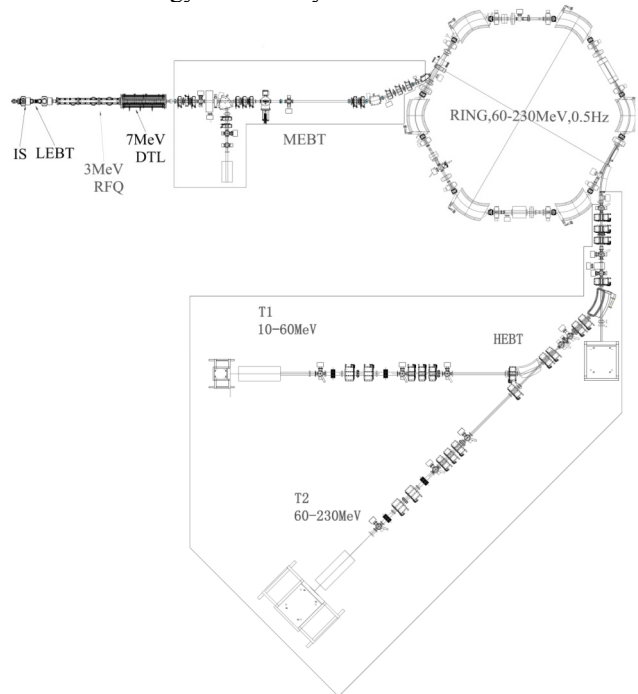


Figure 1: Layout of XiPAF accelerator system.

The main features of this accelerator are listed as follow:

- H⁺ injection enables transverse space painting flexibility in order to alleviate space charge effects at low energy [2].
- The 6-fold “Missing-dipole” FODO structure simplifies the lattice design and work point tuning. And it supply large space for injecting and extraction.
- The magnet-alloy loaded cavity simplifies the accelerating system and provides wide beam frequency swing.

[†] wangxuewu@tsinghua.edu.cn